

**ASSESSING THE CYTOTOXICITY OF ENGINEERED NANOPARTICLES:
APPLICATIONS AND IMPLICATIONS**

by
Margaret Fleming

A dissertation submitted to Johns Hopkins University in conformity with the
requirements for the degree of Doctor of Philosophy

Baltimore, Maryland
February 2020

© 2020 Margaret Fleming
All Rights Reserved

Abstract

Assessing the Cytotoxicity of Engineered Nanoparticles: Applications and Implications

This work examines the cytotoxicity of nanoparticles applied in two engineered systems: (I) chemical mechanical planarization (CMP) and (II) membrane water treatment. Nanoparticle cytotoxicity is central to both sections: Part I characterizes the interactions of CMP nanoparticles with cell membranes following their use and Part II investigates the efficacy of antibacterial silver nanoparticles as they are applied in membrane treatment.

During CMP, abrasive silica, ceria, and alumina nanoparticles contact the base of integrated circuit devices, producing an atomically smooth surface. Following CMP, these nanoparticles enter the environment through the wastewater treatment system. CMP nanoparticles were characterized to determine physicochemical changes incurred during processing that may alter their environmental fate and cytotoxicity. No significant changes in size, charge, or aggregation behaviors were observed. Interactions of CMP nanoparticles with model cell membranes were assessed using Quartz Crystal Microbalance with Dissipation Monitoring (QCM-D). Ceria and alumina nanoparticles did not interact strongly with model cell membranes, likely due to stabilizing slurry additives that remained effective even at high dilutions. Silica nanoparticles showed the strongest tendency to attach to supported lipid bilayers, with significant attachment detected at concentrations as low as 1 mg/L. Attachment was correlated with epithelial

cell membrane damage observed by collaborators at North Carolina A&T State University.

In Part II of this dissertation effort, I explored how the antibacterial nature of silver nanoparticles, when coupled with the hydrophilicity of polydopamine, can be harnessed to decrease the detrimental impact of biofouling on low pressure membranes. This work demonstrated that the hydrophilicity provided by the polydopamine coating decreased the initial rate of bacterial deposition by almost 50%. However, over the course of 3 days of filtration, only the combination of both polydopamine and silver nanoparticles was able to improve the rate of clean water production, increasing the flux to more than 175% of the unmodified membrane.

The unique properties associated with nanomaterials can be implemented in a variety of innovative environmental engineering applications. In designing these applications, the full life cycle of the nanoparticles must be considered.

Advisors: Dr. Edward Bouwer and Dr. Harihar Rajaram

Committee: Dr. William Ball, Dr. Xitong Liu, Dr. Sarah Preheim

Acknowledgements

First and foremost, I would like to express my deepest gratitude to my advisor Dr. Ed Bouwer. Even before he generously offered to oversee my Ph.D. research, Ed was one of my favorite teachers. He was incredibly knowledgeable and always made time to meet when I needed advice regarding research, writing, or building a career. He made the department feel like a family and cared about each of us on both an academic and a personal level. I will always be so grateful for everything he did to support me and create a feeling of belonging. He is profoundly missed.

I am greatly indebted to Dr. Kai Loon Chen, my first advisor, for his role in developing my research projects. His expert guidance and emphasis on precision taught me so much about planning experiments and communicating science. I would like to thank Dr. Hari Rajaram, for overseeing the completion of my Ph.D., along with my other committee members, Drs. Bill Ball, Sarah Preheim, and Xitong Liu. The advice and insight they provided as committee members and as teachers through my years at Johns Hopkins were invaluable. Xitong deserves special recognition for patiently guiding me through many levels of my Ph.D., from my first days in the laboratory to my final dissertation submission.

I would like to acknowledge my funding sources, the IGERT: Water, Health, and Climate program, the NSF GOALI program, and the departmental fellowship. Participating as an IGERT trainee was an especially enlightening experience and I am so grateful to Dr. Grace Brush for her work developing and leading the program.

I would like to thank Drs. Lynn Roberts and Alan Stone for their willingness to share their expertise through both their wonderful courses and one-on-one meetings. I am

also grateful to Drs. Mike Betenbaugh, Howard Fairbrother, Joe Jacangelo and Chuck Young for participating as members of my GBO committee. Their insights broadened my research perspective and improved the quality of my work.

I would like to acknowledge Dr. Shyam Aravamudhan for his collaboration and guidance in the effort to produce research that is both practical and compelling. I would like to recognize Dr. Mike Bevan for generously allowing me access to the Zetasizer Nano-ZS. Additional thanks to his student, Jenny Jumai'an, for providing training and facilitating my lab work. I would also like to thank Michael McCaffery and Erin Pryce of the Integrated Imaging Center for providing confocal microscope access and training.

I greatly appreciate the patience and support of the front office staff: Jessica Elroy, Michael Lester, Denise Nowlin, Zoe Petersen, and Tugba Yildiz. Special thanks to Huan Luong, who served as the lab manager for most of my time at Johns Hopkins and without whom I could not have succeeded in the lab.

I cannot adequately express my appreciation for my friends and colleagues within EHE. I am so grateful to my work family the Bouwer Group, Chris Brueck, Dr. Steven Chow, and Hannah Gray, for the endless emotional support and intellectual feedback they provided. I am thankful to Dr. Li Tang for introducing me to the Hopkins laboratories and for training me on membrane modification and bacterial work. Dr. Mike Rose has been an incredibly thoughtful officemate and labmate and I am very grateful for his friendship. The enthusiasm and hard work of my trainees, Ayella Maile-Moskowitz and Isabela Sampaio, made the laboratory a brighter place. I am deeply appreciative of all of my colleagues, including Keith Arora-Williams, Cassie Cosans, Andrea Fraser, Dr. David Goodwin, Dr. Robin Hytowitz, Dr. Jessica Lawson, Dr. Stephanie Lau, Weichen

Liao, David Litwin, Alex Lorentz, Dr. Shane Putnam, Dr. Eric Sakowski, Dr. Elina Spyrou, Veronica Wallace, Dr. Dano Wilusz, and Yue Zhang, for making EHE such a wonderful place to work.

I am indescribably grateful to my roommates and closest friends, Hannah, Rachel, and Keith, for making Baltimore my home. They have supported me through every up and down of my Ph.D. and kept me motivated and inspired with their dedication, insight, and humor. I can't imagine the last five and a half years without them.

Finally, I want to express profound gratitude to my family for the countless ways they've supported me. I am very thankful for my parents, Russ and Kathy Fleming, who remain my greatest sources of day-to-day advice and larger wisdom. I would also like to thank my siblings, David and Natalie, for being the very best, built-in, life-long friends. I am so grateful to have all of you to laugh with and learn from.

I have a very clear memory from my first day at Johns Hopkins of my advisor, Ed, describing the department as a family. A family is exactly what I found, and I am so grateful to everyone who has gone out of their way to make this such an amazing experience.

Thank you.

Table of Contents

Abstract.....	ii
Acknowledgements	iv
Table of Contents	vii
List of Tables	xi
List of Figures.....	xii
Chapter 1. Brief Overview of the Nature, Fate, and Effects of Engineered	
Nanomaterials	1
1.1 Nanomaterial Production	1
1.2 Human Exposure and Health Effects	1
1.3 Environmental Health Effects.....	3
1.4 Regulatory Landscape.....	5
1.4.1 Challenges.....	5
1.4.2 Food and Drug Administration	6
1.4.3 Environmental Protection Agency	7
1.4.4 Occupational Safety and Health Administration.....	8
1.4.5 European Commission	9
1.5 Disposal	9
1.5.1 Landfills	9
1.5.2 Wastewater Treatment	10
1.6 Environmental Fate.....	16
1.6.1 Water.....	16
1.6.2 Soil.....	19
1.6.3 Air	20
1.7 Dissertation Objectives	20
1.8 Dissertation Organization	21
1.9 References.....	24

Chapter 2. Introduction to Chemical Mechanical Planarization Nanoparticles 29

2.1 CMP Process.....	29
2.2 Airborne Exposure.....	30
2.3 Wastewater.....	31
2.4 Environmental Fate.....	33
2.5 Toxicity.....	34
2.5.1 Pristine Nanoparticles.....	34
2.5.2 CMP Nanoparticles.....	36
2.6 Summary.....	38
2.7 References.....	40

**Chapter 3. Predicting the Environmental Fate of Waste Chemical Mechanical
Planarization Nanoparticles Through Physicochemical Characterization and**

Interactions with Model Cell Membranes 43

3.1 Abstract.....	43
3.2 Introduction.....	44
3.3 Materials and Methods.....	46
3.3.1 Nanoparticle Slurries.....	46
3.3.2 Electrophoretic Mobility.....	48
3.3.3 Size and Aggregation.....	49
3.3.4 Quartz Crystal Microbalance with Dissipation Monitoring.....	50
3.3.5 QCM-D Solution Preparation.....	51
3.3.6 Attachment Efficiency.....	52
3.3.7 Vesicle Disruption.....	53
3.4 Results and Discussion.....	54
3.4.1 Nanoparticle Slurry Characteristics.....	54
3.4.2 Electrophoretic Mobility.....	56
3.4.3 Size and Aggregation.....	58
3.4.4 Attachment Efficiency.....	60
3.4.3 Vesicle Disruption.....	64
3.5 Conclusion.....	66
3.5 References.....	68

Chapter 4. Assessing Changes in CMP Nanoparticle Cytotoxicity Using Model Cell

Membranes	72
4.1 Abstract.....	72
4.2 Introduction.....	73
4.3 Materials and Methods.....	75
4.3.1 Nanoparticle Slurry Characterization.....	75
4.3.2 Supported Lipid Bilayer Attachment	77
4.3.3 Vesicle Disruption	78
4.3.4 Cytotoxicity Assays	79
4.4 Results and Discussion	80
4.4.1 Nanoparticle Slurry Characterization.....	80
4.4.2 QCM-D Attachment.....	81
4.4.3 Vesicle Disruption	88
4.4.4 Implications for Cytotoxicity	90
4.5 Conclusions.....	92
4.6 References.....	94

Chapter 5. Introduction to Water Filtration Membranes Modified with Silver

Nanoparticles to Delay Biofouling.....	98
5.1 Low Pressure Membrane Systems	98
5.2 Biological Fouling in Membrane Systems.....	99
5.3 Current Cleaning Methods	99
5.4 Membrane Modification with Polydopamine	102
5.4 Environmental Fate of Silver Nanoparticles.....	105
5.6 Silver Nanoparticle Toxicity.....	107
5.7 Summary	108
5.8 References.....	109

Chapter 6. Modifying Water Purification Membranes with Bioinspired

Polydopamine and Silver Nanoparticles for Biofilm Prevention	113
6.1 Abstract.....	113
6.2 Introduction.....	114

6.3 Materials and Methods.....	116
6.3.1 Membrane Fabrication and Modification	116
6.3.2 Preparation of Bacterial Solution.....	117
6.3.3 Direct Observation System	118
6.3.4 Biofilm Formation System.....	119
6.3.5 Silver Leaching	121
6.3.6 Biofilm Imaging.....	122
6.4 Results and Discussion	122
6.4.1 Direct Observation System	122
6.4.2 Biofilm Formation System.....	124
6.4.3 Silver Leaching	127
6.4.4 Biofilm Imaging.....	127
6.5 Conclusions.....	132
6.6 References.....	134
Chapter 7. Conclusions, Significance, and Suggestions for Future Work.....	137
7.1 Impact of CMP on Nanoparticle Characteristics	137
7.2 Stabilization Effects of Slurry Additives	138
7.3 Pairing Model Cell Membrane and Cytotoxicity Studies	139
7.4 Improving Polymeric Membrane Performance with Polydopamine and Silver Nanoparticle Modification.....	140
7.5 Engineering and Research Significance.....	141
7.5.1 Metal Oxide Nanoparticles Applied in Chemical Mechanical Planarization	141
7.5.2 Silver Nanoparticles Applied in Membrane Water Treatment	142
7.6 Future Research Directions.....	144
7.6.1 CMP Nanoparticle Characterization	144
7.6.2 Developing Membranes Modified with Polydopamine and Silver Nanoparticles.....	146
7.7 References.....	147
Curriculum Vitae.....	148

List of Tables

Table 3.1. Identifiers for nanoparticle slurries before and after CMP. Altogether there are seven slurry types tested, including three pre-CMP (Si, Ce, and Al) and four post-CMP (Si-Si, Ce-Si, Al-Cu, and Al-W).....	48
Table 3.2. CMP process parameters provided by Dr. Steven Crawford at North Carolina A&T State University. Parameters were set in keeping with associated intended uses: alumina slurries for metal removal, ceria and silica slurries for interlayer dielectrics (ILD) and shallow trench isolation (STI).....	48
Table 3.3. CMP slurry characteristics.....	56
Table 4.1. pH range of various physiological fluids.....	76
Table 4.2. Concentrations at which 50% of cells were inhibited (IC ₅₀) following 48 hours of exposure to silica, ceria, and alumina nanoparticles, before (Si, Ce, Al) and after (Si-Si, Ce-Si, Al-Cu) exposure to the CMP process. Values provided by Dr. Shyam Aravamudhan and Dr. Steven Crawford of North Carolina A&T State University.....	91

List of Figures

Figure 3.1. Transmission Electron Microscopy (TEM) images of (a) fumed SiO₂, (b) CeO₂, and (c) Al₂O₃ nanoparticles from the manufacturer provided CMP slurries. Images provided by Dr. Shyam Aravamudhan and collected by Dr. Steven Crawford at North Carolina A&T State University. 47

Figure 3.2. Electrophoretic mobilities (EPMs) of the nanoparticles, before (Al, Ce, Si) and after (Al-Cu, Al-W, Ce-Si, Si-Si) CMP, diluted 1/1000 in 0.4 mM NaHCO₃ buffer and varying concentrations of NaCl. EPMs are represented as the average and standard deviation of four replicate measurements. 57

Figure 3.3. Hydrodynamic diameters of CMP nanoparticles (diluted to 1 mg/L in DI water) represented as the average and standard deviation of four replicate measurements. 59

Figure 3.4. (a) Hydrodynamic diameters of silica nanoparticles, before (Si) and after (Si-Si) CMP and (b) corresponding rates of aggregation. Silica nanoparticles were diluted to a concentration of 1 mg/L and allowed to aggregate over 20 minutes. 60

Figure 3.5. Attachment efficiency of silica NPs, before (Si) and after (Si-Si) CMP, diluted on the order of 1 mg/L with NaHCO₃ buffer and varying NaCl concentration. Represented as the average and standard deviation of triplicate experiments. Asterisk (*) indicates $p < 0.05$ for both Si and Si-Si nanoparticles. 62

Figure 3.6. Representative QCM-D frequency profile as silica nanoparticles deposit onto vesicles (0-40 min) followed by exposure to the membrane solubilizer, which releases all CF dye contained within the vesicles (40-60 min). 64

Figure 3.7. (a) Carboxyfluorescein dye in outflow of QCM-D as vesicles are exposed to 1 mg/L silica nanoparticles (before (Si) and after (Si-Si) CMP) dispersed in 150 mM NaCl and bicarbonate buffer for 40 minutes. Following the nanoparticle exposure period, 32 mM Triton X-100, a membrane solubilizer, was pumped through the system for 20 minutes. Enlargement of silica nanoparticle exposure period is show in (b). 65

Figure 4.1. Hydrodynamic diameters of silica, ceria, and alumina nanoparticles, before (Si, Ce, Al) and after (Si-Si, Ce-Si, Al-Cu, Al-W) CMP processing, diluted to 1 mg/L in 150 mM NaCl and 0.4 mM NaHCO₃. Data represents the average and standard deviation of four replicate measurements. 81

Figure 4.2. Representative profiles of the frequency change that occurred as silica nanoparticles attached to the supported lipid bilayer over 40 minutes of exposure. Nanoparticles diluted in 150 mM NaCl and bicarbonate buffer (pH 7.4). 82

Figure 4.3. Initial rate of frequency change as silica nanoparticles, before (Si) and after (Si-Si) CMP, attach to the supported lipid bilayer in 150 mM NaCl and bicarbonate buffer (pH 7.4). Represented by the average and standard deviation of three replicate runs. Asterisk (*) indicates $p < 0.05$ for both Si and Si-Si nanoparticles. Asterisks (**) indicate $p < 0.025$ for both Si and Si-Si nanoparticles. 82

Figure 4.4. Representative profiles of the frequency change that occurred as ceria nanoparticles attached to the supported lipid bilayer over 40 minutes of exposure. Nanoparticles diluted in 150 mM NaCl and bicarbonate buffer (pH 7.4). 83

Figure 4.5. Initial rate of frequency change as ceria nanoparticles, before (Ce) and after (Ce-Si) CMP, attach to the supported lipid bilayer in 150 mM NaCl and bicarbonate

buffer (pH 7.4). Represented by the average and standard deviation of three replicate runs. Asterisk (*) indicates $p < 0.05$ for both Ce and Ce-Si nanoparticles..... 84

Figure 4.6. Representative profiles of the frequency change that occurred as alumina nanoparticles attached to the supported lipid bilayer over 40 minutes of exposure.

Nanoparticles diluted in 150 mM NaCl and bicarbonate buffer (pH 7.4). 84

Figure 4.7. Initial rate of frequency change as alumina nanoparticles (before CMP (Al), after polishing copper (Al-Cu), and after polishing tungsten (Al-W)) attach to the supported lipid bilayer in 150 mM NaCl and bicarbonate buffer (pH 7.4). Represented by the average and standard deviation of three replicate runs. Asterisk (*) indicates $p < 0.1$ for Al, Al-Cu, and Al-W nanoparticles. Asterisks (**) indicate $p < 0.025$ for Al, Al-Cu, and Al-W nanoparticles. 85

Figure 4.8. LDH released from A549 lung epithelial cells normalized by the negative control (e.g. 1.5 = 150% of LDH released during negative control) following 48 hours of nanoparticle exposure. Figure provided by Dr. Shyam Aravamudhan and Dr. Steven Crawford of North Carolina A&T State University 87

Figure 4.9. Representative profiles of 500 mg/L silica, ceria, and alumina nanoparticles (diluted in 150 mM NaCl and 0.4 mM NaHCO_3) depositing onto the DOPC vesicle layer over 40 minutes followed by 20 minutes of exposure to 32 mM Triton X-100 (membrane solubilizer). 88

Figure 4.10. Carboxyfluorescein dye released from vesicles as a function of time over 40 minutes of nanoparticle exposure. Vesicles exposed to 500 mg/L silica, ceria, and alumina nanoparticles before (Si, Ce, and Al) and after (Si-Si, Ce-Si, Al-Cu, and Al-W) exposure to the CMP process and diluted in 150 mM NaCl and bicarbonate buffer (pH

7.4). QCM-D effluent collected over five-minute intervals. Data represents average and standard deviation of triplicate runs..... 89

Figure 4.11. Percent of total carboxyfluorescein dye released from vesicles upon exposure to 500 mg/L silica, ceria, and alumina nanoparticles before (Si, Ce, and Al) and after (Si-Si, Ce-Si, Al-Cu, and Al-W) exposure to the CMP process and diluted in 150 mM NaCl and bicarbonate buffer (pH 7.4). Percentage represented by average and standard deviation of triplicate runs. Asterisk (*) indicates $p < 0.1$ and asterisks (**) indicate $p < 0.05$ 90

Figure 6.1. Direct observation system schematic. The system is pressurized to 20 psi. Bacterial feed solution in the pressure vessel is pumped through a flow meter and a polycarbonate flow cell set on the stage of a fluorescent microscope. The polycarbonate flow cell holds the membrane. The crossflow stream runs over the surface of the membrane, while the permeate stream passes through the membrane. Both the crossflow and permeate streams are recirculated to the pressure vessel. 119

Figure 6.2. Biofilm formation system schematic. The system is pressurized to 5 psi, maintained using a pressure regulator and two pressure gauges. Bacterial feed solution is pumped through a flow meter and a polycarbonate flow cell which holds the membrane. The crossflow stream runs over the surface of the membrane, while the permeate stream passes through the membrane. Both the crossflow and permeate streams are recirculated to the feed solution container. 121

Figure 6.3. (a) Number of bacteria deposited on base polysulfone, PD modified, and PD/Ag modified membranes over 20 minutes of filtration through the direct observation system. Data represent average and standard deviation of triplicate experiments. (b)

Initial deposition rate of *P. aeruginosa* onto base polysulfone, PD modified, and PD/Ag modified membranes. Rate calculated by normalizing the initial slopes presented in (a) by the membrane area (870 μm x 729 μm) and the concentration of bacteria in the feed solution (ca. 10^5 cells/L). Asterisk (*) indicates $p < 0.025$ 123

Figure 6.4. Flux decline over three days of *P. aeruginosa* filtration in the biofilm formation system through base, PD modified, and PD/Ag modified membranes. Flux measured by weighing the output of the permeate stream collected over a period of three minutes and converting to a flow rate. Data represent average and standard deviation of triplicate experiments..... 125

Figure 6.5. Representative top view confocal images of the live cells (green) and dead cells (red) attached to the surfaces of (a) base membranes, (b) PD modified membranes, and (c) PD/Ag modified membranes after three days of bacterial filtration. Each row contains three images to demonstrate the wide range of bacterial growth that developed on each type of membrane surface in the biofilm formation system. Each image is 225 μm x 225 μm 128

Figure 6.6. Live cell, dead cell, and extracellular polysaccharide (used as an indicator of EPS) COMSTAT biovolumes measured on base, PD modified, and PD/Ag modified membranes. The extracellular polysaccharide biovolume associated with PD/Ag modified membranes (*) cannot be seen as the average value is $0.0025 \pm 0.003 \mu\text{m}$. Data represent average and standard deviation of triplicate experiments. 129

Chapter 1. Brief Overview of the Nature, Fate, and Effects of Engineered Nanomaterials

1.1 Nanomaterial Production

Nanomaterials may be produced through natural processes, including volcanic eruptions, forest fires, and rock weathering, or through anthropogenic manufacturing processes [1]. Engineered nanomaterials are manufactured for their novel properties, including antibacterial (e.g. silver nanoparticles in clothing), magnetic (e.g. iron oxide nanoparticles in diagnostic imaging), and catalytic (e.g. ceria nanoparticles in diesel fuels) functionality. Over 1000 kg of engineered nanomaterials are produced annually [2] for use in medicinal, electronic, industrial, and environmental applications [1, 3-6]. About half of the nanoparticles in commercial products are metals and metal oxides (e.g. silver, zinc oxide, copper oxide, titanium dioxide, iron oxide) followed by silicon and carbon-based nanomaterials [1, 7]. Using only voluntary product submissions, the Project on Emerging Nanotechnologies has compiled a database of over 1800 consumer products from 622 companies in 32 countries [7].

1.2 Human Exposure and Health Effects

Human exposure to engineered nanomaterials can occur through three routes: inhalation, ingestion, and dermal contact. Inhalation is the exposure route associated with the greatest health risk [8]. Although long-range inhalation effects are not considered likely, airborne levels will be concentrated around nanoparticle production processes and construction activities involving nanoparticle-laden materials (e.g. cement and concrete), increasing the risks experienced by workers [8]. Inhaled nanoparticles can be absorbed

through contact with lung epithelial cells or become trapped in mucous which is subsequently swallowed, entering the ingestion pathway [8]. Other ingestion exposures include consumption of food and water contaminated by nanoparticles and hand-to-mouth contact. Engineered nanoparticles that have been ingested will be transported to the intestines, where they are exposed to acidic conditions that may alter nanoparticle properties that determine uptake [8]. Dermal contact, the most common exposure route due to human interaction with commercial products, has been shown to be the least likely to result in nanoparticle entry to the body. Nanoparticles generally do not travel through skin layers; however, the likelihood of absorption increases if skin has been damaged by cuts or burns [8].

Following human exposure and nanoparticle adsorption, engineered nanoparticles are distributed throughout the body. Their ability to penetrate biological barriers allows them to be transported from systemic circulation into most organs, including the brain [8]. Nanomaterials may access the brain by means of passive diffusion through the blood-brain barrier (BBB), through receptor-mediated endocytosis or pinocytosis, or through the olfactory nervous system [8]. While the extent of absorption into the brain is likely limited [9], signs of inflammation and changes to neuron morphology have been observed in animals following exposure to carbon black, TiO₂ nanoparticles, and carbon nanotubes [8].

Within organs, nanoparticles can enter cells through passive diffusion or through the active uptake processes of phagocytosis, pinocytosis, and endocytosis [8]. During phagocytosis, nanoparticles are engulfed by lysosomes that contain digestive enzymes. This acidic environment can solubilize metallic nanoparticles, releasing metal ions [8].

Other nanoparticles, including metal oxide nanoparticles, are recalcitrant even in lysosomal environments and can persist for months before removal from the cell through exocytosis [8].

The health effects of nanomaterials have most commonly been studied in mammalian systems [8]. Oxidative stress, caused by the generation of reactive oxygen species (ROS), is one of the primary toxicity mechanisms associated with nanomaterial exposure and can cause DNA damage and cancer [8]. In addition, high concentrations of toxic metal ions can be released from the large surface area provided by nanoparticles after they have entered biological systems. Nanoparticle exposure can alter cellular activities involved in growth and proliferation as well as cause cell death through necrosis or apoptosis. Nanoparticle exposure has also been shown to cause inflammation in organs including the lungs, liver and skin, which can lead to diseases including atherosclerosis, rheumatoid arthritis, and cancer [8].

1.3 Environmental Health Effects

The effects of nanoparticles on microorganisms have received less attention than those on eukaryotic organisms [10]. On the cellular level, nanoparticle attachment is an important step in both eukaryotic and prokaryotic-nanoparticle interactions [11]. Increased adhesion is associated with physical damage to the cell membrane and increased cellular uptake. Attachment is also associated with increased damage from the release of toxic metal ions and ROS from the nanoparticle surface, leading to destabilization of the cell membrane and subsequent leakage [12]. Attached nanoparticles may decrease the chances of cell survival by forming an additional barrier to feeding and movement [13]. Studies have shown that carbon nanotube, graphene oxide nanosheet,

and ZnO nanoparticle attachment to *Escherichia coli* cells all result in toxic effects [12]. Furthermore, nanoparticles like Ag and TiO₂ are commonly used specifically for their antibacterial properties .

Aquatic species are exposed to contaminated water through skin, gills, and/or ingestion. For fish, submersion makes the distinction between dermal contact and ingestion routes less distinct [8], but transport through the skin may be limited due to the protective mucous layer [14]. Fish uptake of metallic nanoparticles, including Au, Cu, Ag, and Ti, has been demonstrated [8]. Benthic organisms will primarily be exposed to nanomaterials that settle out of the water column. Titanium nanoparticles and fullerenes have both been found in marine bivalves [15, 16]. Metal nanoparticles are likely to cause damage to the digestive gland of mollusks [17], while carbon nanotubes have been shown to cause inflammatory reactions [15].

Nanoparticles may enter terrestrial plants through root uptake from the soil or through atmospheric deposition to the leaves [18]. The extent and effects of nanoparticle absorption is dependent on both the nanomaterial type and plant species. Studies have reported observations of growth reduction, growth increase, and no detectable change [8]. Nanoparticle induced toxicity has been observed following exposure to fullerenes, carbon nanotubes, Al nanoparticles, Zn nanoparticles, TiO₂ nanoparticles, and ZnO nanoparticles [8]. Once nanoparticles are incorporated into plant systems, organisms that feed on these plants are consequently exposed.

Nanoparticles may be transferred from one organism to another through food consumption. There are a few studies that have reported these types of exchanges, reviewed by Boyes et al. [8]. While quantum dots can be transferred from protozoans to

rotifers through ingestion, no biomagnification has been observed [19]. Biomagnification of quantum dots did occur when *Pseudomonas aeruginosa* was consumed by *Tetrahymena thermophila* protozoa [20]. Gold nanoparticles experienced size-dependent biomagnification as they moved from tobacco plants to tobacco hornworms [21]. Ceria nanoparticles traveled from kidney bean plants to Mexican bean beetles, with larvae experiencing lower accumulation than adults [22]. Further biomagnification was demonstrated when the contaminated Mexican bean beetles were consumed by spined soldier bugs [22]. While biomagnification of nanomaterials has been shown to occur, few studies address nanoparticle movement through food webs/chains [8]. An important pathway that needs further investigation is the accumulation of settled nanoparticles in mollusks that are then consumed by humans [23].

1.4 Regulatory Landscape

1.4.1 Challenges

Regulating the manufacture, importation, and processing of nanomaterials presents several challenges. While many regulatory bodies argue that nanomaterials fit into existing policy structures, concerns have been raised over the need to differentiate nanomaterials from their bulk counterparts. A fundamental consideration in designing policy is determining the definition of a nanomaterial. While many defer to the classical definition of a solid substance having at least one dimension on the nanoscale (< 100 nm), this cut-off is arbitrary [10]. Instead, the unique properties that make materials at the nanoscale valuable, including differences from bulk scale conductivity, strength, and reactivity, are the characteristics of interest that may call for special regulatory focus. Despite the challenges inherent in regulation, nanoparticles are already marketed

globally. Given the public interest in the potential hazards of exposure to nanomaterials, several United States agencies have made various efforts to address these concerns.

1.4.2 Food and Drug Administration

The official position of the Food and Drug Administration (FDA) is that nanomaterials can be regulated under existing statutes [24]. Materials, including nanomaterials, are subject to different regulatory standards depending on their intended use. A subset, including medical devices and foods, require premarket authorization, a process involving the submission of information related to product safety and efficacy. Other products, including cosmetics and dietary supplements, do not require premarket review and are only regulated if safety issues arise after they are sold. Through this traditional process, the FDA reviewed the use of titanium dioxide nanoparticles in sunscreens. These nanoparticles were determined to be generally recognized as safe and effective (GRASE) on the basis that the nanoparticles were not shown to penetrate skin [25, 26]. Other factors, such as environmental fate and aquatic toxicity were not considered.

The FDA's Nanotechnology Task Force was formed in 2006 and released a report the following year recommending pathways to improve the understanding and regulation of nanomaterials [27]. While the task force concluded that existing regulations are flexible enough to cover nanomaterials, the report authors expressed concern over mass production of nanomaterials not subject to premarket authorization and suggested adjustments including receiving additional data from manufacturers. The FDA Nanotechnology Regulatory Science Research Plan was released in 2013, outlining a framework to address the gaps in knowledge preventing more efficient regulation [28].

This plan includes the establishment of staff training and professional development programs, laboratory facilities, and collaborative research. Most recently, the FDA released “Guidance for Industry: Considering Whether an FDA-Regulated Product Involved the Application of Nanotechnology,” which helped manufacturers identify nanomaterials and encouraged them to consult with the FDA on their use [29]. Such consultation would be voluntary.

1.4.3 Environmental Protection Agency

Chemical manufacturing is regulated by the Environmental Protection Agency through the Toxic Substances Control Act (TSCA). Through this legislation, companies must notify the EPA of their plans to manufacture new chemicals. This notification includes available toxicity data, but no testing is required [30]. The EPA probes potential chemical toxicity through the use of models that rely on structure-activity relationships [30]. To prevent the manufacturing of a new chemical, within 90 days of receiving the submission the EPA must prove the chemical presents a risk to public and/or environmental health and requires further toxicity testing [30]. As a result, the portion of new chemicals prevented from going to market is very low.

Nanomaterials were regulated under the general TSCA until January 2017 when the EPA published a new rule, “Chemical Substances When Manufactured or Processed as Nanoscale Materials; TSCA Reporting and Recordkeeping Requirements,” in the Federal Registrar [31]. Under this new rule, manufacturers, importers, and processors must electronically submit information about their nanoparticle use, including chemical identity, production volume, and environmental and health effects. Nanomaterials regulated by this rule are not defined on the basis of size per se, but rather as materials

specifically manufactured for the unique properties that arise from their large surface area to volume ratios.

1.4.4 Occupational Safety and Health Administration

Among the U.S. government's regulatory bodies, the Occupational Safety and Health Administration (OSHA) has progressed furthest in recommending safe exposure levels for nanomaterials. As the branch tasked with promoting safe working conditions, OSHA is largely concerned with particulate matter that enters the air during the manufacturing and processing of these materials and reaches workers through inhalation. Nanomaterials fall under the purview of OSHA's standing regulations, including Section 5(a)(1) of the Occupational Safety and Health Act, also known as the General Duty Clause [32]. This clause stipulates that an employer is required to "furnish each of his employees employment and a place of employment which are free from recognized hazards that are causing or are likely to cause death, or serious harm to his employees." Furthermore, nanomaterials are subject to the same OSHA standards that govern other materials, including rules regarding injury and illness reporting, personal protective equipment requirements, sanitation, and hazard communication.

While nanomaterials fall under the general scope of OSHA regulations, awareness of the potential risks associated specifically with nanoparticles has drawn the attention of the National Institute for Occupational Safety and Health (NIOSH), a branch of the CDC that conducts research to inform the OSHA exposure limits. These exposure limits are generally communicated through an 8-hour time-weighted average, or the permissible air concentration a worker is exposed to averaged over an 8-hour shift as part of a 40-hour work week. In 2004, NIOSH established the Nanotechnology Research Center, to apply

this research methodology to nanomaterials. As a result, OSHA has developed recommendations (not enforceable laws) for carbon nanotubes and nanofibers (1 mg/m³ 8-hour time-weighted average) [26] and titanium dioxide nanoparticles (2.4 mg/m³ and 0.3 mg/m³ 10-hour time-weighted averages for fine and ultrafine particles, respectively [33].

1.4.5 European Commission

In contrast to the United States, the European Union bases its chemical manufacturing policy on the precautionary principle, which gives more weight to the risk of the unknown when producing a new chemical substance. Through REACH (Registration, Evaluation, Authorization, and Restriction of Chemicals) regulation, the European Commission requires companies to assess public and environmental health risks associated with all chemical substances produced or imported in quantities greater than 10 tons per year. Nanomaterials fall under this purview, as well as under the Classification Labeling, and Packaging Regulation that requires a new hazard classification evaluation for any changes in a substance's physical state. Several individual members of the European Union have additional regulations that specifically target nanomaterials [34].

1.5 Disposal

1.5.1 Landfills

The majority (ca. 63-91%) of manufactured nanomaterials are disposed of in landfills [35]. The main concern regarding this disposal method is the possibility of engineered nanoparticles traveling through landfill leachate and contaminating soil and

groundwater [36-40]. The interactions of engineered nanomaterials with landfill leachate are likely to result in transformations, including aggregation, dissolution, and redox reactions [8]. These interactions are predicted to alter the surface of nanoparticles, resulting in their destabilization and decreasing the likelihood of their release from the landfill. For instance, Zhu et al. determined that in the high ionic strength environment of landfill leachate, humic acids introduce bridging forces that cause TiO₂ nanoparticles to aggregate [41]. In fact, a simulation of the 5-year fate of TiO₂ nanoparticles modeled by de Castro et al., showed TiO₂ nanoparticles adsorbing to landfill soil and remaining immobile [42]. Generally, engineered nanoparticles are expected to be well confined in landfills that are appropriately sealed and treated [43]. Furthermore, the presence of engineered nanomaterials has not impacted microbial degradation of the organic matter contained in landfills [8].

1.5.2 Wastewater Treatment

Current and expected production rates indicate that significant concentrations of engineered nanomaterials will be discharged into environmental waters and reach wastewater treatment facilities [43]. Furthermore, the incorporation of engineered nanoparticles into wastewater treatment has been suggested to improve the efficacy of water filtration and disinfection [44]. Indeed, commonly used nanomaterials have already been detected in municipal wastewater treatment systems. Gottschalk et al. estimated that TiO₂ nanoparticles, Ag nanoparticles, carbon nanotubes, and fullerenes are present in treated wastewater at concentrations of 1.8-4.3 ng/L, 0.3-0.4 ng/L, 21.0-42.5 ng/L, 8.6-14.8 ng/L, and 3.8-5.2 ng/L, respectively [45].

While wastewater treatment systems are not designed for removal of particles on the nanoscale, many of the treatment processes are able to remove a large fraction of nanoparticles, mostly through a combination of sorption, aggregation, and settling [46]. Water treatment processes that have demonstrated varying degrees of success include coagulation, flocculation, sedimentation, filtration, sorption, and biological treatment. Considering the behavior and removal of nanoparticles as they move through these treatment processes is an important step in evaluating their environmental fate [46].

Coagulation/Flocculation/Sedimentation

One of the fundamental wastewater treatment processes is sedimentation, which provides time for solids in the waste stream to settle out of solution. The settling time of nanoparticles, calculated through Stokes' Law, is not fast enough for this type of removal to be effective. In order to increase the fraction of nanoparticles removed, particles are exposed to coagulation, a critical, antecedent step in which chemicals are added to the influent to promote the formation of aggregates [47, 48]. Coagulation of negatively charged particles is usually achieved by adding alum or ferric salt (ferric sulfate or ferric chloride) to influent water. The addition of these salts causes destabilization of particles, resulting in homo-aggregation (with other nanoparticles of the same type) and hetero-aggregation (with other wastewater constituents) [47]. Flocculation refers to the process in which particles are allowed to mix with the coagulants and form aggregates, or flocs. Following coagulation and flocculation, nanoparticles can be effectively removed through sedimentation or flotation.

The efficiency of coagulation, flocculation, and sedimentation is dependent on factors including nanoparticle type, coagulant type, coagulant dosage, and source water

parameters [43]. Kinsinger et al. found that TiO₂ particles smaller than 450 nm were not removed through flocculation and sedimentation [49]. Several studies have shown incomplete metal and metal oxide nanoparticle removal, with efficiencies ranging from 20% to more than 90% [43]. This may be due to incomplete particle destabilization and aggregation. The presence of natural organic matter (NOM) has been shown to decrease the removal of nanoparticles, either through sequestration of available coagulant or through stabilization of the nanoparticles [43, 47].

Biological Treatment

Biological treatment is unlikely to be the primary means chosen to treat industrial wastewaters containing nanoparticles. However, following initial treatment, many industrial waste streams are discharged to municipal wastewater treatment plants with activated sludge facilities. Nanoparticles may experience cellular uptake, biodegradation, and/or sorption to biomass [50]. More than 90% of engineered nanomaterials are expected to be removed during biological treatment, the majority through attachment to the concentrated biomass [50, 51]. Nanomaterial exposure may also impact the activity and efficacy of microorganisms involved in biological treatment. To monitor these potential changes, researchers have measured oxygen uptake rate, carbon and nitrogen removal efficiency, abundance of microbes, and enzyme activity [47].

The conditions present in biological wastewater treatment systems lessen the impact of antibacterial nanoparticles. Bacteria in attached-growth systems form biofilms, a protected form of growth discussed in detail in Chapters 5 and 6 [52, 53]. Microbial communities have also been shown to adapt to low concentrations of antimicrobial exposure over time [52]. Through the combination of these factors, biological treatment

is not likely to be significantly affected by predicted levels of engineered nanoparticles, including those with known antibacterial characteristics [51].

Membrane Filtration

During membrane filtration, applied pressure forces water to pass through the filter's pores while larger contaminants are retained. Ultrafiltration membranes, with pore sizes between 0.001 and 0.1 μm , are effective in the removal of nanoparticles.

Microfiltration membranes, with pore sizes greater than 0.1 μm , have also shown some capacity to remove nanoparticles from the water stream [43, 51]. As most particles are removed through size exclusion, the formation of aggregates will increase the efficacy of membrane treatment. Beyond physical straining, nanoparticles can be removed through electrostatic or hydrophobic interactions with the membrane [51]. Ladner et al. showed that nanoparticles modified with positively charged functional groups were removed through sorption to polymeric membranes (generally negatively charged) [54].

Negatively charged nanoparticles were less efficiently removed, likely due to the lack of electrostatic attraction between nanoparticles and the membrane surface. Metal and metal oxide nanoparticles have been successfully rejected from ultrafiltration membranes while fullerols have shown breakthrough [43].

Granular Media Filtration

As in membrane filtration, removal of nanoparticles through granular media filtration can be achieved through size exclusion or as a result of electrostatic interactions. Most nanoparticle removal occurs through the transportation of the nanoparticle to the surface of a filter grain and subsequent attachment [55]. Once at the surface of these grains, the interaction of van der Waals and electrostatic forces can result

in the trapping of these nanoparticles in a primary energy minimum [43]. Nanoparticle removal can also be achieved through pore straining, when the buildup of rejected contaminants on the granular media results in smaller pores for the nanoparticles to pass through. Li et al. conducted a study testing the efficacy of sand removal of coated and uncoated ZnO, CeO₂, TiO₂, and Ag nanoparticles, which showed that while uncoated nanoparticles experienced high removal, polymer coatings greatly diminished their retention [56].

Sorption

Due to the high surface area to volume ratio of nanoparticles, exposure to a sorbent is likely to result in efficient removal. Activated carbon, including granular activated carbon (GAC) and powdered activated carbon (PAC), is the most common sorbent used in water treatment. Other materials, including zeolites, synthetic polymer resins, and activated alumina have also been applied [43]. A variety of active carbon types have been shown to remove Ag nanoparticles from aqueous solution, with increasing efficacy correlated with increasing ionic strength and complete removal observed at NaCl concentrations of 30 mM [57].

Total Removal

A limited number of studies investigate the success of a full wastewater treatment train on the removal of engineered nanoparticles. In part, this is due to the difficulty of tracing the path of engineered nanoparticles through a wastewater treatment system [47, 51]. Distinguishing between dissolved, nanoparticle, and larger particle forms of a material can be difficult. Traditionally, a dissolved species is defined by its ability to pass through a 0.45 µm filter, but this definition includes nanomaterials [47]. In addition,

particle size distributions are difficult to accurately measure as larger particles block the smaller particles from being detected. Furthermore, the bulk form counterparts of nanomaterials may be present in water treatment chemicals, as is the case with SiO₂ and Al₂O₃.

Despite these challenges, several attempts at tracking engineered nanoparticle removal through continuous-flow wastewater treatment systems have been made [47]. Silver nanoparticles have been reported in wastewater effluent on the scale of ng/L [58, 59]. Chang et al. demonstrated poor removal (<10%) of silicate nanoparticles by biological treatment, followed by coagulation with polyaluminum chloride and sedimentation [60]. Most of the silicate nanoparticles above 450 nm settled out of the wastewater stream, but less than 10% of nanoparticles smaller than 450 nm were removed. Farre et al. monitored effluent from 22 municipal wastewater treatment plants in Spain and detected fullerenes in half of the samples collected with nine containing concentrations on the µg/L scale [61]. The fate of TiO₂ nanoparticles in wastewater treatment plants has received some attention, with several studies demonstrating greater than 90% removal [51]. Limbach et al. investigated the movement of CeO₂ nanoparticles and estimated that, while most sorbed to sludge, 6% of influent nanoparticles made it through treatment and were discharged into surface waters [62].

Biosolid Disposal

Biosolids generated during wastewater treatment are disposed of through land application, landfilling, or incineration. In the United States, the majority of biosolids (50-60%) are applied to farmland as fertilizer [45], which serves as the main source of engineered nanomaterials in soils [8]. The Targeted National Sewage Sludge Survey

reported the average concentrations of engineered nanoparticles in biosolids from 74 wastewater treatment plants. Ag, Zn/ZnO, Ti/TiO₂, and Cu/CuO nanoparticles were detected at average concentrations of 31.6, 994, 286, and 558 mg/kg, respectively [63]. Incineration is responsible for disposal of about 20% of the biosolids generated at wastewater treatment plants in the United States [8]. The ash resulting from incineration is then landfilled.

1.6 Environmental Fate

1.6.1 Water

Measuring the concentrations of engineered nanoparticles in environmental waters is made difficult by the low concentrations present and the challenges implicit in distinguishing engineered nanoparticles from other forms [64]. Neal et al. modeled engineered nanomaterial release and estimated Ag nanoparticles, ZnO nanoparticles, CeO₂ nanoparticles, and carbon nanotubes to be present in surface waters in concentrations on the scale of ng/L and TiO₂ nanoparticle concentrations up to µg/L [39]. When these nanoparticles enter surface waters, their fate is primarily governed by their tendency to aggregate. Nanoparticles may experience chemical transformation or form complexes with suspended solids, dissolved organic matter, or colloids. Nanoparticles or aggregates are then transported by means of advection, sedimentation, and Brownian motion. Most engineered nanomaterials are predicted to aggregate with organic matter and settle into the sediment, subject to periodic disturbances that result in remobilization [8, 15, 43].

The behavior of nanoparticles in surface waters is largely determined by their stability. Nanoparticles of the same type are often stabilized by electrostatic repulsion.

However, at a certain electrolyte concentration known as the critical coagulation concentration (CCC), charge screening or neutralization occurs, completely destabilizing the particle suspension. At the CCC, every particle collision results in attachment [43]. The levels of CaCl_2 in moderately hard waters are in the CCC range of many engineered nanomaterials, including carbon nanotubes, fullerenes, and TiO_2 , Fe_2O_3 , ZnO , CeO_2 , and Ag citrate nanoparticles [43]. Increasing electrolyte concentration also results in increased hetero-aggregation. Other relevant forces include steric hindrance and hydration forces [65].

As mentioned, the most common fate of nanoparticles released to surface waters is hetero-aggregation followed by sedimentation [66]. Studies have shown that TiO_2 , Fe_2O_3 nanoparticles, ZnO nanoparticles, CeO_2 nanoparticles, and carbon nanotubes all agglomerate in surface waters, forming aggregates on the scale of hundreds of nm to a few mm [66]. Ag nanoparticles stabilized with a citrate coating are the only nanoparticles reported to remain stable in natural waters [66]. Aggregation and sedimentation removes nanoparticles from the water column, limiting their bioavailability and interactions primarily to benthic organisms [15, 67].

The organic matter present in surface waters can coat nanoparticles, altering aggregation behaviors, solubility and toxicity [37]. Typically, dissolved organic carbon is present in surface waters at concentrations between 0.1 and 10 mg/L [68]. NOM refers to the many organic compounds found in surface waters resulting from plant and animal decay. Primarily humic acids, fulvic acids, carbohydrates, amino acids, and proteins, NOM contains functional groups including thiols, phenols, quinones, aldehydes, ketones,

carboxyls, and methoxyls [1]. This array of functional groups gives NOM the ability to complex with a wide variety of materials, including most engineered nanoparticles.

NOM can modify the surface properties of engineered nanomaterials through several pathways. In the environment, organic matter is generally negatively charged due to the presence of carboxylic and phenolic groups [1]. Therefore, aggregation between NOM and positively charged nanoparticles is likely. The carboxylic and phenolic groups that provide NOM's negative charge are also available for complexation with engineered nanomaterials [1]. For instance, these groups allow NOM to form an irreversible coating around metal oxide nanoparticles through ligand exchange [69]. More hydrophobic particles, including carbon nanomaterials and quantum dots, can also experience hydrophobic forces that result in agglomeration [68]. Other NOM-nanoparticle interactions include hydrogen bonding, π - π attraction, and cation bridging [68].

At concentrations typically observed in surface waters, NOM is expected to increase the stability of particles through a combination of electrostatic repulsion and steric hindrance [68]. While this stability is associated with increased bioavailability, DOM coatings have been shown to ameliorate the toxic effects of metal, metal oxide, and carbon nanomaterials [70]. While the mechanisms have not been clearly proven, DOM is theorized to decrease nanotoxicity by binding toxic metal ions, preventing direct contact with the nanoparticle, and reacting with ROS generated at the nanoparticle surface [55, 70].

Groundwater is not a likely environmental sink for engineered nanoparticles, as filtration through the soil offers a natural barrier to entry [43]. As discussed in the previous filtration section, nanoparticles are removed from the mobile water phase

through pore straining (size exclusion) or attachment to the soil (depth filtration), the latter being dominant for particles on the nanoscale [55]. Nanoparticles may be transported from landfill leachate, land application of biosolids, or nanopesticides to groundwater sources [43]. When groundwater pollution does occur, contaminants are often persistent. Given the low concentrations of organic matter and high concentrations of CaCl_2 and MgCl_2 often present in groundwaters, nanoparticles that enter these systems are predicted to experience aggregation [43].

1.6.2 Soil

Engineered nanomaterials can enter soil through the primary pathway of biosolid application or through nanomaterial spray or atmospheric deposition [8]. Once introduced into soil environments, nanoparticles may sorb to soil or mobilize and travel with pore water. Nanomaterials may experience aggregation, sorption, dissolution, and/or redox reactions. The behaviors of these nanomaterials are often specific and depend on the physical, biological, and chemical characteristics of the soil. In addition, nanoparticles may be taken up by soil organisms. Copper nanoparticles, for example, have been shown to be consumed by earthworms [51].

Homo-aggregation between nanoparticles and hetero-aggregation of nanoparticles with the soil matrix can result in immobilization [1]. Immobilization due to homo-aggregation is often a result of pore straining [1]. For example, CuO nanoparticles have been shown to homo-aggregate and become trapped in channels within the soil matrix [71].

The characteristics of the soil are also important determinants, with increasing surface heterogeneity and roughness promoting attachment [1]. Soil composition,

including the presence and amount of clay, extractable cations, and natural organic matter impacts nanoparticle deposition [1]. Soils are generally rich in organic matter and, as in aquatic systems, nanoparticle interactions with DOM can result in increased nanoparticle stability [1].

Engineered nanoparticles are likely to experience chemical transformations within the soil matrix, including dissolution and redox reactions. Gold, copper, and silver nanoparticles have all been shown to solubilize and complex with NOM and other chelating agents [72]. Metal oxide nanoparticle dissolution is generally precipitated by redox reactions. Other reactions, including sulfidation of silver nanoparticles and phosphatidation of zinc oxide nanoparticles, have also been reported [1].

1.6.3 Air

Only about 0.1-1.5% of engineered nanomaterial mass reaches the environment through air emissions [35]. Nanoparticles can be released into the atmosphere through combustion and through spray products including coatings and disinfectants [1, 8]. Diesel fuels containing CeO₂ additives for decreased particulate emissions release nano-CeO₂ into the air [73]. Nanomaterials released into the atmosphere are transported in air currents and may be transformed through a variety of processes, including aggregation, photooxidation, condensation, and chemical reactions via nucleation [1, 8]. Ultimately, nanoparticles released to the atmosphere will be deposited in soil and water.

1.7 Dissertation Objectives

As evident from the preceding discussion, the novel functionality of nanoparticles can be harnessed for a variety of engineering applications, but not without the potential for harmful effects on humans and/or ecological systems. Therefore, the design of

nanoparticles and their new uses should be accompanied by a careful consideration of their fate in the environment and associated ecosystem and health risks. This body of work adds to the necessary database for such considerations by exploring and elucidating the implications and applications of nanomaterial cytotoxicity in two engineered systems.

In Part I, abrasive metal oxide nanoparticles that are used in chemical mechanical planarization (CMP) were characterized to achieve the following objectives:

1. Determine the charge, primary particle size, and aggregation behaviors of nanoparticles in aqueous solutions, before and after exposure to the CMP process, to inform projections of their environmental fate.
2. Assess CMP nanoparticle interactions with model cell membranes to investigate whether changes following CMP exposure are likely to affect their cytotoxicity.

In Part II, low pressure water filtration membranes were modified with hydrophilic polydopamine and antibacterial silver nanoparticles to:

1. Investigate changes to initial bacterial adhesion through direct observation experiments.
2. Determine how modification affects membrane performance through longer term biofouling tests that simulate the conditions of a working treatment plant.

1.8 Dissertation Organization

This dissertation is organized into the following chapters:

Chapter 2 introduces Part I, concerning the environmental and human health impacts of CMP nanoparticles. This chapter provides a description of CMP, the role of silica, ceria, and alumina nanoparticles in this process, and the disposal pathways that

lead to their environmental release. Current literature reports of CMP nanoparticle toxicity are also reviewed.

Chapter 3 describes the characterization of the physicochemical properties and model cell membrane interactions of CMP nanoparticles. Size and electrophoretic mobilities of silica, ceria, and alumina nanoparticles were measured in aqueous solutions of neutral pH and varying NaCl concentrations. The aggregation behaviors of CMP nanoparticles in NaCl, NaNO₃, and CaCl₂ solutions were investigated. Attachment and disruption of model cell membranes under various aqueous solution conditions were studied. For all characterizations conducted, differences in nanoparticle behavior before and after exposure to the CMP process were assessed.

Chapter 4 continues to present the assessment of nanoparticles before and after use in CMP with a focus on their potential interactions with human cells. Under aqueous solution conditions that mimic physiological fluids (pH 7.4, 150 mM NaCl), CMP nanoparticle attachment and disruption of model cell membranes was investigated. Finally, these mechanistic studies were compared with cytotoxicity studies conducted by collaborators at North Carolina A&T State University.

Chapter 5, which serves as an introduction to Part II, concerns the use of silver nanoparticles in improving the performance of membrane filters. A review of low pressure membranes and membrane modification studies, including previous work addressing polydopamine modification, is presented. Literature describing the toxicity and environmental fate of silver nanoparticles is also reviewed.

Chapter 6 describes the investigation of the ability of polydopamine and silver nanoparticle membrane modification to decrease biofouling and, as a result, increase the

energy efficiency of membrane treatment. A direct observation system was used to determine the initial rate of attachment of *Pseudomonas aeruginosa* bacteria to the surface of unmodified membranes, membranes modified with hydrophilic polydopamine, and membranes modified with both polydopamine and antibacterial silver nanoparticles. The performance of these membranes was also assessed by measuring the rate of clean water production over 3 days of bacterial filtration in a constant pressure system. Finally, silver leaching from the modified membranes was evaluated.

Chapter 7 reviews the key findings introduced in experimental chapters 3, 4, and 6. Broader impacts and future directions of this research are discussed.

1.9 References

1. Goswami, L., et al., *Engineered nano particles: Nature, behavior, and effect on the environment*. Journal of Environmental Management, 2017. **196**: p. 297-315.
2. Janković, N.Z. and D.L. Plata, *Engineered nanomaterials in the context of global element cycles*. Environmental Science: Nano, 2019. **6**(9): p. 2697-2711.
3. Grillo, R., A.H. Rosa, and L.F. Fraceto, *Engineered nanoparticles and organic matter: A review of the state-of-the-art*. Chemosphere, 2015. **119**: p. 608-619.
4. Xu, L., et al., *ZnO-SnO₂ nanotubes surface engineered by Ag nanoparticles: Synthesis, characterization, and highly enhanced HCHO gas sensing properties*. Journal of Materials Chemistry C, 2013. **1**(11): p. 2174-2182.
5. Das, P., et al., *Novel synthesis of an iron oxalate capped iron oxide nanomaterial: A unique soil conditioner and slow release eco-friendly source of iron sustenance in plants*. RSC Advances, 2016. **6**(105): p. 103012-103025.
6. Sarmah, K. and S. Pratihar, *Synthesis, Characterization, and Photocatalytic Application of Iron Oxalate Capped Fe, Fe-Cu, Fe-Co, and Fe-Mn Oxide Nanomaterial*. ACS Sustainable Chemistry and Engineering, 2017. **5**(1): p. 310-324.
7. Vance, M.E., et al., *Nanotechnology in the real world: Redeveloping the nanomaterial consumer products inventory*. Beilstein Journal of Nanotechnology, 2015. **6**(1): p. 1769-1780.
8. Boyes, W.K., et al., *A comprehensive framework for evaluating the environmental health and safety implications of engineered nanomaterials*. Critical Reviews in Toxicology, 2017. **47**(9): p. 767-810.
9. Pietrojusti, A., L. Campagnolo, and B. Fadeel, *Interactions of engineered nanoparticles with organs protected by internal biological barriers*. Small, 2013. **9**(9-10): p. 1557-1572.
10. Lead, J.R., et al., *Nanomaterials in the environment: Behavior, fate, bioavailability, and effects—An updated review*. Environmental Toxicology and Chemistry, 2018. **37**(8): p. 2029-2063.
11. Lesniak, A., et al., *Nanoparticle adhesion to the cell membrane and its effect on nanoparticle uptake efficiency*. Journal of the American Chemical Society, 2013. **135**(4): p. 1438-1444.
12. Chen, K.L. and G.D. Bothun, *Nanoparticles meet cell membranes: Probing nonspecific interactions using model membranes*. Environmental Science and Technology, 2014. **48**(2): p. 873-880.
13. Karimi, S., et al., *Acute and chronic toxicity of metal oxide nanoparticles in chemical mechanical planarization slurries with *Daphnia magna**. Environmental Science: Nano, 2018. **5**(7): p. 1670-1684.
14. Handy, R.D., et al., *Manufactured nanoparticles: Their uptake and effects on fish - A mechanistic analysis*. Ecotoxicology, 2008. **17**(5): p. 396-409.
15. De Marchi, L., et al., *Engineered nanomaterials: From their properties and applications, to their toxicity towards marine bivalves in a changing environment*. Environmental Research, 2019. **178**.
16. Marisa, I., et al., *Invitro exposure of haemocytes of the clam *Ruditapes philippinarum* to titanium dioxide (TiO₂) nanoparticles: Nanoparticle*

- characterisation, effects on phagocytic activity and internalisation of nanoparticles into haemocytes*. Marine Environmental Research, 2015. **103**: p. 11-17.
17. Gomes, T., et al., *Accumulation and toxicity of copper oxide nanoparticles in the digestive gland of Mytilus galloprovincialis*. Aquatic Toxicology, 2012. **118-119**: p. 72-79.
 18. Dietz, K.J. and S. Herth, *Plant nanotoxicology*. Trends in Plant Science, 2011. **16**(11): p. 582-589.
 19. Holbrook, R.D., et al., *Trophic transfer of nanoparticles in a simplified invertebrate food web*. Nature Nanotechnology, 2008. **3**(6): p. 352-355.
 20. Werlin, R., et al., *Biomagnification of cadmium selenide quantum dots in a simple experimental microbial food chain*. Nature Nanotechnology, 2011. **6**(1): p. 65-71.
 21. Judy, J.D., J.M. Unrine, and P.M. Bertsch, *Evidence for biomagnification of gold nanoparticles within a terrestrial food chain*. Environmental Science and Technology, 2011. **45**(2): p. 776-781.
 22. Majumdar, S., et al., *Cerium Biomagnification in a Terrestrial Food Chain: Influence of Particle Size and Growth Stage*. Environmental Science and Technology, 2016. **50**(13): p. 6782-6792.
 23. Ferry, J.L., et al., *Transfer of gold nanoparticles from the water column to the estuarine food web*. Nature Nanotechnology, 2009. **4**(7): p. 441-444.
 24. *FDA's Approach to Regulation of Nanotechnology Products*. FDA, 2019.
 25. *Center for Drug Evaluation and Research Nanotechnology Programs*. FDA, 2018.
 26. *OSHA Fact Sheet: Working Safely with Nanomaterials*, O.S.H. Administration, Editor. 2013.
 27. *Nanotechnology Task Force Report 2007*. FDA, 2020.
 28. *2013 Nanotechnology Regulatory Science Research Plan*. FDA, 2019.
 29. *Considering Whether an FDA-Regulated Product Involves the Application of Nanotechnology*. U.S. Food and Drug Administration, 2019.
 30. Vogel, S.A. and J.A. Roberts, *Why the toxic substances control act needs an overhaul, and how to strengthen oversight of chemicals in the interim*. Health Affairs, 2011. **30**(5): p. 898-905.
 31. *Chemical Substances When Manufactured or Processed as Nanoscale Materials; TSCA Reporting and Recordkeeping Requirements*. Federal Register, 2017.
 32. *OSH Act of 1970 | Occupational Safety and Health Administration*.
 33. *Current intelligence bulletin 63: occupational exposure to titanium dioxide*. 2017.
 34. *Regulations on Nanomaterials in EU and Nano Register 2016*.
 35. Keller, A.A., et al., *Global life cycle releases of engineered nanomaterials*. Journal of Nanoparticle Research, 2013. **15**(6).
 36. Bolyard, S.C., D.R. Reinhart, and S. Santra, *Behavior of engineered nanoparticles in landfill leachate*. Environmental Science and Technology, 2013. **47**(15): p. 8114-8122.
 37. Reinhart, D.R., et al., *Emerging contaminants: Nanomaterial fate in landfills*. Waste Management, 2010. **30**(11): p. 2020-2021.

38. Blaser, S.A., et al., *Estimation of cumulative aquatic exposure and risk due to silver: Contribution of nano-functionalized plastics and textiles*. Science of the Total Environment, 2008. **390**(2-3): p. 396-409.
39. Gottschalk, F., T. Sun, and B. Nowack, *Environmental concentrations of engineered nanomaterials: Review of modeling and analytical studies*. Environmental Pollution, 2013. **181**: p. 287-300.
40. Sun, T.Y., et al., *Comprehensive probabilistic modelling of environmental emissions of engineered nanomaterials*. Environmental Pollution, 2014. **185**: p. 69-76.
41. Zhu, M., et al., *The effect of humic acid on the aggregation of titanium dioxide nanoparticles under different pH and ionic strengths*. Science of the Total Environment, 2014. **487**(1): p. 375-380.
42. De Castro, J.A., et al., *Modeling the transport phenomena of TiO₂ nanoparticles into leachate of municipal waste landfills*, in *Materials Science Forum*. 2012. p. 1695-1700.
43. Troester, M., H.J. Brauch, and T. Hofmann, *Vulnerability of drinking water supplies to engineered nanoparticles*. Water Research, 2016. **96**: p. 255-279.
44. Theron, J., J.A. Walker, and T.E. Cloete, *Nanotechnology and water treatment: Applications and emerging opportunities*. Critical Reviews in Microbiology, 2008. **34**(1): p. 43-69.
45. Gottschalk, F., et al., *Modeled environmental concentrations of engineered nanomaterials (TiO₂, ZnO, Ag, CNT, fullerenes) for different regions*. Environmental Science and Technology, 2009. **43**(24): p. 9216-9222.
46. Otero-González, L., et al., *Stability of alumina, ceria, and silica nanoparticles in municipal wastewater*. Water Science and Technology, 2014. **70**(9): p. 1533-1539.
47. Speed, D.E., *Environmental aspects of planarization processes*, in *Advances in Chemical Mechanical Planarization (CMP)*. 2016. p. 1-269.
48. Popowich, A., Q. Zhang, and X.C. Le, *Removal of nanoparticles by coagulation*. Journal of Environmental Sciences (China), 2015. **38**: p. 168-171.
49. Kinsinger, N., et al., *Titanium dioxide nanoparticle removal in primary prefiltration stages of water treatment: Role of coating, natural organic matter, source water, and solution chemistry*. Environmental Engineering Science, 2015. **32**(4): p. 292-300.
50. O'Brien, N. and E. Cummins, *Ranking initial environmental and human health risk resulting from environmentally relevant nanomaterials*. Journal of Environmental Science and Health - Part A Toxic/Hazardous Substances and Environmental Engineering, 2010. **45**(8): p. 992-1007.
51. Westerhoff, P.K., A. Kiser, and K. Hristovski, *Nanomaterial removal and transformation during biological wastewater treatment*. Environmental Engineering Science, 2013. **30**(3): p. 109-117.
52. Zhang, C., et al., *Governing factors affecting the impacts of silver nanoparticles on wastewater treatment*. Science of the Total Environment, 2016. **572**: p. 852-873.
53. Sheng, Z. and Y. Liu, *Effects of silver nanoparticles on wastewater biofilms*. Water Research, 2011. **45**(18): p. 6039-6050.

54. Ladner, D.A., et al., *Functionalized nanoparticle interactions with polymeric membranes*. Journal of Hazardous Materials, 2012. **211-212**: p. 288-295.
55. Crittenden, J.C., et al., *MWH's Water Treatment: Principles and Design: Third Edition*. MWH's Water Treatment: Principles and Design: Third Edition. 2012.
56. Li, Z., et al., *Transport of nanoparticles with dispersant through biofilm coated drinking water sand filters*. Water Research, 2013. **47**(17): p. 6457-6466.
57. Gicheva, G. and G. Yordanov, *Removal of citrate-coated silver nanoparticles from aqueous dispersions by using activated carbon*. Colloids and Surfaces A: Physicochemical and Engineering Aspects, 2013. **431**: p. 51-59.
58. Mitrano, D.M., et al., *Detecting nanoparticulate silver using single-particle inductively coupled plasma-mass spectrometry*. Environmental Toxicology and Chemistry, 2012. **31**(1): p. 115-121.
59. Hoque, M.E., et al., *Detection and characterization of silver nanoparticles in aqueous matrices using asymmetric-flow field flow fractionation with inductively coupled plasma mass spectrometry*. Journal of Chromatography A, 2012. **1233**: p. 109-115.
60. Chang, M.R., D.J. Lee, and J.Y. Lai, *Nanoparticles in wastewater from a science-based industrial park-Coagulation using polyaluminum chloride*. Journal of Environmental Management, 2007. **85**(4): p. 1009-1014.
61. Farré, M., et al., *First determination of C60 and C70 fullerenes and N-methylfulleropyrrolidine C60 on the suspended material of wastewater effluents by liquid chromatography hybrid quadrupole linear ion trap tandem mass spectrometry*. Journal of Hydrology, 2010. **383**(1-2): p. 44-51.
62. Limbach, L.K., et al., *Removal of oxide nanoparticles in a model wastewater treatment plant: Influence of agglomeration and surfactants on clearing efficiency*. Environmental Science and Technology, 2008. **42**(15): p. 5828-5833.
63. *Targeted National Sewage Sludge Survey Sampling and Analysis Technical Report*. 2009, U.S. Environmental Protection Agency.
64. von der Kammer, F., et al., *Analysis of engineered nanomaterials in complex matrices (environment and biota): General considerations and conceptual case studies*. Environmental Toxicology and Chemistry, 2012. **31**(1): p. 32-49.
65. Dwivedi, A.D., et al., *Fate of engineered nanoparticles: Implications in the environment*. Coordination Chemistry Reviews, 2015. **287**: p. 64-78.
66. Quik, J.T.K., et al., *Heteroaggregation and sedimentation rates for nanomaterials in natural waters*. Water Research, 2014. **48**(1): p. 269-279.
67. Di Toro, D.M., et al., *Technical basis for establishing sediment quality criteria for nonionic organic chemicals using equilibrium partitioning*. Environmental Toxicology and Chemistry, 1991. **10**(12): p. 1541-1583.
68. Yu, S., et al., *Interactions between engineered nanoparticles and dissolved organic matter: A review on mechanisms and environmental effects*. Journal of Environmental Sciences (China), 2018. **63**: p. 198-217.
69. Yang, K., D. Lin, and B. Xing, *Interactions of humic acid with nanosized inorganic oxides*. Langmuir, 2009. **25**(6): p. 3571-3576.
70. Glisovic, S., et al., *Emerging technologies and safety concerns: a condensed review of environmental life cycle risks in the nano-world*. International Journal of Environmental Science and Technology, 2017. **14**(10): p. 2301-2320.

71. Jeong, S.W. and S.D. Kim, *Aggregation and transport of copper oxide nanoparticles in porous media*. Journal of Environmental Monitoring, 2009. **11**(9): p. 1595-1600.
72. Unrine, J.M., et al., *Evidence for bioavailability of Au nanoparticles from soil and biodistribution within earthworms (Eisenia fetida)*. Environmental Science and Technology, 2010. **44**(21): p. 8308-8313.
73. Cassee, F.R., et al., *Exposure, health and ecological effects review of engineered nanoscale cerium and cerium oxide associated with its use as a fuel additive*. Critical Reviews in Toxicology, 2011. **41**(3): p. 213-229.

Chapter 2. Introduction to Chemical Mechanical Planarization Nanoparticles

2.1 CMP Process

Chemical mechanical planarization (CMP) is a semiconductor fabrication process used to polish the wafer base of integrated circuits, the small chips used in common electronics. First applied in 1965 by Monsanto for glasses manufacturing [1], CMP is now used to decrease the surface roughness of copper, tungsten, and silica wafers to less than 10 Å across 300 mm [2]. The resulting planarized surfaces are required for the proper placement of hundreds of millions of transistors that make up integrated circuit devices. While crucial to the \$325.4 billion semiconductor industry, CMP is in itself an industry valued at over \$1.5 billion annually [3].

During CMP, a wafer carrier is pushed against a polyurethane polishing pad by an applied downward force. As both the pad and the wafer carrier spin, the pad brings the wafer into direct contact with the CMP slurry [4]. The slurry contains a range of additives depending on the specific application, but generally contains water, abrasive nanoparticles, acids or bases for pH control, anti-coagulants, corrosion inhibitors, surfactants, polymers, oxidizers, buffers, chelating or complexing agents, and bactericides and fungicides [4-6]. This slurry smooths the wafer surface through a combination of chemical etching and mechanical abrasion. Chemicals are added to soften certain surfaces and form a protective layer around others. Chelating agents and surfactants are added to stabilize nanoparticles, preventing aggregation and the resulting surface defects and scratches [5, 7]. Silica, ceria, and alumina nanoparticles, generally in

the size range of 2-200 nm, are the main source of mechanical polishing [5, 6]. For a 200 nm particle, the force applied for wafer contact is estimated to be between 100-1000 nN [7].

The specific mechanism of CMP polishing involves several steps. First, a passive oxide film is formed on the surface of the wafer, through interactions with either water or CMP slurry oxidizers. Common oxidizers include hydrogen peroxide, potassium ferricyanide, ferric chloride, and potassium iodate [5, 7]. This oxide film decreases the surface energy of the wafer, preventing further reactions [2]. The oxide layer is then removed by contact with the abrasive nanoparticles, allowing dissolution of the underlying wafer material [2, 5, 8]. Oxidation quickly re-passivizes the wafer and the cycle repeats. This process results in a removal rate more than two orders of magnitude greater than that achieved through mechanical polishing alone [5]. Overall, interaction with the CMP slurry should result in high removal rates (2000-8000 Å/minute), planarity, surface quality, and layer selectivity [5].

2.2 Airborne Exposure

Although no NIOSH recommendations exist for ceria, alumina, or silica nanoparticles, OSHA has established general 8-hour time-weighted average legal airborne permissible exposure limits for alumina and silica at 5 mg/m³ and 0.8 mg/m³ respectively. Studies done at CMP facilities found very low concentrations of airborne particulate matter. In fact, with the exception of one silica reading of 0.478 mg/m³, all other mass readings were below the detection limit [9, 10]. Furthermore, the particles that were detected were largely aggregates, with none falling below the 100 nm threshold.

The studies concluded that the workers at these CMP facilities experience low exposure to nanoparticles through inhalation.

2.3 Wastewater

The wastewater from the semiconductor industry is regulated under the category of Electrical and Electronics Components (E&EC) effluent of the National Pollutant Discharge and Elimination System (NPDES). Through these regulations, water quality parameters including concentrations of total toxic organics, copper, chromium, and lead are enforced. However, the metal oxides used as abrasive nanoparticles in CMP are not included in discharge regulation. In 2018, the EPA began conducting a detailed study of E&EC effluent in order to update the regulations and properly account for changes to the volume and composition of waste streams, the method of discharge, and the treatment technology [11]. The results of that study have not been released.

Semiconductor fabrication facilities generate large quantities of wastewater, typically over 400 million gallons a year [12], 30-40% of which is attributed to CMP producing 10 or more liters per wafer polished [6]. CMP wastewater has been found to have fairly high concentrations of metal oxide nanoparticles, with upper estimates of silica, alumina and ceria nanoparticles on the order of 1000 mg/L, 100 mg/L, and 1 mg/L [6]. Silica nanoparticle concentrations between 1300 and 8500 mg/L have been detected in the CMP wastewater from fabrication plants in China and Taiwan [13].

CMP wastewater treatment is specific to the individual fabrication facility. Some fabs have on-site treatment, in which CMP wastewater is diluted and mixed with wastewater from other processes and subjected to physical, chemical, and/or biological treatment before discharge into surface waters [6, 14]. Other fabs pretreat their effluent

before discharging to municipal wastewater treatment plants that typically subject waste streams to screening, grit removal, biological treatment, and disinfection [6, 14, 15].

Tracing CMP nanoparticles through wastewater treatment systems is challenging due to the difficulties of discerning the source of the metal oxides and distinguishing nanoparticles from other forms. Ceria nanoparticles are the easiest to track because of their low solubility and limited use in semiconductor manufacturing [6]. Limbach et al. were able to demonstrate their movement through a wastewater treatment system and estimated 6% of influent CeO₂ nanoparticles reach surface waters [16].

In CMP wastewater treatment, lime is a commonly added coagulant to facilitate copper removal. This addition of Ca²⁺ ions also destabilizes negatively charged metallic oxide nanoparticles, allowing them to aggregate and settle [6]. Coagulation followed by flotation can be an effective treatment method, with one bench-scale study showing removal of 92% of total solids using CTAB and alum as coagulants [17]. Several studies showed the addition of alum resulted in more than 95% removal of silica nanoparticles [6]. The presence of other wastewater constituents can facilitate aggregation; both alumina and ceria nanoparticles have been shown to form large aggregates in wastewater, while silica nanoparticles demonstrate exceptional stability [18]. Additives in CMP wastewaters stabilize these nanoparticles, but dilution may decrease their efficacy [18].

High removal (>90%) of alumina and ceria nanoparticles can be achieved through biological treatment [6]. Silica nanoparticle outcomes show more variance, but sorption to biomass is theorized to be the largest sink [6]. Investigation of ceria nanoparticles used in CMP showed 94% removal in a continually mixed activated sludge system [16]. With regard to the impact of nanoparticle exposure on the microorganisms used in biological

treatment, CMP nanoparticle concentrations of 50 mg/L have shown significant (22-50%) inhibition of denitrifying and ammonia oxidizing bacteria [6].

2.4 Environmental Fate

Through the wastewater treatment process, SiO₂, CeO₂, and Al₂O₃ nanoparticles will be sequestered in biosolids or released to surface waters. While slurries that move through wastewater treatment systems are typically diluted to concentrations orders of magnitude below 1 g/L, a small portion of CMP nanoparticles will be transported with treated effluent into the environment [3, 6, 15]. The fraction of nanoparticles in the generated biosolids will range from less than 1 wt % to over 75 wt % [19]. This sludge is then applied to agricultural land (ca. 60%), incinerated and landfilled (ca. 20%), or landfilled directly (ca. 20%) [19]. Walser et al. investigated CeO₂ nanoparticle interactions through the incineration process and found that these nanoparticles were not emitted into the air, but remained in the ash that was ultimately landfilled [20].

The environmental fate of CMP nanoparticles following disposal will depend on their physicochemical characteristics. The pK_a values of silica, alumina, and ceria are about 2, 9, and 6-8, respectively. This means that in environmental waters, silica nanoparticles will be negatively charged, alumina nanoparticles will be positively charged, and ceria nanoparticles will be near neutral. Under environmental pH conditions, metal oxide nanoparticles are not likely to experience significant dissolution [21], but they have been shown to form complexes with dissolved organic matter (DOM). This occurs when the protonated hydroxyl groups on the nanoparticle surface interact with the carboxyl or phenolic groups of NOM resulting in a ligand exchange and the formation of an inner-sphere complex [22]. Ceria and alumina nanoparticles are prone to

aggregation and are likely to settle into sediment, while silica nanoparticles are predicted to resist agglomeration [6]. Because environmental studies of CMP nanoparticles have been limited, their ultimate fate remains unclear.

2.5 Toxicity

Developing nanoparticle toxicity profiles is difficult due to conflicting reports from studies with a variety of test subjects, doses, durations, and end points [19]. The dependency of toxicity on small changes in nanoparticle size, shape, and surface characteristics creates an additional barrier to accurately assessing potential health risks. While silica, alumina, and ceria nanoparticles are generally not considered hazardous [19], they have shown toxic effects in a variety of in vitro and in vivo studies [27]. These toxic effects are commonly communicated in terms of the IC₅₀, EC₅₀, or LC₅₀, or the concentration at which 50% of cells or organisms are inhibited, affected, or killed.

2.5.1 Pristine Nanoparticles

Fumed silica (f-SiO₂), the silica nanoparticle form assessed in this work, is associated with greater cytotoxicity than its colloidal counterpart. This may be due to the aggregated, chain-like nature of f-SiO₂ providing greater surface area and hydroxyl radical generation [23]. Drawing conclusions about the toxicity of f-SiO₂ nanoparticles based on the literature is challenging [24]. Ha et al. found over 75% of the populations of RAW 264.7 cells, NCIH411 cells, HUVECs cells, HepG2 cells, HEK293 cells, BMSC cells, and A549 cells remained viable after three days of exposure to the highest concentration tested (1 g/L) [25]. Casado et al. also did not reach 50% inhibition after exposing RTG-2 cells to 96 hours of contact with 1 g/L f-SiO₂ nanoparticles [26]. While Yu et al. did not find exposure to 500 µg/L f-SiO₂ nanoparticles to have a significant

effect on A549 cells after 24 hours, the same concentration decreased viability of RAW 264.7 cells by over 50% [27]. Exposure to silica nanoparticles on the order of hundreds of mg/L over 1-2 days has been shown to result in the death of 50% of water flea (*Daphnia magna*) populations [19]. The majority of ecotoxicity studies involving silica nanoparticles and the microalgae *Pseudokirchneriella subcapitata* have found EC/LC₅₀ concentrations in the range of 50-100 mg/L [19]. Overall, exposure to silica nanoparticles is correlated with inflammation, toxicity, hemolysis, and the generation of ROS, with exposure to smaller nanoparticles resulting in greater cytotoxicity [24].

The results of ceria nanotoxicity testing are also varied. De Marzi et al. and Lanone et al. reported 24-hr IC₅₀ concentrations greater than 1 g/L for ceria nanoparticle exposure to THP-1 cells [28], A549 cells [28, 29], CaCo2 cells [29], and HepG2 cells [29]. De Marzi et al. further investigated the effects of 10 days of exposure and found ceria nanoparticle concentrations of 0.5 mg/L, 2 mg/L, and 0.5 mg/L decreased the viability of A549 cells, CaCo2 cells, and HepG2 cells by more than 50% [29]. Park et al. and Lin et al. determined IC₅₀ values following 72 hours of exposure to be ca. 20 mg/L for BEAS-2B cells [30] and A549 cells [31]. No morphological or toxic effects were observed in J774A.1 murine macrophages following 24-hr exposure to 10 μM ceria nanoparticle solution [32]. Exposure to ceria nanoparticles on the order of tens of mg/L has resulted in toxic effects in crustacean species *Daphnia magna* and *Daphnia pulex* over durations ranging from 2 – 23 days [19]. Ceria ecotoxicity has also been tested using the microalgae *P. subcapitata* and found the highest concentration (100 mg/L) did not have significant toxic effects over 4.5 hours [33]. Ceria nanoparticles have been reported to both cause oxidative stress and to exhibit antioxidant properties [24].

In vitro studies with alumina nanoparticles have reported limited exposure damage, with effective concentrations on the scale of hundreds of mg/L. Radziun et al. found exposure to 400 mg/L alumina nanoparticles had a significant effect on BJ and L929 cells, but cell viability remained above 90% [34]. Wagner et al. determined the 24-hr LC₅₀ concentrations for NR8383 cells to be 250 mg/L [35]. Sun et al. did not observe any toxic effect in HCMECs cells following exposure to 100 mg/L alumina nanoparticles over 24 hours [36]. Braydich-Stolle et al. found that although Al₂O₃ nanoparticles were not very toxic by themselves, they decreased the ability of U937 cells to fight the pathogen *Staphylococcus aureus* [37].

In vivo studies of alumina nanoparticles have been conducted in both aquatic and terrestrial organisms. In algae, concentrations ranging from tens to hundreds of mg/L were found to cause significant toxic effects in algae species including *Chlorella sp.*, *Scenedesmus sp.*, and *P. subcapitata* with exposures lasting between 4.5 hours and 6 days [19]. In crustaceans (*Daphnia magna* and *Ceriodaphnia dubia*), the concentration at which 50% of the organisms died following 1-3 days of exposure fell into the range of 50-175 mg/L [19]. Prabhakar et al. found dose-dependent oxidative stress reactions in rats exposed to alumina nanoparticle oral treatment [38]. At the highest concentration of 2000 mg/kg, this oxidative stress resulted in the development of liver lesions.

2.5.2 CMP Nanoparticles

Despite some knowledge of pristine alumina, ceria, and silica nanoparticle toxicity, these results are not necessarily applicable to CMP nanoparticles. Flaherty et al. made a direct comparison between pristine metal oxide nanoparticles and those dispersed in CMP slurries [39]. While exposure to 1 g/L ceria and alumina nanoparticles (in all

solutions) over 24 hours did not result in decreased mouse alveolar macrophage viability, the impact of silica nanoparticle exposure depended on the solution tested. Twenty-four hours of exposure to 1 g/L silica nanoparticles in aqueous solution reduced cell viability to 40%, while exposure to the same silica nanoparticle concentration in three different CMP slurries reduced viability to 18%, 35%, and 77%.

Due to the specificity of toxicity testing, CMP nanoparticles must be investigated under diluted slurry conditions, which few studies have considered. Kosaraju et al. reported the 48-hr toxicity of ceria nanoparticles in CMP slurries, both before and after use in the CMP process [40]. They observed toxic effects to A549 epithelial cells at a concentration of 6.67 g/L for both pre and post-CMP ceria nanoparticles, with post-CMP exposure resulting in slightly greater toxicity. Speed et al. conducted in vitro studies with A549 epithelial cells to determine the EC₅₀ values of silica, ceria, and alumina nanoparticles on cell proliferation, viability, and membrane integrity [19]. In these studies, pristine nanoparticles were dispersed in simplified CMP slurries, but not exposed to the polishing process. A549 cells in contact with f-SiO₂ nanoparticles were associated with average EC₅₀ values for proliferation, viability, and integrity of 3.6 mg/mL, 1.5 mg/mL, and 3.1 mg/mL, respectively. At the highest concentration of ceria nanoparticle exposure (2 mg/mL), less than 10% of cell proliferation was inhibited. No other effects following ceria or alumina exposure were observed.

In vivo toxicity effects of CMP nanoparticles have rarely been studied, but those studies undertaken have shown mixed results. Fumed silica, ceria, and alumina nanoparticles in a simplified CMP slurry found low or no inhibition of *Aliivibrio fischeri* (marine bacterium) bioluminescence at concentrations of ca. 1 mg/mL [19]. Alumina

nanoparticle exposure resulted in the largest impact (28.4% inhibition), followed by ceria (4.3% inhibition) and silica (0% inhibition). Karimi et al. investigated acute and chronic effects of CMP nanoparticle exposure on *D. magna*, finding that half of the *D. magna* population died after 96 hours of exposure to 1.1 mg/L alumina nanoparticles [15]. Ceria and alumina nanoparticle exposure both resulted in significant declines in the body size in the acute studies and decreased the rate of reproduction in the chronic studies. Ceria and alumina nanoparticles also accumulated in *D. magna* digestive tracts, potentially limiting movement and hindering nutrient access. In another study, waste ceria CMP nanoparticles were exposed to zebrafish embryos to determine potential developmental impacts, but no significant results were observed after 5 days of exposure [41]. General conclusions regarding CMP nanotoxicity are difficult to form as outcomes depend on the exposure concentration, duration, endpoints tested, and specific nanoparticle characteristics that can be changed through the CMP process.

2.6 Summary

The use of abrasive metal oxide nanoparticles is necessary to the production of modern integrated circuit devices. Following their use in CMP, silica, ceria, and alumina nanoparticles enter the environment through the wastewater treatment system. Since small physicochemical changes can significantly impact nanotoxicity, characterizing variations that arise from exposure to the CMP process is a critical step in assessing the risks posed by nanoparticle release. This work will investigate the size, charge, and aggregation of CMP nanoparticles with the goal of informing predictions of their environmental fate. Furthermore, the attachment of CMP nanoparticles to model cell membranes and subsequent damage will be studied. By characterizing CMP

nanoparticles under conditions reminiscent of surface waters and physiological fluids, we aim to help elucidate likely interactions in both environmental and human health contexts.

2.7 References

1. Chen, H., et al., *Mechanical model of nanoparticles for material removal in chemical mechanical polishing process*. Friction, 2016. **4**(2): p. 153-164.
2. Ng, D., et al., *Oxidation and removal mechanisms during chemical-mechanical planarization*. Wear, 2007. **263**(7-12 SPEC. ISS.): p. 1477-1483.
3. Roth, G.A., N.M. Neu-Baker, and S.A. Brenner, *SEM analysis of particle size during conventional treatment of CMP process wastewater*. Science of the Total Environment, 2015. **508**: p. 1-6.
4. Brahma, N. and J.B. Talbot, *Effects of CMP slurry additives on the agglomeration of alumina nanoparticles I: General aggregation rate behavior*. Journal of Colloid and Interface Science, 2014. **419**: p. 56-60.
5. Singh, R.K., et al., *Fundamentals of slurry design for CMP of metal and dielectric materials*. MRS Bulletin, 2002. **27**(10): p. 752-760+748.
6. Speed, D.E., *Environmental aspects of planarization processes*, in *Advances in Chemical Mechanical Planarization (CMP)*. 2016. p. 1-269.
7. Ilie, F. and G. Ipate, *Chemical-mechanical impact of nanoparticles and pH effect of the slurry on the CMP of the selective layer surfaces*. Lubricants, 2017. **5**(2).
8. Kaufman, F.B., et al., *Chemical-Mechanical Polishing for Fabricating Patterned W Metal Features as Chip Interconnects*. Journal of the Electrochemical Society, 1991. **138**(11): p. 3460-3465.
9. Brenner, S.A., et al., *NIOSH field studies team assessment: Worker exposure to aerosolized metal oxide nanoparticles in a semiconductor fabrication facility*. Journal of Occupational and Environmental Hygiene, 2016. **13**(11): p. 871-880.
10. Brenner, S.A., et al., *Occupational exposure to airborne nanomaterials: An assessment of worker exposure to aerosolized metal oxide nanoparticles in a semiconductor fab and subfab*. Journal of Occupational and Environmental Hygiene, 2016. **13**(9): p. D138-D147.
11. *Electrical and Electronic Components Effluent Guidelines*. US EPA, 2016.
12. Chun, J.-H., *Searching for a Sustainable Manufacturing Process: Rapid Pad Conditioning in ULSI Fabrication* 2010.
13. Liu, Y., et al., *Nanoparticles in wastewaters: Hazards, fate and remediation*. Powder Technology, 2014. **255**: p. 149-156.
14. Karimi, S., et al., *Acute and chronic toxicity to Daphnia magna of colloidal silica nanoparticles in a chemical mechanical planarization slurry after polishing a gallium arsenide wafer*. NanoImpact, 2019. **13**: p. 56-65.
15. Karimi, S., et al., *Acute and chronic toxicity of metal oxide nanoparticles in chemical mechanical planarization slurries with Daphnia magna*. Environmental Science: Nano, 2018. **5**(7): p. 1670-1684.
16. Limbach, L.K., et al., *Removal of oxide nanoparticles in a model wastewater treatment plant: Influence of agglomeration and surfactants on clearing efficiency*. Environmental Science and Technology, 2008. **42**(15): p. 5828-5833.
17. Liu, J.C. and C.Y. Lien, *Dissolved air flotation of polishing wastewater from semiconductor manufacturer*, in *Water Science and Technology*. 2006. p. 133-140.

18. Otero-González, L., et al., *Stability of alumina, ceria, and silica nanoparticles in municipal wastewater*. *Water Science and Technology*, 2014. **70**(9): p. 1533-1539.
19. Speed, D., et al., *Physical, chemical, and in vitro toxicological characterization of nanoparticles in chemical mechanical planarization suspensions used in the semiconductor industry: Towards environmental health and safety assessments*. *Environmental Science: Nano*, 2015. **2**(3): p. 227-244.
20. Walser, T., et al., *Persistence of engineered nanoparticles in a municipal solid-waste incineration plant*. *Nature Nanotechnology*, 2012. **7**(8): p. 520-524.
21. Troester, M., H.J. Brauch, and T. Hofmann, *Vulnerability of drinking water supplies to engineered nanoparticles*. *Water Research*, 2016. **96**: p. 255-279.
22. Yu, S., et al., *Interactions between engineered nanoparticles and dissolved organic matter: A review on mechanisms and environmental effects*. *Journal of Environmental Sciences (China)*, 2018. **63**: p. 198-217.
23. Zhang, H., et al., *Processing pathway dependence of amorphous silica nanoparticle toxicity: Colloidal vs pyrolytic*. *Journal of the American Chemical Society*, 2012. **134**(38): p. 15790-15804.
24. Karlsson, H.L., M.S. Toprak, and B. Fadeel, *Toxicity of Metal and Metal Oxide Nanoparticles*, in *Handbook on the Toxicology of Metals: Fourth Edition*. 2015. p. 75-112.
25. Ha, S.W., et al., *Bio-active engineered 50nm silica nanoparticles with bone anabolic activity: Therapeutic index, effective concentration, and cytotoxicity profile in vitro*. *Toxicology in Vitro*, 2014. **28**(3): p. 354-364.
26. Casado, M.P., A. Macken, and H.J. Byrne, *Ecotoxicological assessment of silica and polystyrene nanoparticles assessed by a multitrophic test battery*. *Environment International*, 2013. **51**: p. 97-105.
27. Yu, T., A. Malugin, and H. Ghandehari, *Impact of silica nanoparticle design on cellular toxicity and hemolytic activity*. *ACS Nano*, 2011. **5**(7): p. 5717-5728.
28. Lanone, S., et al., *Comparative toxicity of 24 manufactured nanoparticles in human alveolar epithelial and macrophage cell lines*. *Particle and Fibre Toxicology*, 2009. **6**.
29. De Marzi, L., et al., *Cytotoxicity and genotoxicity of ceria nanoparticles on different cell lines in vitro*. *International Journal of Molecular Sciences*, 2013. **14**(2): p. 3065-3077.
30. Park, E.J., et al., *Oxidative stress induced by cerium oxide nanoparticles in cultured BEAS-2B cells*. *Toxicology*, 2008. **245**(1-2): p. 90-100.
31. Lin, W., et al., *Toxicity of cerium oxide nanoparticles in human lung cancer cells*. *International Journal of Toxicology*, 2006. **25**(6): p. 451-457.
32. Hirst, S.M., et al., *Anti-inflammatory properties of cerium oxide nanoparticles*. *Small*, 2009. **5**(24): p. 2848-2856.
33. Velzeboer, I., et al., *Aquatic ecotoxicity tests of some nanomaterials*. *Environmental Toxicology and Chemistry*, 2008. **27**(9): p. 1942-1947.
34. Radziun, E., et al., *Assessment of the cytotoxicity of aluminium oxide nanoparticles on selected mammalian cells*. *Toxicology in Vitro*, 2011. **25**(8): p. 1694-1700.

35. Wagner, A.J., et al., *Cellular interaction of different forms of aluminum nanoparticles in rat alveolar macrophages*. Journal of Physical Chemistry B, 2007. **111**(25): p. 7353-7359.
36. Sun, J., et al., *Cytotoxicity, permeability, and inflammation of metal oxide nanoparticles in human cardiac microvascular endothelial cells: Cytotoxicity, permeability, and inflammation of metal oxide nanoparticles*. Cell Biology and Toxicology, 2011. **27**(5): p. 333-342.
37. Braydich-Stolle, L.K., et al., *Nanosized aluminum altered immune function*. ACS Nano, 2010. **4**(7): p. 3661-3670.
38. Prabhakar, P.V., et al., *Oxidative stress induced by aluminum oxide nanomaterials after acute oral treatment in Wistar rats*. Journal of Applied Toxicology, 2012. **32**(6): p. 436-445.
39. Flaherty, N.L., et al., *Comparative analysis of redox and inflammatory properties of pristine nanomaterials and commonly used semiconductor manufacturing nano-abrasives*. Toxicology Letters, 2015. **239**(3): p. 205-215.
40. Kosaraju, K., S. Crawford, and S. Aravamudhan. *Cellular toxicity assessment and environmental impact of pre-and post-CMP Nanoparticle Slurries*. in ECS Transactions. 2015.
41. Dumitrescu, E., et al., *Interaction, transformation and toxicity assessment of particles and additives used in the semiconducting industry*. Chemosphere, 2018. **192**: p. 178-185.

Chapter 3. Predicting the Environmental Fate of Waste Chemical Mechanical Planarization Nanoparticles Through Physicochemical Characterization and Interactions with Model Cell Membranes¹

3.1 Abstract

Chemical mechanical planarization (CMP) is a semiconductor fabrication process that produces the atomically smooth wafer bases of integrated circuits. The wafers are planarized through the combination of chemical etching and mechanical polishing provided by the CMP slurry containing abrasive metal oxide nanoparticles. CMP wastewater treatment is site-specific and releases unknown concentrations of SiO₂, CeO₂, and Al₂O₃ nanoparticles into surface waters. Because small physicochemical changes can result in significant alterations in nanotoxicity, determining the impact of the CMP process on nanoparticle characteristics is a necessary step in assessing their associated environmental risks. This work found that exposure to the CMP process caused no significant change in nanoparticle charge, size, or aggregation. Furthermore, the interactions of these nanoparticles with model cell membranes remained unaltered. No CeO₂ or Al₂O₃ nanoparticle attachment to supported lipid bilayers (SLBs) was observed at environmentally relevant concentrations, likely due to the presence of polymeric stabilizers in the original slurry. Although SiO₂ nanoparticles did show attachment to

¹ This chapter is being prepared for publication. Dr. Xitong Liu provided guidance on experimental methodology, data interpretation and editorial suggestions. Dr. Shyam Aravamudhan and Dr. Steven Crawford of North Carolina A&T State University provided the CMP slurries, CMP process parameters, and Transmission Electron Microscope images.

SLBs, this contact was not associated with the release of fluorescent dye from phospholipid vesicles, indicating a lack of disruptive damage. Further characterization is required to make definitive conclusions; however, the unchanged nature of waste CMP nanoparticles observed in this work does not indicate that exposure to the CMP process increases the environmental risks posed by nanoparticle release.

3.2 Introduction

Chemical mechanical planarization (CMP) is a key process in the production of integrated circuits, the small chips used in the electronics we rely on daily (e.g. computers, cell phones, and home appliances). During CMP, a slurry containing abrasive nanoparticles contacts the wafer base of the integrated circuit, decreasing its surface roughness to less than a nanometer [1]. The production of each wafer generates 10 or more L of CMP wastewater [2]. The most commonly used abrasive nanoparticles, SiO₂, CeO₂, and Al₂O₃ are present in CMP wastewater at concentrations on the order of 1000 mg/L, 100 mg/L, and 1 mg/L, respectively [3].

Semiconductor fabrication facilities are subject to Clean Water Act regulations that require the removal of wastewater constituents including toxic organics, copper, chromium, and lead [4]. Treatment is site-specific and may include dilution with wastewater from other fabrication processes, physical and/or biological treatment [3, 5, 6]. CMP nanoparticles are not regulated and their paths through these treatment processes are difficult to trace [2]. Of the most commonly used nanomaterials, CeO₂ nanoparticles are the easiest to follow due to their insolubility and lack of use in wastewater treatment, with 6% of influent concentrations predicted to remain in treated effluent [7]. Although

large environmental discharges are not usually expected, nanoparticles will nonetheless reach surface waters following their use in CMP, raising questions regarding their potential impact.

A major component of environmental risk assessment is the characterization of a product's cytotoxicity, but the mechanisms of nanoparticle cytotoxicity are not always clear [8]. Previous literature has demonstrated that common pathways are enabled by direct contact between nanoparticles and cell membranes [9-13]. This may be due to the advantage of proximity when releasing toxic ions or reactive oxygen species (ROS), the ability to enter cells on contact, or physical destruction of the cell membrane. The complicated composition of cell membranes, with varied distributions of lipids and proteins, fluid movement, and characteristics that depend on the stage of growth, make it difficult to study general mechanisms of attachment [14-16]. Model supported lipid bilayers (SLBs) and vesicles that self-assemble in aqueous solution, with mechanical and electrical properties similar to those of cell membranes, have been used for over 30 years in biomedical research and can be applied to cytotoxicity studies [17].

Although the nanoparticles used in CMP are generally believed to be innocuous, there is evidence to suggest that they can exhibit cytotoxic effects. Metal oxide nanoparticles are known to generate ROS, interfere with lipid metabolism, and damage DNA [6]. Furthermore, large changes in nanotoxicity have been attributed to small changes in physicochemical characteristics (e.g. nanoparticle size, surface reactivity, and shape) [3, 6, 18, 19]. Therefore, characterizing the changes these nanoparticles may experience as a result of the CMP process is an important aspect of assessing the environmental risks posed by their release.

This research focuses on characterizing silica, ceria, and alumina nanoparticles in CMP slurries both before and after polishing silicon, copper, or tungsten wafers. This includes determining the size, charge, and aggregation dynamics of CMP nanoparticles as well as the potential impact of these nanoparticles on cell membranes. The tendency of CMP nanoparticles to attach to SLBs is investigated using a Quartz Crystal Microbalance with Dissipation Monitoring (QCM-D). In addition, zwitterionic vesicles containing fluorescent dye are used to determine if the CMP nanoparticles puncture phospholipid bilayers upon attachment. This research aims to provide insight into the interactions of CMP nanoparticles in aquatic environments through characterization of the physicochemical properties of the CMP nanoparticles as well as nanoparticle attachment to and disruption of model biological membranes.

3.3 Materials and Methods

3.3.1 Nanoparticle Slurries

There are a variety of commercially available slurries for use in CMP; this study focused on a few that cover the most common nanoparticle/wafer combinations [19]. Slurries containing fumed SiO₂ nanoparticles (Cabot Semisperse 12 E), CeO₂ nanoparticles (AGCEM CES 333F-2.5), and Al₂O₃ nanoparticles (Eminess Ultra-sol A20) were purchased from their respective manufacturers. Nanoparticle slurries are proprietary and their detailed characterization is unknown. However, the basic compositions of the slurries were provided through their associated Material Safety Data Sheets (MSDS). Slurries have been further characterized through measurements of Total Organic Carbon (TOC-L Analyzer, Shimadzu Scientific Instruments, Columbia, MD) and conductivity (HQ40D Portable Multi Meter, HACH Company, Loveland, CO).

Transmission Electron Microscopy (TEM) images of the CMP nanoparticles (Figure 3.1) were provided by collaborators at North Carolina A&T State University.

The slurries were exposed to CMP processes simulated at North Carolina A&T State University as described by Crawford et al. [19]. From the three original pristine slurries, four post-CMP slurries were created. The names of the slurries before and after polishing various wafer types is provided in Table 3.1. Polishing was accomplished using a rigid, micro-porous polyurethane polishing pad (Eminess DOW IC1000) and a fully automated CMP Polisher (Speedfam-IPEC Avanti 472). Generally, the process was designed to achieve a high removal rate and promote nanoparticle transformation while retaining acceptable polishing quality. CMP parameters, including intended use, time, speed and pressure, remained in the realistic range and are reported in Table 3.2 [19].

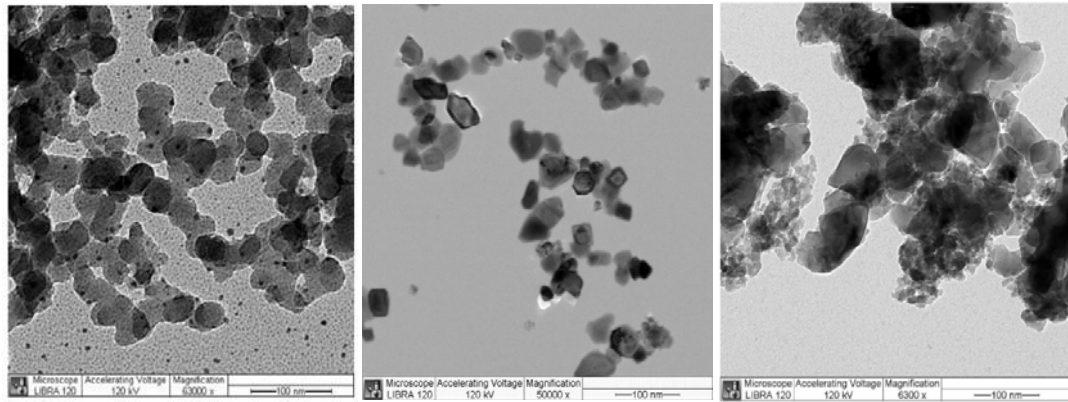


Figure 3.1. Transmission Electron Microscopy (TEM) images of (a) fumed SiO₂, (b) CeO₂, and (c) Al₂O₃ nanoparticles from the manufacturer provided CMP slurries. Images provided by Dr. Shyam Aravamudhan and collected by Dr. Steven Crawford at North Carolina A&T State University.

Table 3.1. Identifiers for nanoparticle slurries before and after CMP. Altogether there are seven slurry types tested, including three pre-CMP (Si, Ce, and Al) and four post-CMP (Si-Si, Ce-Si, Al-Cu, and Al-W).

Slurry	Nanoparticle Type	Wafer Polished	Pre-CMP ID	Post-CMP ID
Cabot Semisperse 12 E	Silica (SiO ₂)	Silicon	Si	Si-Si
AGCEM CES 333F-2.5	Ceria (CeO ₂)	Silicon	Ce	Ce-Si
Eminess Ultra-sol A20	Alumina (Al ₂ O ₃)	Copper	Al	Al-Cu
Eminess Ultra-sol A20	Alumina (Al ₂ O ₃)	Tungsten	Al	Al-W

Table 3.2. CMP process parameters provided by Dr. Steven Crawford at North Carolina A&T State University. Parameters were set in keeping with associated intended uses: alumina slurries for metal removal, ceria and silica slurries for interlayer dielectrics (ILD) and shallow trench isolation (STI).

Slurry	Substrate	Time (mm:ss)	Platen Speed (rpm)	Carrier Speed (rpm)	Down Force (psi)	Back Pressure (psi)	Substrate Size (mm)
Alumina	Copper	2:00	30	36	10	2	200
Alumina	Tungsten	2:00	30	36	10	2	200
Ceria	Silicon	2:00	60	72	12	2	200
Silica	Silicon	5:00	60	60	6	1.5	200

3.3.2 Electrophoretic Mobility

ZetaPALS Zeta Potential Analyzer (Brookhaven Instruments Corp., Holtsville, NY) was used to measure the electrophoretic mobilities (EPMs) of the nanoparticles diluted 1/1000 in 0.4 mM NaHCO₃ solution over a range of NaCl concentrations. The Zeta Potential Analyzer measures EPMs through Phase Analysis Light Scattering, a process in which nanoparticle motion is caused by the application of an oscillating electric field. The movement of the particles toward the positive or negative electrode, depending on their surface charge, will scatter incoming laser light. The phase shift caused by this scatter indicates the velocity at which the particle is moving. The EPM is presented as the average and standard deviation of 4 runs (10 cycles per run). EPMs are

reported at a maximum NaCl concentration of 100 mM as measurements taken at higher ionic strengths were inconsistent due to charge screening.

3.3.3 Size and Aggregation

The hydrodynamic diameters of the nanoparticles (slurries diluted to a concentration of 1 mg/L with DI water) were measured using the Dynamic Light Scattering (DLS) function of the Zetasizer Nano-ZS (Malvern Panalytical, Westborough, MA). DLS determines particle size through the characterization of the particle's Brownian motion, defined as the movement that results from collisions with surrounding solvent molecules. During DLS, a laser light is directed through the particle suspension and the intensity of the scattered light is detected. The autocorrelation function measures the time it takes for the intensity profile observed to be completely uncorrelated with the initial intensity profile. The more quickly this occurs, the faster the particles are moving and the smaller the particle size. These measurements allow for the discernment of a diffusion coefficient (D), which can be related to the hydrodynamic diameter of the particle (d_h) through the Stokes-Einstein equation (Equation 3.1) with the additional inputs of the Boltzmann constant (k) and the solvent's viscosity (η) and temperature (T).

Equation (3.1)
$$d_h = \frac{kT}{3\pi\eta D}$$

Four replicate measurements were recorded for each nanoparticle type and solution condition.

To characterize aggregation behaviors, nanoparticles were exposed to commonly occurring salts, including up to 1 M NaCl, 1 M NaNO₃, and 0.5 M CaCl₂ solutions. All salt solutions were adjusted to neutral pH using NaHCO₃. Following initial dispersion, nanoparticles were allowed to aggregate for 20 minutes prior to performing DLS. If an

increase in average size was observed, an additional sizing protocol was conducted to determine aggregation rate. For this set of measurements, DLS was initiated immediately following the introduction of the nanoparticles to the salt solution. A measurement was then recorded every 15 seconds over a period of 20 minutes. The rate of aggregation, calculated using linear least-square regression, was determined from duplicate runs.

3.3.4 Quartz Crystal Microbalance with Dissipation Monitoring

In the QCM-D system (Biolin Scientific, Västra Frölunda, Sweden), a model cell membrane can be deposited on a quartz crystal sensor oscillating at a specific frequency. When nanoparticles are then introduced to the model cell membrane, attachment decreases the frequency, providing information on the deposited layer's mass in real-time with a sensitivity of tens of nanograms [14, 20-22]. Furthermore, when paired with dye leakage assays, the QCM-D can be used to assess membrane damage [14, 16, 23, 24].

To clean the quartz sensors prior to use, they were soaked in 1% Hellmanex for 30 minutes before rinsing with DI water and drying with a stream of nitrogen gas. As a final cleaning step to remove organics, the sensors were exposed to a UV ozone system (Procleaner 110, BioForce Nanosciences, Inc., Ames, IA) for 20 minutes. To clean the QCM-D chambers, 1% Hellmanex solution was pumped through the system for 30 minutes at a flow rate of ca. 0.3 mL/min followed by rinsing with DI water for 30 minutes. After the DI water rinse, the chambers were dried with a stream of nitrogen gas [25]. When clean sensors were introduced into the QCM-D chambers, the frequencies at each resonance were compared with dissipation values specified by the manufacturer. If the values at each resonance were within 20% of those specified, the QCM-D system was deemed ready for use.

3.3.5 QCM-D Solution Preparation

Several HEPES Buffer solutions were introduced into the QCM-D system, identified as PLL Buffer (10 mM HEPES and 150 mM NaCl), SLB Buffer (10 mM HEPES and 150 mM NaCl adjusted to neutral pH), and Vesicle Buffer (20 mM HEPES and 150 mM NaCl adjusted to neutral pH). NP Buffers were solutions composed of 0.4 mM NaHCO₃ and varying concentrations of NaCl. CMP nanoparticles were diluted in their respective NP Buffer solutions to a concentration of 1 mg/L, considered a conservative estimate of the highest concentration that may be expected in environmental waters.

The zwitterion 1,2-dioleoyl-sn-glycero-3-phosphocholine (DOPC) was used as a model cell membrane. 25 g/L DOPC chloroform solution was obtained from Avanti Polar Lipids, Inc. (Alabaster, AL). The DOPC was dried by evaporating the chloroform with a stream of nitrogen gas and placing the resulting DOPC film in a vacuum desiccator for at least 4 hours. For the SLB attachment and vesicle disruption studies, the DOPC film was rehydrated to a concentration of 1 g/L with SLB Buffer and 100 mM carboxyfluorescein (CF) dye in Vesicle Buffer respectively. DOPC solutions were then stirred for at least 30 minutes. To produce DOPC vesicles made up of single bilayers, 1 g/L DOPC solutions were extruded (Avanti Lipids, Inc.) 15 times through a .05 μm membrane and diluted with either the SLB or the Vesicle Buffer to a final concentration of 0.05 g/L DOPC. The diameter of the resulting DOPC vesicles was ca. 130 nm, on the same size order as the CMP nanoparticles, a drawback of using these model cells. Real cells are generally much larger, with bacterial cells ranging from 0.2-10 μm. As curvature is inversely related to size, this change in diameter is likely to impact cell-nanoparticle interactions [26, 27].

Steps were taken to eliminate bubbles from solutions entering the QCM-D chambers. This includes degassing all solutions (except for the phospholipids) for five minutes as well as submerging all solutions in a water bath in order to achieve a temperature equal to that of the QCM-D chambers ($T = 25^{\circ}\text{C}$). The QCM-D system was run under continuous flow conditions at a rate of 0.1 mL/min.

3.3.6 Attachment Efficiency

For nanoparticles to attach to a surface, they must first be brought into contact via the long-range transport mechanisms of advection, sedimentation, and Brownian motion. Once nanoparticles are within proximity of the surface, short-range forces determine nanoparticle attachment, with electrostatic interactions often acting as a hindrance [28]. As nanoparticles move through the QCM-D system, the slope of the decrease in frequency ($\Delta f/dt$) provides a rate of attachment. The metric of attachment efficiency (α) was used to compare the tendency of nanoparticles to attach to model cell membranes under different solution chemistries (Equation 3.2). Attachment efficiency normalizes the rate of frequency change that occurs as nanoparticles attach to a surface by the rate of frequency change that occurs as nanoparticles attach to a favorable surface ($\Delta f/dt_{fav}$) [23, 29-33].

Equation (3.2)
$$\alpha = \frac{\Delta f/dt}{\Delta f/dt_{fav}}$$

A favorable surface is defined as a surface that is electrostatically attractive to the nanoparticles. In other words, this metric normalizes attachment by the rate observed if every nanoparticle-surface contact is predicted to result in attachment. For the positively charged alumina nanoparticles, this favorable surface is a silica coated quartz crystal

sensor (Biolin Scientific QSX 303). For the negatively charged silica and ceria nanoparticles, a positively charged layer must be deposited over the silica sensor. To achieve this positively charged surface, PLL Buffer is pumped through the system to develop a stable baseline, defined as a change of frequency less than 0.2 Hz over 10 minutes, before introducing 0.01 g/L poly-L-lysine (PLL) in PLL Buffer to the QCM-D system. Upon establishment of the PLL layer on the sensor surface, the system was rinsed with PLL Buffer for 10 minutes.

To determine the extent of nanoparticle attachment to the DOPC SLB, SLB Buffer was pumped through the QCM-D chambers containing silica coated sensors until the frequency stabilized. Then, 0.05 g/L DOPC in SLB Buffer was introduced. When a critical concentration of deposited vesicles was reached, the forces on the vesicles caused a chain reaction of vesicle rupture, resulting in the formation of a DOPC SLB [34, 35]. The successful deposition of this layer is demonstrated through the characteristic frequency and dissipation changes of -25 ± 0.5 Hz and 0.1×10^{-6} , respectively [25, 34-36]. Upon establishment of the SLB on the sensor surface, the system was rinsed with SLB Buffer for 10 minutes.

When the desired sensor surface was established, the NP Buffer solution was introduced to the system. When the frequency once again reached a stable baseline, the diluted nanoparticle slurry was pumped through the QCM-D chambers. Triplicate experiments were conducted for each nanoparticle type and solution condition.

3.3.7 Vesicle Disruption

To establish a layer of DOPC vesicles on a QCM-D sensor surface, Vesicle Buffer was pumped through the system until stabilization was reached. DOPC vesicles

were then introduced into the QCM-D chambers housing gold sensors (Biolin Scientific QSX 301) and allowed to deposit for ca. 30 minutes. Unlike the vesicle interactions with silica sensors, deposition onto gold sensors results in a layer of vesicles that remained intact [34, 35]. After vesicle deposition, the system was rinsed with Vesicle Buffer for two hours before the NP Buffer was introduced. Again, stabilization was achieved before nanoparticles in 150 mM NaCl NP Buffer were introduced into the system. Nanoparticles were pumped through the flow chambers over a period of forty minutes followed by twenty minutes of 32 mM Triton X-100, a membrane solubilizer, to release the CF dye contained within the vesicles. During this time, effluent was collected over five-minute intervals. Following QCM-D, a fluorometer (Qubit 3.0, Thermo Fisher Scientific, Waltham, Massachusetts) was used to measure the CF dye concentration in the QCM-D effluent using an excitation wavelength of 470 nm and emission wavelengths between 510-580 nm. The total mass of dye released over the course of the experiment was calculated by multiplying the concentration of dye in the effluent by the flow rate (0.1 mL/min) and time length of effluent collection (5 minutes).

3.4 Results and Discussion

3.4.1 Nanoparticle Slurry Characteristics

While the composition of CMP slurries are proprietary, information provided by the MSDS is listed in Table 3.3. The measured total organic carbon (TOC) concentrations and conductivities are also listed. Slurries are generally composed of water, abrasive nanoparticles, buffers and acids or bases for pH control, anti-coagulants, corrosion inhibitors, surfactants, polymers, oxidizers, chelating or complexing agents, and bactericides and fungicides [2, 37, 38]. As the aggregation of abrasive nanoparticles

causes increased wafer defectivity, one of the main considerations in developing a slurry is maintaining nanoparticle stability [37]. Stabilizers prevent aggregation through electrostatic and/or steric repulsion. Common polymeric stabilizers include polyacrylic acid, polyethylene glycol, cetyl trimethyl ammonium bromide and polyethylene cetyl ether [2].

The alumina slurry has the greatest measured concentrations of organic carbon and conductivity, followed by the ceria and silica slurries, indicating the alumina slurry contains the greatest levels of organic and inorganic additives. With regard to the specific slurry composition, the KOH reported in the silica slurry is commonly used as a chemical etchant for silicon surfaces [39]. As mentioned previously, the polyacrylic acid in the ceria slurry is well-known as a polymeric stabilizer. The source of the ammonia listed in the alumina slurry MSDS is unspecified, but ammonium salts are a common source of CMP stabilization [40-43]. Generally, these slurry characteristics, both provided and measured, indicate a significantly greater presence of polymeric stabilizers in the ceria and alumina slurries than in the silica slurry.

Table 3.3. CMP slurry characteristics.

Slurry Characteristic	Al ₂ O ₃	CeO ₂	f-SiO ₂
Wt % NP ^a	15-25	1	12
Wt % Water ^a	75-85	~ 96.5	> 87%
Other Component ^a	Ammonia, aqueous solution (< 1%)	Poly Acrylic Acid (2.5%)	Potassium hydroxide (< 1%)
pH ^a	5-6	~6	10.9-11.2
NP Size (nm) ^a	240	140	170
TOC (g/L) ^b	19.42	0.75	0.03
Conductivity (S/m) ^c	3.74	0.31	1.11

^a Provided by the manufacturer MSDS

^b Measured with the Shimadzu TOC-L Analyzer

^c Measured with the HACH HQ40D Multi Meter

3.4.2 Electrophoretic Mobility

The EPMs of each type of nanoparticle, before and after CMP, are shown in Figure 3.2. The charge measurements are in fair agreement with relevant literature values [3, 19, 23]. The silica and ceria nanoparticles have very similar profiles, with negative charges approaching 0 as the ionic strength increases. The alumina nanoparticles are all positively charged, also approaching 0 with increasing NaCl concentration. The increasing concentration of ions in solution results in charge screening, decreasing the effective surface charge of the nanoparticles [44]. Polishing did not significantly impact the EPMs, indicating the preservation of surface functional groups through the CMP process.

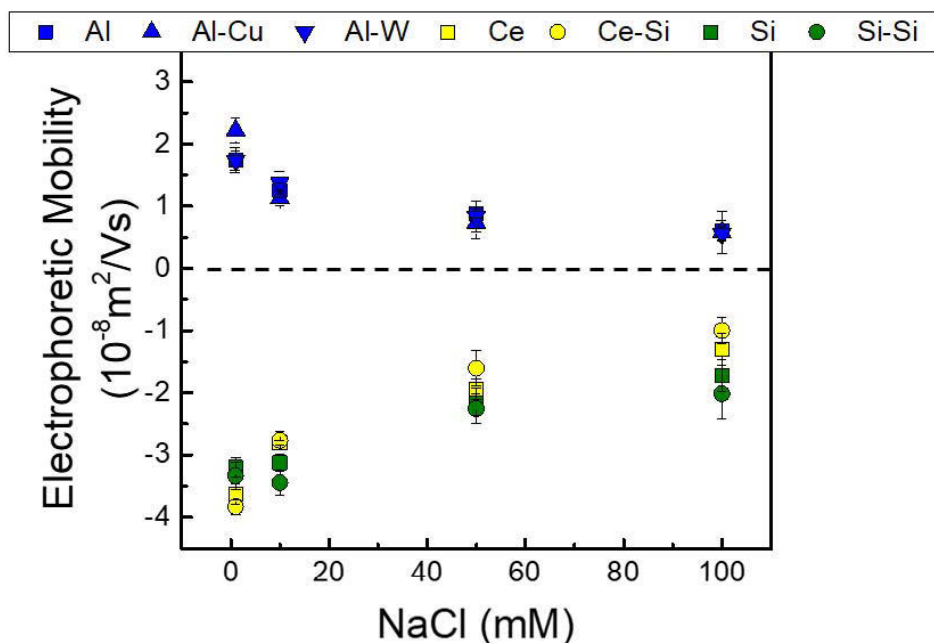


Figure 3.2. Electrophoretic mobilities (EPMs) of the nanoparticles, before (Al, Ce, Si) and after (Al-Cu, Al-W, Ce-Si, Si-Si) CMP, diluted 1/1000 in 0.4 mM NaHCO₃ buffer and varying concentrations of NaCl. EPMs are represented as the average and standard deviation of four replicate measurements.

The salt levels in surface waters are an important consideration when predicting the environmental fates of CMP nanoparticles based on surface charge. Lakes and rivers generally have low salinity corresponding with ionic strengths between 1-5 mM while seawater reaches ionic strengths around 700 mM. Therefore, in fresh waters these nanoparticles retain their charge, increasing particle stability and decreasing the chance of homo-aggregation. As most particles have a net negative charge in environmental waters, the positively charged alumina nanoparticles are likely to experience hetero-aggregation [45]. Negatively charged nanoparticles, including silica and ceria, are more likely to resist aggregation and remain bioavailable [46]. However, in sea water, with decreased effective surface charge, nanoparticles are more prone to attachment, leading to the formation of aggregates that settle out of the water column. Therefore, in saline waters,

the nanoparticles are likely to end up in sediment, emphasizing the importance of their potential interactions with benthic organisms [47].

3.4.3 Size and Aggregation

The average observed hydrodynamic diameters of Si (173 nm) and Ce (144 nm) nanoparticles are consistent with the manufacturer provided sizes of 170 nm and 140 nm respectively (Figure 3.3). The Al nanoparticles, with an average hydrodynamic diameter of 367 nm, are slightly larger than the manufacturer description of 240 nm. This may indicate some aggregation of the nanoparticles in solution, which, according to the manufacturer, has been shown to occur in slurries of adjusted pH. Hetero-aggregation may also be occurring, as slurry additives such as a stabilizing polymers can attach to nanoparticles and increase their effective size [24]. Alternatively, this may be due to the discrepancy demonstrated between measurements taken using DLS and microscopy, as light scattering methods have been shown to favor the detection of larger particles [3, 48]. None of the nanoparticles experience a significant change in size as a result of exposure to the CMP process, with average hydrodynamic diameters of Si-Si, Ce-Si, Al-Cu, and Al-W nanoparticles of 163 nm, 148 nm, 358 nm, and 318 nm, respectively.

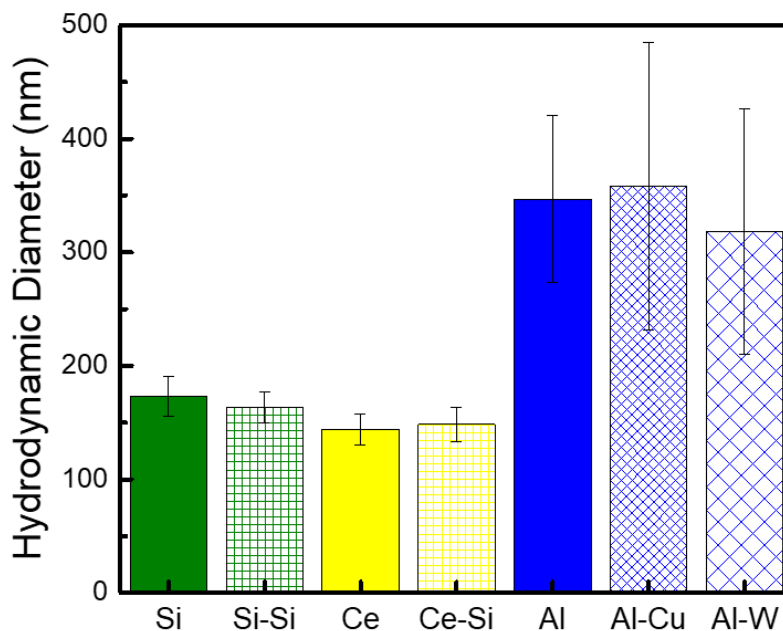


Figure 3.3. Hydrodynamic diameters of CMP nanoparticles (diluted to 1 mg/L in DI water) represented as the average and standard deviation of four replicate measurements.

The CMP nanoparticles were generally stable, with ceria and alumina nanoparticles demonstrating no substantial aggregation in any of the salt solutions. The hydrodynamic diameters of the silica nanoparticles did increase with increasing CaCl_2 concentration (Figure 3.4a) beginning at 10 mM. As silica nanoparticles exhibited a greater tendency to aggregate in the presence of CaCl_2 than in NaCl or NaNO_3 solutions of equivalent ionic strength, increased aggregation may be due to preferential binding of Ca^{2+} ions [25] to the negatively charged silanol groups rather than to charge screening effects. The aggregation rates were similar for silica nanoparticles before and after the CMP process, overlapping at CaCl_2 concentrations of 10 and 500 mM (Figure 3.4b).

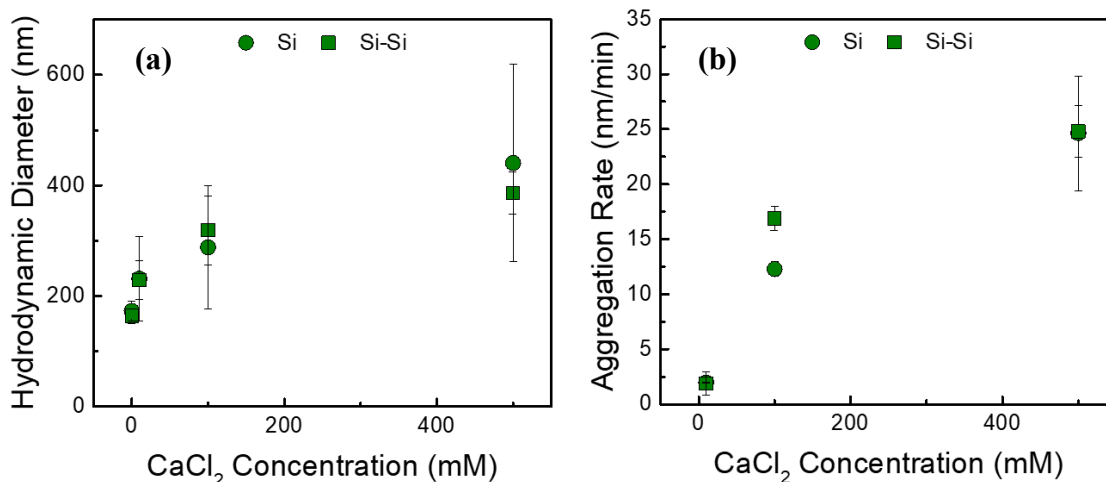


Figure 3.4. (a) Hydrodynamic diameters of silica nanoparticles, before (Si) and after (Si-Si) CMP and (b) corresponding rates of aggregation. Silica nanoparticles were diluted to a concentration of 1 mg/L and allowed to aggregate over 20 minutes.

While silica nanoparticles have demonstrated particular resistance to aggregation [23, 49, 50], likely due to the “hairy layer” [50] of flexible segments of poly(silicic acid) protruding from the surface, the Si and Si-Si nanoparticles were found to be the least stable. The comparative stability of ceria and alumina nanoparticles observed in this study indicate the presence of slurry dispersants that are actively preventing aggregation. While the effects of these additives are expected to be less dominant when CMP nanoparticles are released into environmental waters [49], these DLS measurements demonstrate the ability of nanoparticles to retain their stability even after dilution by a factor of over 100,000.

3.4.4 Attachment Efficiency

Under constant solution conditions, the extent of nanoparticle attachment to a lipid bilayer will depend on the characteristics of the nanoparticle, including its surface charge, functionality, size, shape, surface heterogeneity, and hydrophobicity [10, 12, 27, 51]. Electrostatic forces generally govern the short-range motion of nanoparticles and

have been subject to the most extensive investigation regarding nanoparticle-membrane attachment [14, 17, 25, 35, 52]. In fact, the metric of attachment efficiency is built on the idea that attachment will occur under electrostatically favorable conditions.

However, other important forces can challenge this assumption of electrostatic dominance. Hydration forces resulting from the adherence of water molecules to the hydrophobic phospholipid bilayer can increase resistance to attachment, as the water molecules must be moved out of the way in order for attachment to proceed [14, 25, 27]. Hydration forces are especially relevant in this context as the hydrophilic phospholipid bilayer tightly binds water molecules [25]. Steric forces can also create a barrier, as protrusions from the surface (e.g. polymers) physically prevent the nanoparticles from moving close enough to experience van der Waals attraction and subsequent attachment [2, 27, 53]. Furthermore, electrostatic forces become less dominant at higher ionic strengths as the effective surface charge decreases. At 150 mM NaCl, the salt concentration is high enough to expect charges to be screened at nm distances [27]. Indeed, it has been shown that at this ionic strength the negative surface charge of the DOPC layer is effectively screened [25, 35].

Exposure to the CMP process does not appear to impact the tendency of any of the nanoparticles to attach to the lipid bilayer. The attachment efficiencies for silica nanoparticles before and after polishing are shown in Figure 3.5. The attachment efficiency increases with increasing ionic strength until it reaches unity at 100 mM NaCl, likely due to charge screening decreasing the electrostatic repulsion between silica nanoparticles and the DOPC SLB. The presence of sodium ions has also been theorized to result in a reduction of the repulsive hydration forces [25, 35, 54, 55]. After the

attachment efficiency reaches unity, it remains there at 150 mM NaCl as the repulsive forces have been neutralized. At 10 mM NaCl, salt concentrations above those commonly observed in fresh waters, the rate of silica nanoparticle attachment was less than 10% of the rate observed under favorable conditions.

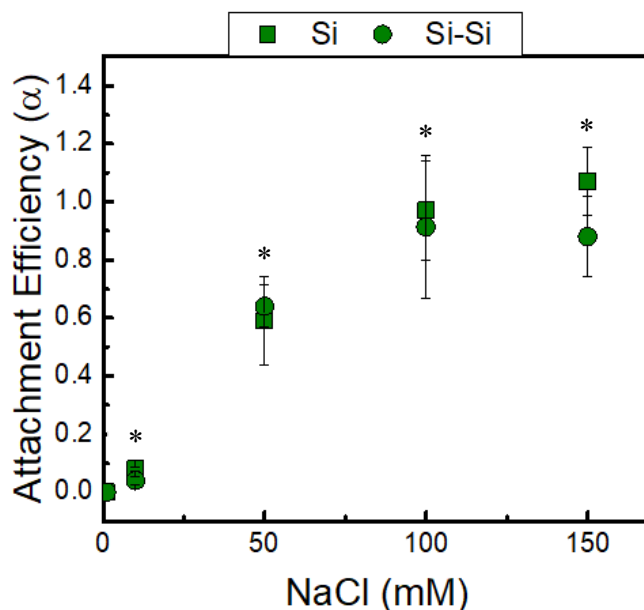


Figure 3.5. Attachment efficiency of silica NPs, before (Si) and after (Si-Si) CMP, diluted on the order of 1 mg/L with NaHCO₃ buffer and varying NaCl concentration. Represented as the average and standard deviation of triplicate experiments. Asterisk (*) indicates $p < 0.05$ for both Si and Si-Si nanoparticles.

While the attachment profile we observe for silica nanoparticles is predictable based on electrostatic forces, ceria and alumina nanoparticles did not show attachment under any solution conditions. Ceria nanoparticles, shown to have very similar charge profiles to silica nanoparticles over varying ionic strengths (Figure 3.2), did not attach to the SLB in the presence of NaCl concentrations up to 300 mM. This disagrees with a previous study conducted by Liu et al., in which ceria nanoparticle attachment occurred in 100 mM NaCl solution [23]. Given the known characteristics of the ceria slurry used in

this study, this difference likely arises from the presence of polyacrylic acid. This polymer can attach to ceria nanoparticles through electrostatic attraction at low pH, and remain fixed to the nanoparticle as the pH is raised [56]. The addition of polyacrylic acid creates a protective cloud around the ceria nanoparticles, providing steric hindrance to attachment while retaining a similar surface charge [42, 57].

No alumina nanoparticle attachment to DOPC SLBs or silica surfaces was observed in solutions containing NaCl concentrations up to 300 mM. As was the case with ceria nanoparticles, this lack of attachment brings attention to the impact of slurry additives. In addition to the stabilizing effect demonstrated in the aggregation studies, the lack of attachment of the positively charged alumina nanoparticles to the negatively charged DOPC SLB indicates that steric repulsion is the dominant short-range force. Although the specific dispersant in the alumina slurry is unknown, given the high TOC content and the retention of the surface charge, a positively charged polymer is likely. In addition, the high ammonium content points to commonly used ammonium based cationic polymers, such as cetyl trimethyl ammonium bromide or dodecyl trimethyl ammonium bromide [2, 58]. Another factor in the resistance of alumina nanoparticle attachment to the sensor surface may be the effect of size on long-range forces. Previous studies have shown an inability of aggregated nanoparticles or nanoparticles of increasing size to attach to the lipid membrane, possibly due to a decrease in the nanoparticle's diffusion coefficient, decreasing collisions between nanoparticles and the SLB [24, 29, 59, 60].

3.4.3 Vesicle Disruption

Silica nanoparticles, as the only CMP nanoparticles to attach to the supported lipid bilayer, were investigated for disruptive effects on micelles containing fluorescent dye. Despite observed attachment to model cell membranes (Figure 3.6), no significant dye leakage was seen from these vesicles over an exposure period of 40 minutes (Figure 3.7). These results are consistent with previous work done by Liu et al., that showed silica nanoparticle attachment in NaCl and phosphate buffer solutions did not correspond with detectable vesicle damage [23]. Therefore, the attachment of silica nanoparticles does not appear to substantially disrupt the phospholipid bilayer.

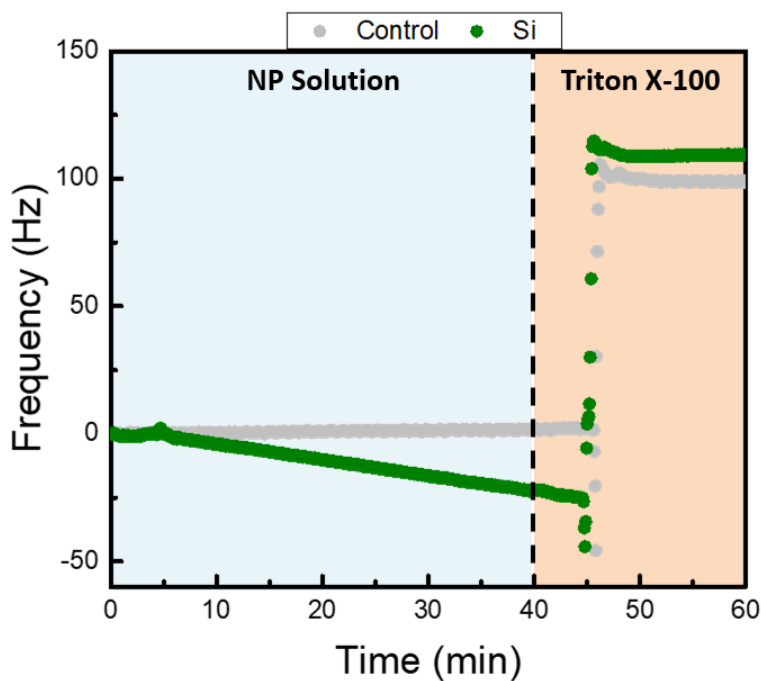


Figure 3.6. Representative QCM-D frequency profile as silica nanoparticles deposit onto vesicles (0-40 min) followed by exposure to the membrane solubilizer, which releases all CF dye contained within the vesicles (40-60 min).

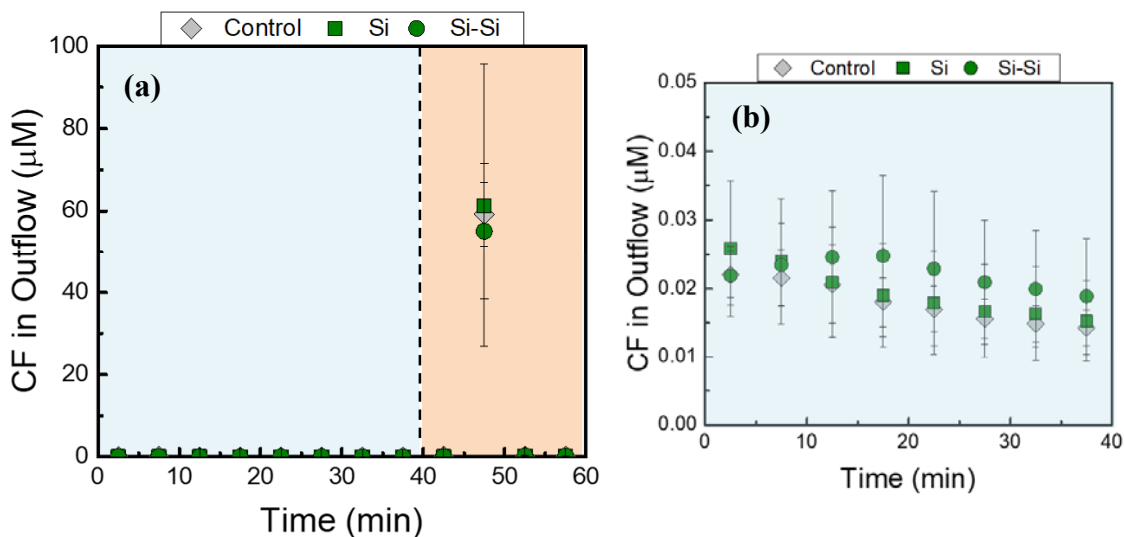


Figure 3.7. (a) Carboxyfluorescein dye in outflow of QCM-D as vesicles are exposed to 1 mg/L silica nanoparticles (before (Si) and after (Si-Si) CMP) dispersed in 150 mM NaCl and bicarbonate buffer for 40 minutes. Following the nanoparticle exposure period, 32 mM Triton X-100, a membrane solubilizer, was pumped through the system for 20 minutes. Enlargement of silica nanoparticle exposure period is show in (b).

While silica nanoparticle attachment did not result in physical damage to the model cell membrane, direct contact may still impact cell viability. Fumed silica nanoparticles have been shown to produce ROS and lead to death in A549 epithelial cells, red blood cells, and Beas-2B bronchial cells [18, 61-63]. ROS react with polyunsaturated fatty acids in the cell membrane and cause lipid peroxidation [14, 64]. This may alter membrane fluidity and permeability, hindering the ability of membrane receptors and enzymes to properly control the intake and excretion of particles and ions [65]. These changes can lead to the production of more ROS and other toxic compounds, creating a positive feedback cycle that may lead to cell death. Oxidative stress can also cause genotoxicity by reacting with the carbohydrates and nitrogen bases that make up DNA [6]. Therefore, attachment, even where it does not result in the puncturing of a micelle, may be important in predicting cell viability after exposure to nanoparticles.

3.5 Conclusion

The CMP process did not result in any significant differences in charge, size, aggregation, or interactions with model cell membranes for the Al₂O₃, CeO₂, or SiO₂ nanoparticles investigated. CMP nanoparticles were found to be generally stable, with Al₂O₃ and CeO₂ likely experiencing enhanced stability through the steric repulsion provided by polymeric dispersants, retained even at high dilutions. Silica was found to homo-aggregate in the presence of CaCl₂ and to attach to model cell membranes. The extent of attachment increased with increasing NaCl concentration and is expected to be fairly low in the salt levels present in surface waters. Even under the conditions in which silica nanoparticles were shown to achieve maximum attachment, they did not cause significant release of fluorescent dye from DOPC vesicles. While this result indicates a lack of physical damage to the model cell membrane, other mechanisms of toxicity, including ROS generation, would be relevant in real systems and exacerbated by direct physical contact.

Although CMP nanoparticles have been shown to demonstrate cytotoxicity, they are generally considered innocuous. SiO₂ and Al₂O₃ nanoparticles fall under the EPA designation “practically non-toxic,” defined as showing no adverse effects at levels less than or equal to 100 mg/L, significantly greater concentrations than we would expect to enter environmental waters. CeO₂ nanoparticles have shown more mixed results, but are in the same category with regard to acute morbidity testing [6]. The lack of distinction in both the physicochemical characterization and model membrane interactions of waste CMP nanoparticles did not indicate an increase in environmental risk. Future work will

directly compare these results with cytotoxicity studies to verify the applicability of model cell membranes in the investigation of cell-nanoparticle interactions.

3.5 References

1. Ng, D., et al., *Oxidation and removal mechanisms during chemical-mechanical planarization*. *Wear*, 2007. **263**(7-12 SPEC. ISS.): p. 1477-1483.
2. Speed, D.E., *Environmental aspects of planarization processes*, in *Advances in Chemical Mechanical Planarization (CMP)*. 2016. p. 1-269.
3. Speed, D., et al., *Physical, chemical, and in vitro toxicological characterization of nanoparticles in chemical mechanical planarization suspensions used in the semiconductor industry: Towards environmental health and safety assessments*. *Environmental Science: Nano*, 2015. **2**(3): p. 227-244.
4. *Electrical and Electronic Components Effluent Guidelines*, U.S.E.P. Agency, Editor. 1983.
5. Karimi, S., et al., *Acute and chronic toxicity to Daphnia magna of colloidal silica nanoparticles in a chemical mechanical planarization slurry after polishing a gallium arsenide wafer*. *NanoImpact*, 2019. **13**: p. 56-65.
6. Karimi, S., et al., *Acute and chronic toxicity of metal oxide nanoparticles in chemical mechanical planarization slurries with Daphnia magna*. *Environmental Science: Nano*, 2018. **5**(7): p. 1670-1684.
7. Limbach, L.K., et al., *Removal of oxide nanoparticles in a model wastewater treatment plant: Influence of agglomeration and surfactants on clearing efficiency*. *Environmental Science and Technology*, 2008. **42**(15): p. 5828-5833.
8. Collins, A.R., et al., *High throughput toxicity screening and intracellular detection of nanomaterials*. *Wiley Interdisciplinary Reviews: Nanomedicine and Nanobiotechnology*, 2017. **9**(1).
9. Geiser, M., et al., *Ultrafine particles cross cellular membranes by nonphagocytic mechanisms in lungs and in cultured cells*. *Environmental Health Perspectives*, 2005. **113**(11): p. 1555-1560.
10. Leroueil, P.R., et al., *Nanoparticle interaction with biological membranes: Does nanotechnology present a janus face?* *Accounts of Chemical Research*, 2007. **40**(5): p. 335-342.
11. Leroueil, P.R., et al., *Wide varieties of cationic nanoparticles induce defects in supported lipid bilayers*. *Nano Letters*, 2008. **8**(2): p. 420-424.
12. Yuan, H., et al., *Variable nanoparticle-cell adhesion strength regulates cellular uptake*. *Physical Review Letters*, 2010. **105**(13).
13. He, X., et al., *Changing exposure media can reverse the cytotoxicity of ceria nanoparticles for Escherichia coli*. *Nanotoxicology*, 2012. **6**(3): p. 233-240.
14. Chen, K.L. and G.D. Bothun, *Nanoparticles meet cell membranes: Probing nonspecific interactions using model membranes*. *Environmental Science and Technology*, 2014. **48**(2): p. 873-880.
15. Beney, L. and P. Gervais, *Influence of the fluidity of the membrane on the response of microorganisms to environmental stresses*. *Applied Microbiology and Biotechnology*, 2001. **57**(1-2): p. 34-42.
16. Goodman, C.M., et al., *Toxicity of gold nanoparticles functionalized with cationic and anionic side chains*. *Bioconjugate Chemistry*, 2004. **15**(4): p. 897-900.
17. Moghadam, B.Y., et al., *Role of nanoparticle surface functionality in the disruption of model cell membranes*. *Langmuir*, 2012. **28**(47): p. 16318-16326.

18. Flaherty, N.L., et al., *Comparative analysis of redox and inflammatory properties of pristine nanomaterials and commonly used semiconductor manufacturing nano-abrasives*. Toxicology Letters, 2015. **239**(3): p. 205-215.
19. Crawford, S., *Cytotoxicity of Engineered Nanoparticles used in Industrial Processing*. 2019, Univeristy of North Carolina at Greensboro.
20. Rodahl, M., et al., *Simultaneous frequency and dissipation factor QCM measurements of biomolecular adsorption and cell adhesion*. Faraday Discussions, 1997. **107**: p. 229-246.
21. Melby, E.S., et al., *Formation of supported lipid bilayers containing phase-segregated domains and their interaction with gold nanoparticles*. Environmental Science: Nano, 2016. **3**(1): p. 45-55.
22. Yousefi, N. and N. Tufenkji, *Probing the interaction between nanoparticles and lipid membranes by quartz crystal microbalance with dissipation monitoring*. Frontiers in Chemistry, 2016. **4**(DEC).
23. Liu, X. and K.L. Chen, *Aggregation and interactions of chemical mechanical planarization nanoparticles with model biological membranes: Role of phosphate adsorption*. Environmental Science: Nano, 2016. **3**(1): p. 146-156.
24. Gal, N., et al., *Interaction of Size-Tailored PEGylated Iron Oxide Nanoparticles with Lipid Membranes and Cells*. ACS Biomaterials Science and Engineering, 2017. **3**(3): p. 249-259.
25. Yi, P. and K.L. Chen, *Interaction of Multiwalled Carbon Nanotubes with Supported Lipid Bilayers and Vesicles as Model Biological Membranes*. Environmental Science & Technology, 2013. **47**(11): p. 5711-5719.
26. Farnoud, A.M. and S. Nazemidashtarjandi, *Emerging investigator series: interactions of engineered nanomaterials with the cell plasma membrane; what have we learned from membrane models?* Environmental Science: Nano, 2019. **6**(1): p. 13-40.
27. Nel, A.E., et al., *Understanding biophysicochemical interactions at the nano-bio interface*. Nature Materials, 2009. **8**(7): p. 543-557.
28. Benjamin, M.M. and D.F. Lawler, *Water quality engineering: Physical/chemical treatment processes*. 2013: John Wiley & Sons.
29. Chen, K.L. and M. Elimelech, *Interaction of fullerene (C60) nanoparticles with humic acid and alginate coated silica surfaces: Measurements, mechanisms, and environmental implications*. Environmental Science and Technology, 2008. **42**(20): p. 7607-7614.
30. Lin, S. and M.R. Wiesner, *Deposition of aggregated nanoparticles - A theoretical and experimental study on the effect of aggregation state on the affinity between nanoparticles and a collector surface*. Environmental Science and Technology, 2012. **46**(24): p. 13270-13277.
31. Chang, X. and D.C. Bouchard, *Multiwalled carbon nanotube deposition on model environmental surfaces*. Environmental Science and Technology, 2013. **47**(18): p. 10372-10380.
32. Chowdhury, I., et al., *Deposition and release of graphene oxide nanomaterials using a quartz crystal microbalance*. Environmental Science and Technology, 2014. **48**(2): p. 961-969.

33. Song, J., et al., *Deposition of protein-coated multi-walled carbon nanotubes on oxide surfaces and the retention in a silicon micromodel*. Journal of Hazardous Materials, 2019. **375**: p. 107-114.
34. Keller, C.A. and B. Kasemo, *Surface specific kinetics of lipid vesicle adsorption measured with a quartz crystal microbalance*. Biophysical Journal, 1998. **75**(3): p. 1397-1402.
35. Richter, R., A. Mukhopadhyay, and A. Brisson, *Pathways of Lipid Vesicle Deposition on Solid Surfaces: A Combined QCM-D and AFM Study*. Biophysical Journal, 2003. **85**(5): p. 3035-3047.
36. Paxton, W.F., et al., *Adsorption and fusion of hybrid lipid/polymer vesicles onto 2D and 3D surfaces*. Soft Matter, 2018. **14**(40): p. 8112-8118.
37. Singh, R.K., et al., *Fundamentals of slurry design for CMP of metal and dielectric materials*. MRS Bulletin, 2002. **27**(10): p. 752-760+748.
38. Ilie, F. and G. Ipate, *Chemical-mechanical impact of nanoparticles and pH effect of the slurry on the CMP of the selective layer surfaces*. Lubricants, 2017. **5**(2).
39. Pandey, K. and P.M. Pandey. *Chemically Assisted Polishing of Monocrystalline Silicon Wafer Si (100) by DDMAF*. in *Procedia Engineering*. 2017.
40. Armini, S., et al., *Mixed organic/inorganic abrasive particles during oxide CMP*. Electrochemical and Solid-State Letters, 2008. **11**(7): p. H197-H201.
41. Salis, B., et al., *Polymer Coating and Lipid Phases Regulate Semiconductor Nanorods' Interaction with Neuronal Membranes: A Modeling Approach*. ACS Chemical Neuroscience, 2019. **10**(1): p. 618-627.
42. Cho, C.W., et al., *Atomic force microscopy study of the role of molecular weight of poly(acrylic acid) in chemical mechanical planarization for shallow trench isolation*. Journal of Materials Research, 2006. **21**(2): p. 473-479.
43. Park, J.G., et al., *Surfactant effect on oxide-to-nitride removal selectivity of nano-abrasive ceria slurry for chemical mechanical polishing*. Japanese Journal of Applied Physics, Part 1: Regular Papers and Short Notes and Review Papers, 2003. **42**(9 A): p. 5420-5425.
44. Elimelech, M., J. Gregory, and X. Jia, *Particle deposition and aggregation: measurement, modelling and simulation*. 2013: Butterworth-Heinemann.
45. Yu, S., et al., *Interactions between engineered nanoparticles and dissolved organic matter: A review on mechanisms and environmental effects*. Journal of Environmental Sciences (China), 2018. **63**: p. 198-217.
46. Goswami, L., et al., *Engineered nano particles: Nature, behavior, and effect on the environment*. Journal of Environmental Management, 2017. **196**: p. 297-315.
47. De Marchi, L., et al., *Engineered nanomaterials: From their properties and applications, to their toxicity towards marine bivalves in a changing environment*. Environmental Research, 2019. **178**.
48. Roth, G.A., N.M. Neu-Baker, and S.A. Brenner, *SEM analysis of particle size during conventional treatment of CMP process wastewater*. Science of the Total Environment, 2015. **508**: p. 1-6.
49. Otero-González, L., et al., *Stability of alumina, ceria, and silica nanoparticles in municipal wastewater*. Water Science and Technology, 2014. **70**(9): p. 1533-1539.

50. Vigil, G., et al., *Interactions of silica surfaces*. Journal of Colloid And Interface Science, 1994. **165**(2): p. 367-385.
51. Chithrani, B.D., A.A. Ghazani, and W.C.W. Chan, *Determining the size and shape dependence of gold nanoparticle uptake into mammalian cells*. Nano Letters, 2006. **6**(4): p. 662-668.
52. Pera, H., J.M. Kleijn, and F.A.M. Leermakers, *Interaction of silica nanoparticles with phospholipid membranes*. Chemistry Letters, 2012. **41**(10): p. 1322-1324.
53. Brahma, N. and J.B. Talbot, *Effects of CMP slurry additives on the agglomeration of alumina nanoparticles I: General aggregation rate behavior*. Journal of Colloid and Interface Science, 2014. **419**: p. 56-60.
54. Zhang, X., et al., *Interactions of polymeric drug carriers with DDT reduce their combined cytotoxicity*. Environmental Pollution, 2018. **241**: p. 701-709.
55. Karlsson, H.L., et al., *Cell membrane damage and protein interaction induced by copper containing nanoparticles-Importance of the metal release process*. Toxicology, 2013. **313**(1): p. 59-69.
56. Sehgal, A., et al., *Precipitation– Redispersion of Cerium Oxide Nanoparticles with Poly (acrylic acid): Toward Stable Dispersions*. Langmuir, 2005. **21**(20): p. 9359-9364.
57. Torchilin, V.P. and V.S. Trubetskoy, *Which polymers can make nanoparticulate drug carriers long-circulating?* Advanced Drug Delivery Reviews, 1995. **16**(2-3): p. 141-155.
58. Cheemalapati, K., J. Keleher, and Y. Li, *Key Chemical Components in Metal CMP Slurries*, in *Microelectronic Applications of Chemical Mechanical Planarization*. 2007. p. 201-247.
59. Liu, X. and K.L. Chen, *Interactions of graphene oxide with model cell membranes: Probing nanoparticle attachment and lipid bilayer disruption*. Langmuir, 2015. **31**(44): p. 12076-12086.
60. Chen, K.L. and M. Elimelech, *Aggregation and deposition kinetics of fullerene (C60) nanoparticles*. Langmuir, 2006. **22**(26): p. 10994-11001.
61. Irfan, A., et al., *Assessment of temporal dose-toxicity relationship of fumed silica nanoparticle in human lung A549 cells by conventional cytotoxicity and 1H-NMR-based extracellular metabolomic assays*. Toxicological Sciences, 2014. **138**(2): p. 354-364.
62. Zhang, H., et al., *Processing pathway dependence of amorphous silica nanoparticle toxicity: Colloidal vs pyrolytic*. Journal of the American Chemical Society, 2012. **134**(38): p. 15790-15804.
63. Eom, H.J. and J. Choi, *Oxidative stress of silica nanoparticles in human bronchial epithelial cell, Beas-2B*. Toxicology in Vitro, 2009. **23**(7): p. 1326-1332.
64. Cabiscol, E., J. Tamarit, and J. Ros, *Oxidative stress in bacteria and protein damage by reactive oxygen species*. International Microbiology, 2000. **3**(1): p. 3-8.
65. Guan, N., et al., *Microbial response to environmental stresses: from fundamental mechanisms to practical applications*. Applied Microbiology and Biotechnology, 2017. **101**(10): p. 3991-4008.

Chapter 4. Assessing Changes in CMP Nanoparticle Cytotoxicity Using Model Cell Membranes²

4.1 Abstract

Chemical mechanical planarization (CMP) is a key process in the manufacturing of integrated circuits in which the circuit base is smoothed to a surface roughness of less than a nm. Polishing is accomplished through a combination of chemical etching and mechanical abrasion provided by slurries containing SiO₂, CeO₂, or Al₂O₃ nanoparticles. Following CMP wastewater treatment, nanoparticles enter the environment, providing potential routes to human exposure. Investigating CMP nanoparticle cytotoxicity in the context of human health is an important step in assessing the risk associated with nanoparticle exposure to the CMP process and subsequent release. Concentration-dependent CMP nanoparticle attachment and disruption of model cell membranes was compared with human cell toxicity assays (i.e. membrane damage and cell inhibition) conducted by collaborators. SiO₂ nanoparticles were the only CMP nanoparticles to show substantial attachment to model cell membranes and damage to A549 lung epithelial cell membranes. In contrast, CeO₂ and Al₂O₃ nanoparticles showed weak interactions with supported lipid bilayers and were not associated with cell membrane damage. No CMP nanoparticles showed appreciable vesicle disruption at concentrations up to 500 mg/L.

² This chapter is being prepared for publication. Dr. Xitong Liu provided guidance on experimental methodology, data interpretation and editorial suggestions. Dr. Shyam Aravamudhan and Dr. Steven Crawford of North Carolina A&T State University provided the CMP slurries and conducted the cytotoxicity (i.e. membrane damage and inhibition concentration) assays.

Overall, no change in CMP nanoparticle behavior was observed that indicated exposure to the CMP process resulted in increased risk to human cells.

4.2 Introduction

Chemical mechanical planarization (CMP) is a semi-conductor fabrication process involved in the production of integrated circuit devices. To fit as many transistors as possible on the base of these devices, the surface must have a roughness of less than a nm [1]. In order to achieve this level of polishing, a combination of chemical etching and mechanical abrasion is required. To this end, a CMP slurry containing abrasive metal oxide (i.e. SiO₂, CeO₂, Al₂O₃) nanoparticles and a variety of chemicals (e.g. oxidizers, corrosion inhibitors, pH buffers, high molecular weight polymers, and biocides) contacts the base under applied pressure [2-4]. After use in the CMP process, the nanoparticle slurry is subject to wastewater treatment specific to the site of fabrication [5-7]. More than 90% of the CMP nanoparticles are predicted to end up in biosolids with more than half of the generated biosolids disposed of through land application [8]. A smaller fraction of the influent CMP nanoparticles will be released to surface waters [2, 9-12]. These two pathways make wastewater treatment the largest environmental source of CMP nanoparticles, increasing the likelihood of subsequent human exposure [8].

With any emerging contaminant, determining the exposure concentration that poses a potential risk to human health is crucial. Compared to running in vivo studies, conducting in vitro tests of cellular responses to increasing contaminant concentrations is a cost-effective, high-throughput method of developing a toxicity profile [13]. However, results from cytotoxicity studies are often conflicting and hard to interpret. This confusion stems from the range of experimental conditions, including different cell types,

contaminant concentrations, exposure lengths, and toxicity endpoints [8, 14].

Furthermore, with regard to nanoparticles, the specific mechanisms of cytotoxicity often remain unclear. Small changes in size, shape, and surface functionality have been shown to significantly impact nanotoxicity [11, 15-17]. The literature does show that direct contact of the nanoparticles with cell membranes is often a precursor to toxic effects [18-22].

The tendency of nanoparticles to contact and adhere to cell membranes can be studied using self-assembling phospholipid bilayers. This simplified membrane model retains the mechanical and electrical properties of biological membranes, allowing for a controlled characterization of cell-nanoparticle interactions [23]. Studies involving biological cell membranes introduce complicating factors including membrane fluidity, interspersed proteins, and ongoing cellular processes [24, 25]. Furthermore, the stage of the cell's lifecycle and changing environmental conditions will affect cell membrane characteristics. Model cell membranes studies can be paired with cytotoxicity assays to provide mechanistic insights into observed nanotoxicity [17, 26-28].

The majority of model membrane studies use an Atomic Force Microscope (AFM) or a Quartz-Crystal Microbalance with Dissipation Monitoring (QCM-D) [25]. QCM-D, which can sense changes in mass down to tens of nanograms, is the method used in this study [25]. Through QCM-D, a model cell membrane can be deposited on a sensor prior to the introduction of a nanoparticle solution. As the nanoparticles attach to the membrane, the frequency at which the sensor oscillates changes, providing information on the deposited layer's mass [25, 29-31]. While the QCM-D cannot provide information on the distribution of nanoparticles through the membrane as the AFM can, it

allows the user to monitor attachment in real-time [7, 26-28, 32-34]. Furthermore, QCM-D can be paired with fluorescent dye leakage assays to detect physical membrane disruption [1, 7, 23, 27, 28, 35].

The goal of this study was to determine whether exposure to the CMP process resulted in changes to SiO₂, CeO₂, and Al₂O₃ nanoparticle interactions with two model cell membranes and three cell lines. Within the QCM-D system, concentration-dependent nanoparticle attachment to supported lipid bilayers (SLBs) and damage to vesicles was investigated. These mechanistic studies were then compared with cytotoxicity assays conducted by collaborators at North Carolina A&T State University, assessing membrane damage and inhibition of A549 lung epithelial cells, HepG2 liver epithelial cells, and RAW 264.7 macrophages. Through characterization of nanoparticle attachment and disruption of model cell membranes and cytotoxicity, this research aims to provide insight into the impact of CMP exposure on nanoparticle interactions with human cells.

4.3 Materials and Methods

4.3.1 Nanoparticle Slurry Characterization

CMP slurries containing silica (Cabot Semisperse 12 E), ceria (AGCEM CES 333F-2.5), and alumina (Eminess Ultra-sol A20) nanoparticles were purchased from their respective manufacturers. After purchasing, slurries were processed through a CMP polisher (Speedfam-IPEC Avanti 472) at North Carolina A&T State University. CMP slurries were paired with typical wafers under realistic polishing conditions (Table 3.2). CMP slurry identifiers are provided in Chapter 3 (Table 3.1) along with more detailed slurry characterizations. Previous measurements indicated that the presence of slurry additives resulted in a strong stabilization effect on ceria and alumina nanoparticles.

For the purposes of this study, nanoparticles are diluted in a solution representing physiological fluids. An aqueous solution of 150 mM NaCl, referred to as NP Solution, provides the average ionic strength of human bodily fluids [36]. Furthermore, the addition of bicarbonate buffer was used to achieve a pH of 7.4, placing this solution in the pH range of most physiological fluids (Table 4.1) [7]. Specifically, NP Solution matches the ionic strength and pH conditions present in blood [37].

Table 4.1. pH range of various physiological fluids.
Adapted from Liu and Chen Environmental
Science: Nano (2016)

Human Body Fluid	pH
Bile	7.4-8.5
Blood	7.35-7.45
Cerebrospinal fluid	7.35-7.45
Gastric juice	1.0-2.0
Saliva	6.7-7.4
Stool	7.0-7.5
Tears	7.4
Urine	5.0-7.5

Nanoparticles were sized using the Dynamic Light Scattering (DLS) function of the Zetasizer Nano-ZS (Malvern Panalytical, Westborough, MA). Nanoparticles of each type were diluted to 1 mg/L with NP Solution. Four replicate measurements were taken in automatic mode. The NP Solution contains ion concentrations large enough for charge screening to prevent the collection of accurate measurements of electrophoretic mobility (EPM). However, previous EPM measurements (Chapter 3) show the surface charge of positively charged Al₂O₃ nanoparticles, negatively charged CeO₂ nanoparticles, and negatively charged SiO₂ nanoparticles all approaching an effective surface charge of 0 as the NaCl concentration increases from 1-100 mM. Therefore, under conditions

representative of physiological fluids, electrostatic forces are expected to be weakened by charge screening.

4.3.2 Supported Lipid Bilayer Attachment

The phospholipid 1,2-dioleoyl-sn-glycero-3-phosphocholine (DOPC), stored in chloroform, was purchased from Avanti Polar Lipids, Inc. (Alabaster, AL) for use as a model cell membrane. To prepare DOPC for SLB deposition, chloroform was evaporated through exposure to a stream of nitrogen gas. The DOPC film that formed was then vacuum desiccated for at least 4 hours. Following drying, the DOPC layer was rehydrated with SLB Buffer (10 mM HEPES and 150 mM NaCl adjusted to neutral pH) by stirring for ca. 30 minutes, resulting in a 1 g/L DOPC solution. This solution was then extruded through a 0.05 μm membrane 15 times to form single bilayer vesicles that were ca. 130 nm in diameter. The DOPC vesicle solution was further diluted with SLB Buffer to a concentration of 0.05 g/L DOPC. Before introduction to the QCM-D system, SLB Buffer, DOPC solution, and NP Solution were all submerged in a water bath set at a temperature of 27° C. SLB Buffer and NP Solution were additionally degassed through 5 minutes of sonication to prevent the presence of bubbles in the QCM-D system. All solutions were pumped through the system at a flow rate of 0.1 mL/min.

The concentration-dependent attachment of the CMP nanoparticles to the SLB was assessed using the QCM-D system (Biolin Scientific, Västra Frölunda, Sweden). The system was cleaned with 1% Hellmanex and DI water, as described in the previous chapter. SLB Buffer was flowed through the system until stabilization, or a frequency change of less than 0.2 Hz over 10 minutes, was achieved. DOPC solution was then pumped through the system containing SiO₂ sensors (Biolin Scientific QSX 303) for ca.

10 minutes, until the characteristic frequency (-25 Hz) and dissipation (10^{-6}) shifts associated with the deposition of the SLB were observed [34, 38-40]. The system was then rinsed with SLB Buffer for 10 minutes before introduction of the NP Solution. When the frequency equilibrated, CMP nanoparticles in NP Solution were flowed through the system for forty minutes. Model cell membranes were exposed to each type of nanoparticle at concentrations of 0.1 mg/L, 1 mg/L, 10 mg/L, 100 mg/L, 250 mg/L, and 500 mg/L. The initial rates of frequency change (first 5 minutes) that occurred as nanoparticles attached to the SLB were then compared among the various concentrations tested.

4.3.3 Vesicle Disruption

For the vesicle disruption studies, DOPC preparation followed the previously described drying steps to form a DOPC film. Then, the DOPC layer was rehydrated with 100 mM carboxyfluorescein (CF) dye in Vesicle Buffer (20 mM HEPES and 150 mM NaCl adjusted to neutral pH) through stirring for ca. 30 minutes. This 1 g/L DOPC solution was processed through the extrusion protocol detailed above [7], followed by dilution with Vesicle Buffer to a concentration of 0.05 g/L DOPC. As in the SLB attachment study, all solutions (i.e. Vesicle Buffer, DOPC solution, and NP Solution) were submerged in a water bath at 27° C to prevent the formation of bubbles upon introduction to the QCM-D system. In addition, the Vesicle Buffer and NP Solution were degassed through 5 minutes of sonication.

Vesicle Buffer was pumped through the QCM-D system housing gold sensors (Biolin Scientific QSX 301) until stabilization was achieved. Then, 0.05 g/L DOPC vesicles in Vesicle Buffer was flowed through the system for ca. 30 minutes to allow a

layer of vesicles to deposit. The system was then rinsed for two hours with Vesicle Buffer before introducing the NP Solution. When stabilization was once again achieved, 10-500 mg/L CMP nanoparticle solutions were pumped through the system for 40 minutes followed by a membrane solubilizer (32 mM Triton X-100) for 20 minutes. During this time, the QCM-D effluent was collected in five-minute intervals. The fluorescence of the effluent samples was measured using the fluorometer function of the Qubit 3.0 system (Thermo Fisher Scientific, Waltham, Massachusetts).

4.3.4 Cytotoxicity Assays

Cytotoxicity assays were conducted at North Carolina A&T State University by Dr. Steven Crawford and Dr. Shyam Aravamudhan. The assays discussed in this chapter are the membrane damage and cell viability assays described in Dr. Crawford's dissertation entitled, "Cytotoxicity of Engineered Nanoparticles used in Industrial Processing" [16]. A549 lung epithelial cells, HepG2 liver epithelial cells, and RAW 264.7 macrophages were chosen to cover the exposure pathways of inhalation and ingestion. Direct contact with the skin is considered an unlikely exposure route as other metal oxide (i.e. TiO₂ and ZnO) nanoparticles have not penetrated through dermal layers [41-45]. Risks associated with the dermal exposure route are further mitigated by the larger sizes of CMP nanoparticles.

All cytotoxicity assessments were conducted following 48-hour exposures to the nanoparticle slurries before (Si, Ce, Al) and after (Si-Si, Ce-Si, Al-Cu) CMP processing. Al-W nanoparticles have not yet been investigated for cytotoxicity. Concentrations tested were based on the initial dilution levels provided by the slurries and ranged from a lower limit of 50 mg/L to upper limits of 2 g/L, 2 g/L, and 10 g/L, for SiO₂, CeO₂, and Al₂O₃

nanoparticles, respectively. Membrane damage was assessed using a lactate dehydrogenase (LDH) assay (Sigma Aldrich). LDH is an enzyme found in the cytoplasm of most cells and is released into solution when the cell membrane is damaged. Once released, a series of enzymatic reactions takes place that results in a solution color change. The absorbance of the solution is measured and compared to a negative control. Cell viability was assessed using the Alamar Blue assay (Thermo Fisher Scientific). Active cells metabolize Alamar Blue, a resazurin dye, and form fluorescent resofurin products. The resulting fluorescent signal can be measured and compared to a negative control. Cell viability effects are represented by the IC_{50} , or the nanoparticle concentration that results in the inhibition of 50% of exposed cells.

4.4 Results and Discussion

4.4.1 Nanoparticle Slurry Characterization

CMP nanoparticles were sized in solution conditions relevant to physiological fluids using DLS (Figure 4.1). CMP exposure did not result in a significant change in nanoparticle size. These hydrodynamic diameters were also not significantly different from those measured in DI water (Chapter 3), indicating the ion concentrations present did not result in increased nanoparticle aggregation. As discussed in the previous chapter, measured silica and ceria nanoparticle hydrodynamic diameters agree with manufacturer-provided sizes (170 and 140 nm, respectively), while the alumina nanoparticles are larger than specified (240 nm). This may be due to hetero-aggregation with slurry additives (considered likely), homo-aggregation between nanoparticles, or an effect of the measurement technique (Chapter 3).

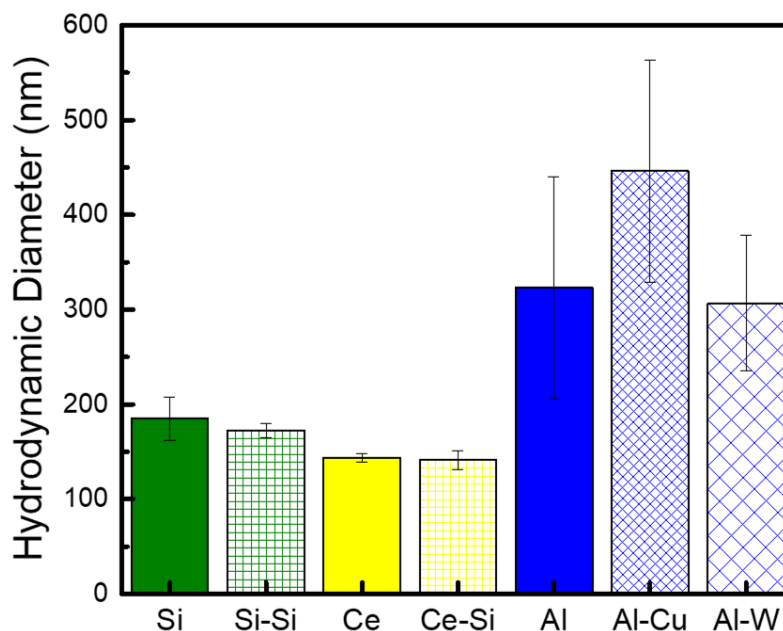


Figure 4.1. Hydrodynamic diameters of silica, ceria, and alumina nanoparticles, before (Si, Ce, Al) and after (Si-Si, Ce-Si, Al-Cu, Al-W) CMP processing, diluted to 1 mg/L in 150 mM NaCl and 0.4 mM NaHCO₃. Data represents the average and standard deviation of four replicate measurements.

4.4.2 QCM-D Attachment

Figure 4.2 shows representative profiles of the change in QCM-D sensor frequency as silica nanoparticles attached to the SLB over forty minutes of exposure. As the Si concentration increased from 0-500 mg/L, the magnitude of the initial rate of frequency change, and therefore initial rate of nanoparticle attachment, also increased. For concentrations greater than 10 mg/L, these rates of attachment did not remain constant, but decreased over time, indicating a maximum nanoparticle mass that can be deposited on the SLB. The data indicates a limited number of attachment sites that, once filled, are no longer available. These same trends, including the average initial slope of attachment, were observed as Si-Si nanoparticles attached to the supported lipid bilayer (Figure 4.3). For both Si and Si-Si nanoparticles, the magnitude of the initial rate of frequency change increases linearly with nanoparticle concentration.

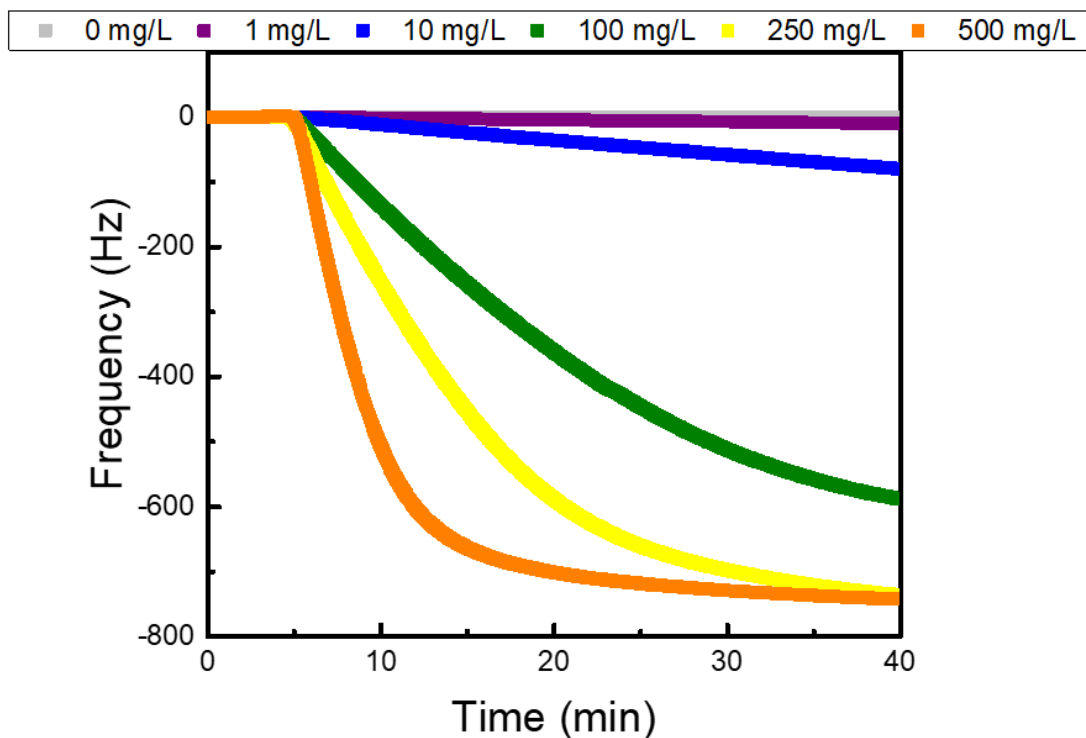


Figure 4.2. Representative profiles of the frequency change that occurred as silica nanoparticles attached to the supported lipid bilayer over 40 minutes of exposure. Nanoparticles diluted in 150 mM NaCl and bicarbonate buffer (pH 7.4).

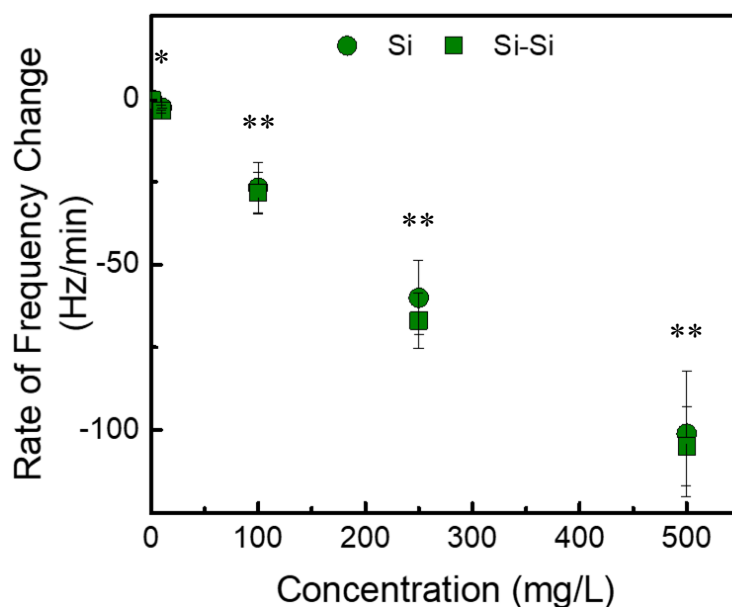


Figure 4.3. Initial rate of frequency change as silica nanoparticles, before (Si) and after (Si-Si) CMP, attach to the supported lipid bilayer in 150 mM NaCl and bicarbonate buffer (pH 7.4). Represented by the average and standard deviation of three replicate runs. Asterisk (*) indicates $p < 0.05$ for both Si and Si-Si nanoparticles. Asterisks (**) indicate $p < 0.025$ for both Si and Si-Si nanoparticles.

The CMP process did not significantly affect nanoparticle attachment to the SLB. Silica nanoparticles showed much greater attachment to the bilayer than either ceria (Figures 4.4 and 4.5) or alumina (Figures 4.6 and 4.7) nanoparticles. Silica, alumina, and ceria nanoparticle exposure first resulted in statistically significant initial frequency changes at concentrations of 1 mg/L, 100 mg/L, and 250 mg/L, respectively. While the introduction of silica nanoparticles caused a sustained frequency change over time, ceria and alumina only significantly altered the frequency upon initial exposure. Even when considering this initial frequency change, the highest concentration (500 mg/L) of Ce, Ce-Si, Al, Al-Cu, and Al-W nanoparticles only resulted in frequency changes on the same order of magnitude as 1 mg/L Si and Si-Si nanoparticles.

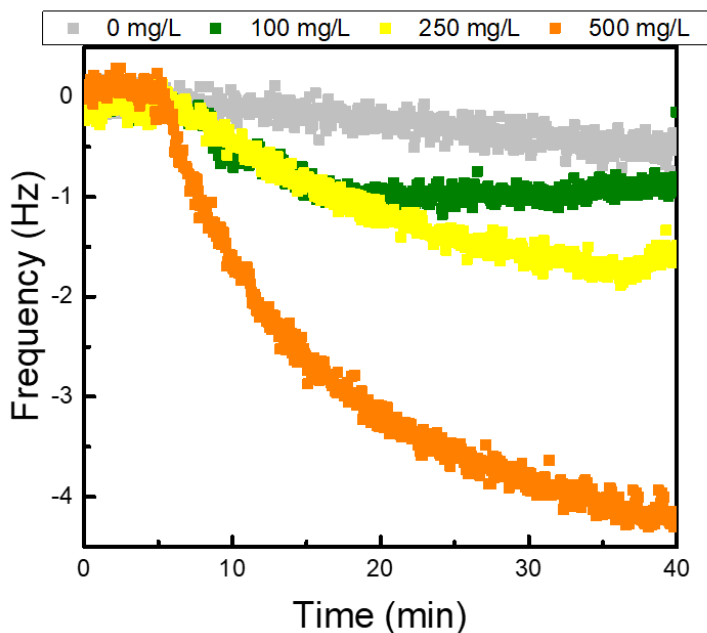


Figure 4.4. Representative profiles of the frequency change that occurred as ceria nanoparticles attached to the supported lipid bilayer over 40 minutes of exposure. Nanoparticles diluted in 150 mM NaCl and bicarbonate buffer (pH 7.4).

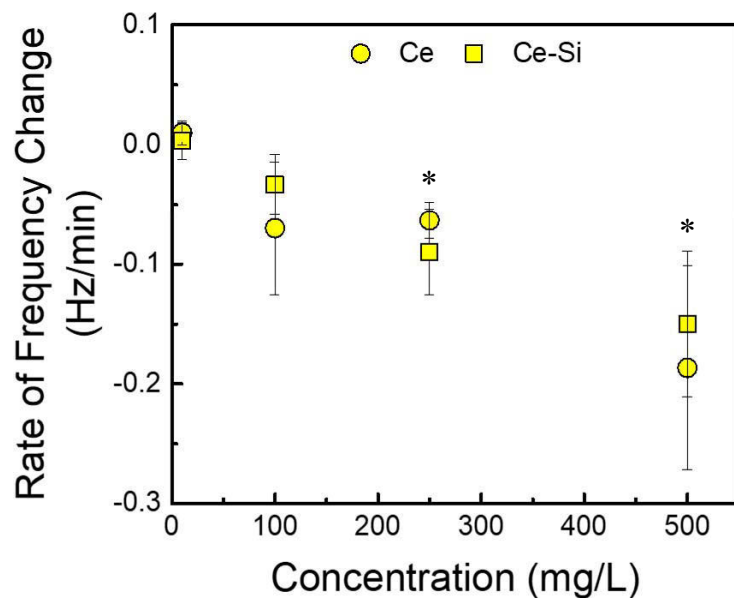


Figure 4.5. Initial rate of frequency change as ceria nanoparticles, before (Ce) and after (Ce-Si) CMP, attach to the supported lipid bilayer in 150 mM NaCl and bicarbonate buffer (pH 7.4). Represented by the average and standard deviation of three replicate runs. Asterisk (*) indicates $p < 0.05$ for both Ce and Ce-Si nanoparticles.

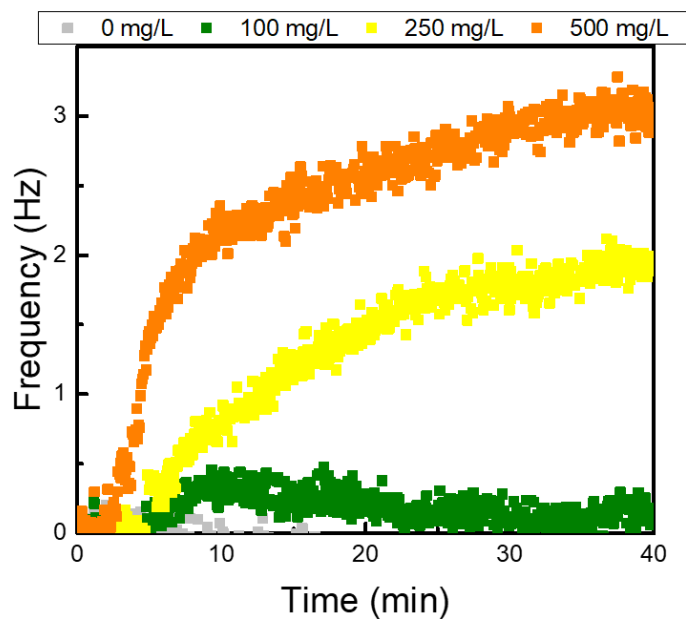


Figure 4.6. Representative profiles of the frequency change that occurred as alumina nanoparticles attached to the supported lipid bilayer over 40 minutes of exposure. Nanoparticles diluted in 150 mM NaCl and bicarbonate buffer (pH 7.4).

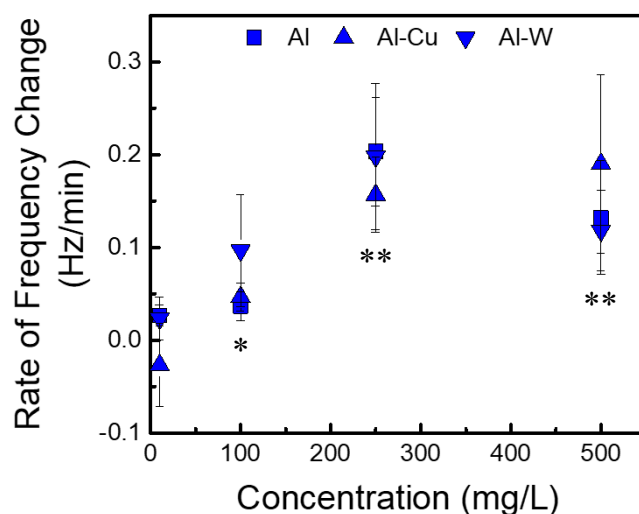


Figure 4.7. Initial rate of frequency change as alumina nanoparticles (before CMP (Al), after polishing copper (Al-Cu), and after polishing tungsten (Al-W)) attach to the supported lipid bilayer in 150 mM NaCl and bicarbonate buffer (pH 7.4). Represented by the average and standard deviation of three replicate runs. Asterisk (*) indicates $p < 0.1$ for Al, Al-Cu, and Al-W nanoparticles. Asterisks (**) indicate $p < 0.025$ for Al, Al-Cu, and Al-W nanoparticles.

The significantly weaker interactions of ceria and alumina nanoparticles with the SLB is in accordance with the aggregation and attachment behavior described in the preceding chapter. As previously discussed, this lack of attachment to the model membrane is likely due to the presence of slurry dispersants. For the ceria nanoparticles, this stabilization effect likely stems from polyacrylic acid (PAA), a polymeric additive listed as a slurry constituent by the manufacturer. PAA is included in the slurry to prevent aggregation of the nanoparticles through steric repulsion [5]. For the alumina nanoparticles, the stabilization source is not provided by the manufacturer. However, because the measured surface charge of the alumina nanoparticles is positive, we can rule out electrostatic repulsion as the stabilizing force. Therefore, the additive present in the alumina slurries is also likely a polymeric stabilizer that prevents attachment through steric repulsion [24, 46]. The presence of these dispersants results in much weaker

interactions between the nanoparticles and the model cell membranes at all concentrations tested.

Unlike ceria and silica nanoparticles, exposure to alumina (Al, Al-Cu, and Al-W) resulted in an initial increase in frequency, indicating a loss of mass from the sensor surface. While alumina nanoparticles did not seem to have a strong tendency to interact with the lipid bilayer (as shown in this and our previous study), it appears that when the two do interact, lipids are removed from the model membrane. This result is likely due to the presence of a cationic polymeric stabilizer. Previous studies have demonstrated the tendency of cationic polymers to distort and compress the cell membrane, leading to cell collapse and the release of intracellular contents [47, 48]. The same forces governing this polymer-cell interaction are likely responsible for the disturbance of the lipid bilayer observed during the QCM-D study.

Although uncommon in the literature, Jiang et al. also observed an increase in QCM-D frequency when investigating the interactions of nanoparticles and model cell membranes [49]. Jiang et al. introduced an aqueous solution of multi-walled carbon nanotubes to a negatively charged supported lipid bilayer (DOPG) deposited on a silica sensor. Their study suggested that the increase in frequency represents the removal of phospholipids from the bilayer as they attach to nanoparticles through hydrogen bonding and van der Waals attraction. This effect has been observed with real bacterial cells using Transmission Electron Microscopy (TEM). Tu. et al. showed lipids were extracted from *E. coli* cell membranes by graphene nanosheets [50]. This extraction decreased lipid density and resulted in the loss of membrane integrity. Therefore, in this study, the initial

increase in frequency observed upon exposure of the SLB to alumina nanoparticles, though small, may be important to cytotoxicity.

These SLB attachment studies can be compared with the membrane damage assays conducted by our collaborators at North Carolina A&T State University (Figure 4.8). Silica nanoparticles, both before and after CMP, are shown to cause membrane damage at all concentrations tested (50-2000 mg/L). No significant membrane damage was observed following cell exposures to ceria and alumina nanoparticles at concentrations up to 2 g/L. Therefore, silica nanoparticles, the only CMP nanoparticle type to show strong attachment to the model cell membranes were also the only type that caused significant damage to A549 lung epithelial cell membranes after 48 hours of exposure.

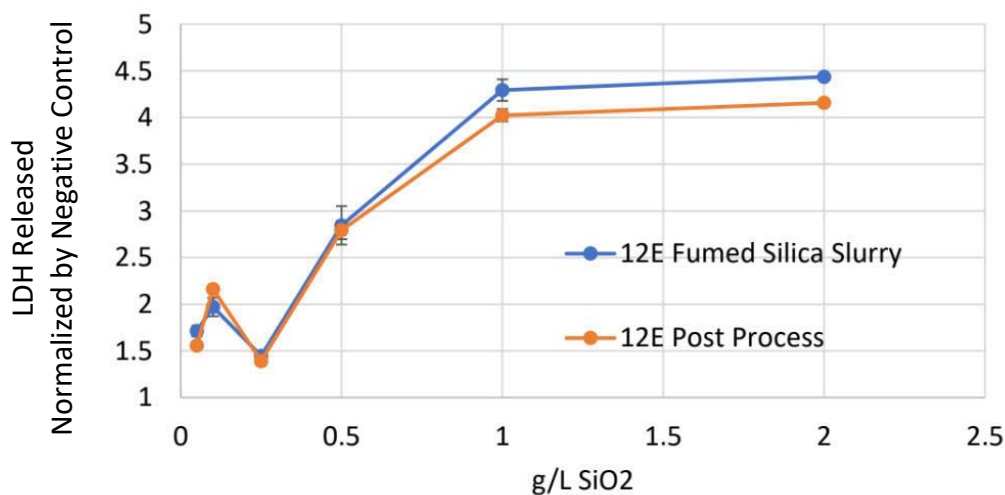


Figure 4.8. LDH released from A549 lung epithelial cells normalized by the negative control (e.g. 1.5 = 150% of LDH released during negative control) following 48 hours of nanoparticle exposure. Figure provided by Dr. Shyam Aravamudhan and Dr. Steven Crawford of North Carolina A&T State University.

4.4.3 Vesicle Disruption

Figure 4.9 shows representative profiles of the decrease in frequency that occurred as 500 mg/L silica, ceria, and alumina nanoparticles attached to the vesicle layer followed by the sudden frequency increase upon exposure to a membrane solubilizer. Silica nanoparticles attached to the vesicular layer and the SLB at about the same rate. Alumina nanoparticles did not show significant attachment to either model cell membrane structure. Ceria nanoparticles showed an increased tendency to attach to the vesicle layer, likely due to the increased surface area available for attachment. The addition of the membrane solubilizer caused the vesicles to rupture, releasing the nanoparticles as well as the fluorescent dye contained within the vesicles, resulting in a final frequency greater than the initial frequency.

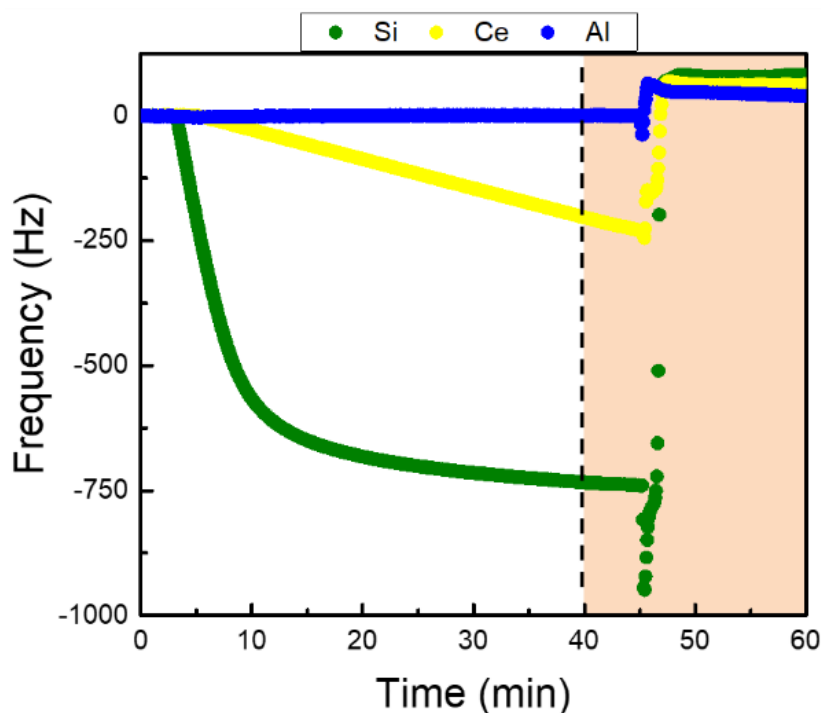


Figure 4.9. Representative profiles of 500 mg/L silica, ceria, and alumina nanoparticles (diluted in 150 mM NaCl and 0.4 mM NaHCO₃) depositing onto the DOPC vesicle layer over 40 minutes followed by 20 minutes of exposure to 32 mM Triton X-100 (membrane solubilizer).

The tendency of nanoparticles to attach to the model cell membranes did not translate to the release of fluorescent dye from the vesicles. Figure 4.10 shows the concentration of fluorescent dye released as a function of time over forty minutes of exposure to 500 mg/L of silica, ceria, and alumina nanoparticles. While a small increase in CF dye release was observed, statistically significant for Ce, Al, Al-Cu, and Al-W nanoparticles, the mass released was a small fraction (<1%) of the total dye contained within the vesicles, indicating limited physical damage (Figure 4.11). Interestingly, Ce-Si nanoparticles showed no significant fluorescent dye release, the only change in nanoparticle behavior based on CMP exposure that was observed in this study. This may be due to CMP being a polishing process that also impacts the nanoparticles exposed, potentially smoothing jagged edges on the ceria nanoparticles.

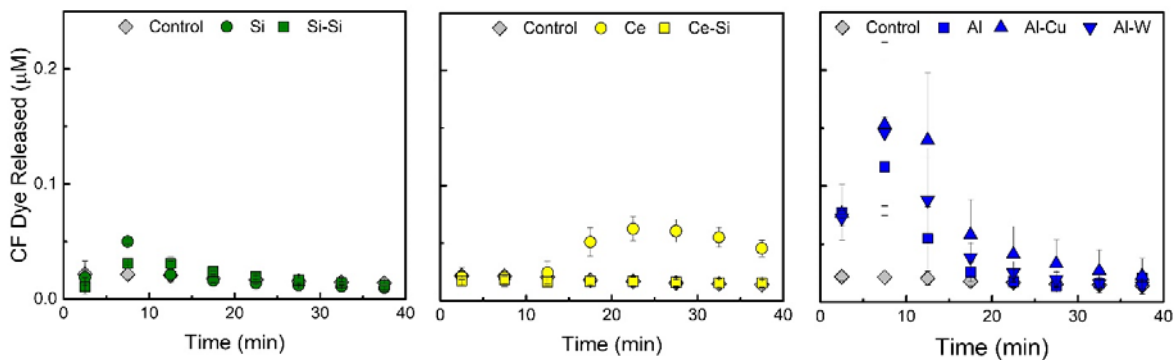


Figure 4.10. Carboxyfluorescein dye released from vesicles as a function of time over 40 minutes of nanoparticle exposure. Vesicles exposed to 500 mg/L silica, ceria, and alumina nanoparticles before (Si, Ce, and Al) and after (Si-Si, Ce-Si, Al-Cu, and Al-W) exposure to the CMP process and diluted in 150 mM NaCl and bicarbonate buffer (pH 7.4). QCM-D effluent collected over five-minute intervals. Data represents average and standard deviation of triplicate runs.

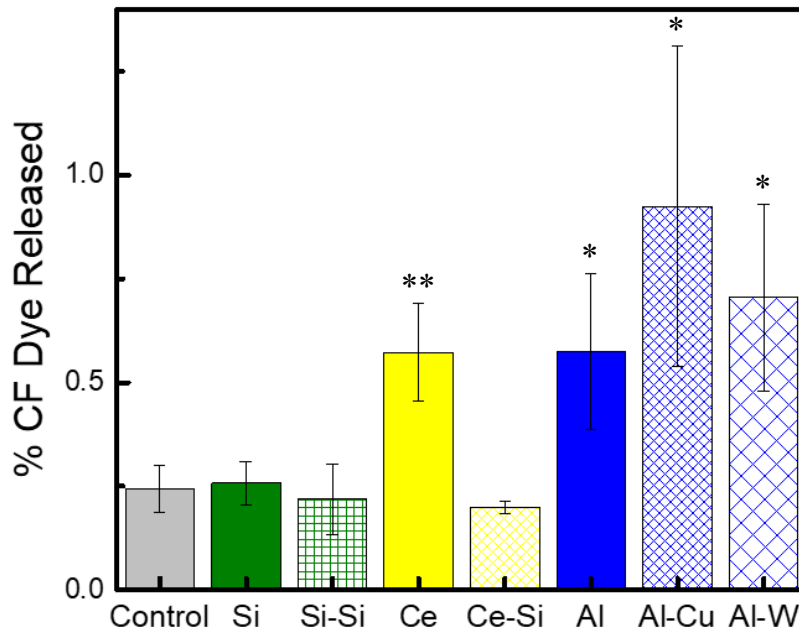


Figure 4.11. Percent of total carboxyfluorescein dye released from vesicles upon exposure to 500 mg/L silica, ceria, and alumina nanoparticles before (Si, Ce, and Al) and after (Si-Si, Ce-Si, Al-Cu, and Al-W) exposure to the CMP process and diluted in 150 mM NaCl and bicarbonate buffer (pH 7.4). Percentage represented by average and standard deviation of triplicate runs. Asterisk (*) indicates $p < 0.1$ and asterisks (**) indicate $p < 0.05$.

4.4.4 Implications for Cytotoxicity

While attachment did not cause substantial physical disruption of the phospholipid bilayer, the tendency of nanoparticles to adhere to the bilayer may still be relevant in predicting nanoparticle cytotoxicity. As discussed in the previous chapter, other common mechanisms of cytotoxicity, including the generation of reactive oxygen species (ROS), are made more potent through increased proximity to the cell. To include consideration of these mechanisms, our model membrane studies were compared with cell viability studies conducted by our collaborators. The IC_{50} concentrations for each nanoparticle and cell combination tested are provided in Table 4.2. No significant differences were observed in the IC_{50} values associated with pre and post-CMP nanoparticles.

Table 4.2. Concentrations at which 50% of cells were inhibited (IC₅₀) following 48 hours of exposure to silica, ceria, and alumina nanoparticles, before (Si, Ce, Al) and after (Si-Si, Ce-Si, Al-Cu) exposure to the CMP process. Values provided by Dr. Shyam Aravamudhan and Dr. Steven Crawford of North Carolina A&T State University.

NP Type	A549 Lung Epithelial	HepG2 Liver Epithelial	RAW 264.7 Macrophage
Si	0.54 g/L	0.22 g/L	0.28 g/L
Si-Si	0.62 g/L	0.25 g/L	0.38 g/L
Ce	> 2 g/L	> 2 g/L	> 2 g/L
Ce-Si	> 2 g/L	> 2 g/L	> 2 g/L
Al	> 10 g/L	4.2 g/L	5.8 g/L
Al-Cu	6.6 g/L	3.5 g/L	6.5 g/L

While the goal of this study was not to make concrete determinations regarding the cytotoxicity of these nanoparticles, we do observe fairly large IC₅₀ values. Silica nanoparticles, which showed the greatest tendency to attach to model cell membranes, was associated with the lowest IC₅₀ concentrations, ranging from 220-620 mg/L. Ceria and alumina nanoparticles, which showed very weak interactions with the SLBs, were associated with IC₅₀ concentrations greater than 2 g/L. Surface water concentrations, even in the event of an accidental spill, will be orders of magnitude less than 1 g/L [2]. While below current detection limits, alumina, silica, and ceria nanoparticles are predicted to be present in surface waters at concentrations in the range of 1-50 ng/L [51]. With respect to the inhalation exposure route, a study conducted by the National Institute of Occupational Health and Safety (NIOSH) found very low airborne concentrations of CMP nanoparticles even in the rooms where processing took place, with all except one measurement falling below detection limits [52]. Therefore, even workers taking part in the CMP process are not likely to inhale nanoparticles at concentrated levels.

4.5 Conclusions

In this study, an association was observed between the attachment of CMP nanoparticles to model cell membranes and the release of cytoplasmic enzymes from A549 lung epithelial cells. At concentrations ranging from 50-500 mg/L, SiO₂ nanoparticles showed significant attachment to SLBs and caused membrane damage to lung cells. CeO₂ and Al₂O₃ nanoparticles both demonstrated weak interactions with SLBs, likely due to the presence of stabilizing additives, and caused no significant membrane damage at the concentrations tested. These attachment studies also showed some relation to the cell viability assays. For all three cell lines tested, the IC₅₀ concentrations associated with SiO₂ nanoparticles were at least an order of magnitude less than those associated with CeO₂ and Al₂O₃ nanoparticles.

The applicability of the vesicle disruption tests to the cytotoxicity assays is harder to assess due to the weak signal of fluorescent dye released for all nanoparticles tested. As CeO₂ and Al₂O₃ nanoparticles showed weak interaction with the phospholipid bilayer, disruption of the vesicles was predictably insubstantial. The IC₅₀ concentrations associated with these nanoparticles were significantly greater than the concentrations tested in the model membrane studies. SiO₂ nanoparticles, which did have IC₅₀ concentrations in the model cell membrane test range, did not cause detectable vesicle disruption. However, the main mechanism attributed to SiO₂ nanoparticle toxicity is not physical damage, but ROS generation. In future work, a positive control with characterized physical membrane disruption should be included.

Exposure to the CMP process did not result in any changes that increased attachment or damage to model cell membranes, membrane damage to A549 lung

epithelial cells, or the viability of A549 lung epithelial cells, HepG2 liver epithelial cells, or RAW 264.7 macrophages. The only significant change observed was in ceria nanoparticles before and after polishing a SiO₂ wafer. Exposure to the post-CMP Ce-Si nanoparticles caused no detectable damage to the vesicles, while exposure to the pre-CMP Ce nanoparticles, at concentrations greater than 100 mg/L, did result in the release of a small fraction (<1%) of the dye contained within the vesicles. In this case, the polishing process resulted in nanoparticles less likely to puncture the phospholipid bilayer. Therefore, in this study, we did not observe any changes in nanoparticle behavior that indicate an increase in cytotoxicity due to exposure to the CMP process.

4.6 References

1. Pera, H., J.M. Kleijn, and F.A.M. Leermakers, *Interaction of silica nanoparticles with phospholipid membranes*. Chemistry Letters, 2012. **41**(10): p. 1322-1324.
2. Speed, D.E., *Environmental aspects of planarization processes*, in *Advances in Chemical Mechanical Planarization (CMP)*. 2016. p. 1-269.
3. Singh, R.K., et al., *Fundamentals of slurry design for CMP of metal and dielectric materials*. MRS Bulletin, 2002. **27**(10): p. 752-760+748.
4. Ilie, F. and G. Ipaté, *Chemical-mechanical impact of nanoparticles and pH effect of the slurry on the CMP of the selective layer surfaces*. Lubricants, 2017. **5**(2).
5. Speed, D., et al., *Physical, chemical, and in vitro toxicological characterization of nanoparticles in chemical mechanical planarization suspensions used in the semiconductor industry: Towards environmental health and safety assessments*. Environmental Science: Nano, 2015. **2**(3): p. 227-244.
6. Karimi, S., et al., *Acute and chronic toxicity to Daphnia magna of colloidal silica nanoparticles in a chemical mechanical planarization slurry after polishing a gallium arsenide wafer*. NanoImpact, 2019. **13**: p. 56-65.
7. Liu, X. and K.L. Chen, *Aggregation and interactions of chemical mechanical planarization nanoparticles with model biological membranes: Role of phosphate adsorption*. Environmental Science: Nano, 2016. **3**(1): p. 146-156.
8. Boyes, W.K., et al., *A comprehensive framework for evaluating the environmental health and safety implications of engineered nanomaterials*. Critical Reviews in Toxicology, 2017. **47**(9): p. 767-810.
9. Limbach, L.K., et al., *Removal of oxide nanoparticles in a model wastewater treatment plant: Influence of agglomeration and surfactants on clearing efficiency*. Environmental Science and Technology, 2008. **42**(15): p. 5828-5833.
10. Roth, G.A., N.M. Neu-Baker, and S.A. Brenner, *SEM analysis of particle size during conventional treatment of CMP process wastewater*. Science of the Total Environment, 2015. **508**: p. 1-6.
11. Karimi, S., et al., *Acute and chronic toxicity of metal oxide nanoparticles in chemical mechanical planarization slurries with Daphnia magna*. Environmental Science: Nano, 2018. **5**(7): p. 1670-1684.
12. Otero-González, L., et al., *Stability of alumina, ceria, and silica nanoparticles in municipal wastewater*. Water Science and Technology, 2014. **70**(9): p. 1533-1539.
13. Collins, A.R., et al., *High throughput toxicity screening and intracellular detection of nanomaterials*. Wiley Interdisciplinary Reviews: Nanomedicine and Nanobiotechnology, 2017. **9**(1).
14. Karlsson, H.L., M.S. Toprak, and B. Fadeel, *Toxicity of Metal and Metal Oxide Nanoparticles*, in *Handbook on the Toxicology of Metals: Fourth Edition*. 2015. p. 75-112.
15. Flaherty, N.L., et al., *Comparative analysis of redox and inflammatory properties of pristine nanomaterials and commonly used semiconductor manufacturing nano-abrasives*. Toxicology Letters, 2015. **239**(3): p. 205-215.
16. Crawford, S., *Cytotoxicity of Engineered Nanoparticles used in Industrial Processing*. 2019, Univeristy of North Carolina at Greensboro.

17. Karlsson, H.L., et al., *Cell membrane damage and protein interaction induced by copper containing nanoparticles-Importance of the metal release process*. Toxicology, 2013. **313**(1): p. 59-69.
18. Geiser, M., et al., *Ultrafine particles cross cellular membranes by nonphagocytic mechanisms in lungs and in cultured cells*. Environmental Health Perspectives, 2005. **113**(11): p. 1555-1560.
19. Leroueil, P.R., et al., *Wide varieties of cationic nanoparticles induce defects in supported lipid bilayers*. Nano Letters, 2008. **8**(2): p. 420-424.
20. Leroueil, P.R., et al., *Nanoparticle interaction with biological membranes: Does nanotechnology present a janus face?* Accounts of Chemical Research, 2007. **40**(5): p. 335-342.
21. Yuan, H., et al., *Variable nanoparticle-cell adhesion strength regulates cellular uptake*. Physical Review Letters, 2010. **105**(13).
22. He, X., et al., *Changing exposure media can reverse the cytotoxicity of ceria nanoparticles for Escherichia coli*. Nanotoxicology, 2012. **6**(3): p. 233-240.
23. Moghadam, B.Y., et al., *Role of nanoparticle surface functionality in the disruption of model cell membranes*. Langmuir, 2012. **28**(47): p. 16318-16326.
24. Nel, A.E., et al., *Understanding biophysicochemical interactions at the nano-bio interface*. Nature Materials, 2009. **8**(7): p. 543-557.
25. Chen, K.L. and G.D. Bothun, *Nanoparticles meet cell membranes: Probing nonspecific interactions using model membranes*. Environmental Science and Technology, 2014. **48**(2): p. 873-880.
26. Coxon, T.P., et al., *A versatile approach towards multivalent saccharide displays on magnetic nanoparticles and phospholipid vesicles*. Organic and Biomolecular Chemistry, 2015. **13**(43): p. 10751-10761.
27. Gal, N., et al., *Interaction of Size-Tailored PEGylated Iron Oxide Nanoparticles with Lipid Membranes and Cells*. ACS Biomaterials Science and Engineering, 2017. **3**(3): p. 249-259.
28. Zhang, X., et al., *Interactions of polymeric drug carriers with DDT reduce their combined cytotoxicity*. Environmental Pollution, 2018. **241**: p. 701-709.
29. Rodahl, M., et al., *Simultaneous frequency and dissipation factor QCM measurements of biomolecular adsorption and cell adhesion*. Faraday Discussions, 1997. **107**: p. 229-246.
30. Melby, E.S., et al., *Formation of supported lipid bilayers containing phase-segregated domains and their interaction with gold nanoparticles*. Environmental Science: Nano, 2016. **3**(1): p. 45-55.
31. Yousefi, N. and N. Tufenkji, *Probing the interaction between nanoparticles and lipid membranes by quartz crystal microbalance with dissipation monitoring*. Frontiers in Chemistry, 2016. **4**(DEC).
32. Chen, K.L. and M. Elimelech, *Aggregation and deposition kinetics of fullerene (C60) nanoparticles*. Langmuir, 2006. **22**(26): p. 10994-11001.
33. Chen, K.L. and M. Elimelech, *Interaction of fullerene (C60) nanoparticles with humic acid and alginate coated silica surfaces: Measurements, mechanisms, and environmental implications*. Environmental Science and Technology, 2008. **42**(20): p. 7607-7614.

34. Yi, P. and K.L. Chen, *Interaction of Multiwalled Carbon Nanotubes with Supported Lipid Bilayers and Vesicles as Model Biological Membranes*. Environmental Science & Technology, 2013. **47**(11): p. 5711-5719.
35. Goodman, C.M., et al., *Toxicity of gold nanoparticles functionalized with cationic and anionic side chains*. Bioconjugate Chemistry, 2004. **15**(4): p. 897-900.
36. Farrell, R.E., *Chapter 8 - Stringency: Conditions that Influence Nucleic Acid Structure*, in *RNA Methodologies (Fourth Edition)*, R.E. Farrell, Editor. 2010, Academic Press: San Diego. p. 173-178.
37. Covington, A.K. and R.A. Robinson, *References standards for the electrometric determination, with ion-selective electrodes, of potassium and calcium in blood serum*. Analytica Chimica Acta, 1975. **78**(1): p. 219-223.
38. Keller, C.A. and B. Kasemo, *Surface specific kinetics of lipid vesicle adsorption measured with a quartz crystal microbalance*. Biophysical Journal, 1998. **75**(3): p. 1397-1402.
39. Richter, R., A. Mukhopadhyay, and A. Brisson, *Pathways of Lipid Vesicle Deposition on Solid Surfaces: A Combined QCM-D and AFM Study*. Biophysical Journal, 2003. **85**(5): p. 3035-3047.
40. Paxton, W.F., et al., *Adsorption and fusion of hybrid lipid/polymer vesicles onto 2D and 3D surfaces*. Soft Matter, 2018. **14**(40): p. 8112-8118.
41. Pflücker, F., et al., *The outermost stratum corneum layer is an effective barrier against dermal uptake of topically applied micronized titanium dioxide*. International Journal of Cosmetic Science, 1999. **21**(6): p. 399-411.
42. Dussert, A.S., E. Gooris, and J. Hemmerle, *Characterization of the mineral content of a physical sunscreen emulsion and its distribution onto human stratum corneum*. International Journal of Cosmetic Science, 1997. **19**(3): p. 119-129.
43. Adachi, K., et al., *In vivo effect of industrial titanium dioxide nanoparticles experimentally exposed to hairless rat skin*. Nanotoxicology, 2010. **4**(3): p. 296-306.
44. Zvyagin, A.V., et al., *Imaging of zinc oxide nanoparticle penetration in human skin in vitro and in vivo*. Journal of Biomedical Optics, 2008. **13**(6).
45. Leite-Silva, V.R., et al., *The effect of formulation on the penetration of coated and uncoated zinc oxide nanoparticles into the viable epidermis of human skin in vivo*. European Journal of Pharmaceutics and Biopharmaceutics, 2013. **84**(2): p. 297-308.
46. Brahma, N. and J.B. Talbot, *Effects of CMP slurry additives on the agglomeration of alumina nanoparticles 1: General aggregation rate behavior*. Journal of Colloid and Interface Science, 2014. **419**: p. 56-60.
47. Broxton, P., et al., *Interaction of some polyhexamethylene biguanides and membrane phospholipids in Escherichia coli*. Journal of Applied Bacteriology, 1984. **57**(1): p. 115-124.
48. Qian, L., et al., *Modified guanidine polymers: Synthesis and antimicrobial mechanism revealed by AFM*. Polymer, 2008. **49**(10): p. 2471-2475.
49. Jiang, W., et al., *Effects of charge and surface defects of multi-walled carbon nanotubes on the disruption of model cell membranes*. Science of the Total Environment, 2017. **574**: p. 771-780.

50. Tu, Y., et al., *Destructive extraction of phospholipids from Escherichia coli membranes by graphene nanosheets*. Nature Nanotechnology, 2013. **8**(8): p. 594-601.
51. Westerhoff, P., et al., *Low risk posed by engineered and incidental nanoparticles in drinking water*. Nature Nanotechnology, 2018. **13**(8): p. 661-669.
52. Brenner, S.A., et al., *NIOSH field studies team assessment: Worker exposure to aerosolized metal oxide nanoparticles in a semiconductor fabrication facility*. Journal of Occupational and Environmental Hygiene, 2016. **13**(11): p. 871-880.

Chapter 5. Introduction to Water Filtration Membranes Modified with Silver Nanoparticles to Delay Biofouling

5.1 Low Pressure Membrane Systems

Low pressure membrane (LPM) systems have garnered attention due to their small footprint and their ability to provide high quality drinking water [1, 2]. Clean water is produced by these systems primarily through mechanical sieving as an applied pressure forces the influent water through the membrane, while solids, including bacteria and cysts, are rejected. Two streams result from this influent: a permeate stream with a lower concentration of total solids than the influent and a concentrate stream with a higher concentration of total solids. Membrane performance is often described in terms of permeate flux (J_w), or the rate of clean water production (Q [L/hr]) relative to the membrane area (A [m²]) (Equation 5.1).

Equation (5.1)
$$J_w = \frac{Q}{A}$$

The Surface Water Treatment Rule (1989) spurred growth of the LPM industry by requiring removal of chlorine resistant species like *Cryptosporidium* oocysts and *Giardia* cysts [3]. The LPM industry also experienced rapid growth in response to outbreaks of cryptosporidiosis in the 1990s [4]. In addition, LPMs are often used as a method of pretreatment for reverse osmosis (RO) systems as communities pursue previously inaccessible water sources through desalination and water reuse [3]. The global water production capacity of LPM systems increased by more than 3000 million gallons per day between 1995 and 2006 [4].

5.2 Biological Fouling in Membrane Systems

The most significant obstacle in long-term membrane use is membrane fouling. Membrane fouling occurs when particles and solutes in the feed solution accumulate and/or adsorb to the membrane surface, resulting in reduced membrane flux, decreased membrane life, and increased energy cost. Biofouling refers to the process in which bacteria contact the membrane surface, attach, form colonies, and produce viscous extracellular polymeric substances (EPS) [5]. The term “biofilm” describes the layer of bacteria embedded in EPS that forms. The EPS can be made up of many classes of organic macromolecules (e.g. humic acids, nucleic acids, lipids, uronic acids), but are primarily polysaccharides and proteins [6]. The expression of EPS components depends on both the specific bacterial community and the environmental conditions present [6]. Biofouling significantly reduces the energy efficiency of the treatment system as the viscoelastic properties of the EPS layer drastically increase the hydraulic resistance of the membrane [7, 8] In addition, biofilms are resistant to traditional membrane cleaning methods, as discussed in the next section. The biofilm’s intractability and deleterious effects on energy efficiency arguably make biofouling the most damaging form of membrane fouling [9].

5.3 Current Cleaning Methods

Fouling is reduced in LPM systems through backwashing, in which water is pushed backwards, from the permeate side of the membrane to the concentrate side. Reversible fouling refers to the fraction of fouling that can be physically removed by these hydrodynamic changes. The frequency and length of backwash varies between treatment plants and in accordance with the needs of each system. Porcelli and Jud

published a review of conventional cleaning methods based on data aggregated from 21 LPM treatment systems [10]. The backwashing frequency fell into the range of 5-96 treatments per day (median of 36 treatments per day) for a duration ranging from 10 seconds to 10 minutes (median of 77 seconds). This range reflects the variety of source water conditions, resulting in trial-and-error determination of optimal cleaning methods.

To remove irreversible fouling, backwashing is often used in combination with chemical treatment. Chemical treatment can include membrane exposure to alkaline (e.g. caustic soda), acidic (e.g. sulfuric acid, nitric acid, hydrochloric acid), oxidative (e.g. hypochlorite, hydrogen peroxide), surfactant (e.g. SDS), and chelating compounds (e.g. EDTA, citric acid) [10]. Alkaline cleaning agents break down weakly acidic organic matter, proteins, and polysaccharides [10]. Acidic reagents catalyze hydrolysis and remove multivalent cations [10]. Oxidation breaks down natural organic matter and inactivates bacteria [10]. Chelating compounds remove minerals and have been shown to hinder biofilm growth [10]. Chemically Enhanced Backflush (CEB), in which chemicals are added during backwash, is scheduled on a daily or weekly basis [10]. Cleaning In Place (CIP), a longer soaking process with higher chemical concentrations, is only scheduled when the rate of water production has fallen below acceptable levels [10]. However, changing the hydrodynamics of the system and treating the membrane chemically does not fully reverse membrane fouling. When irremovable fouling layers prevent CIP from recovering the desired flux, membranes must be replaced.

Biofilms are especially resistant to the cleaning measures implemented to reduce fouling. This resistance is not fully understood but is thought to be partially related to the restriction of chemical penetration as the agents react with the constituents of the biofilm

[11]. Several studies have investigated the effects of conventional cleaning methods on biofilm formation. Bereschenko et al. operated four high pressure stainless-steel flow cells containing RO membranes in parallel with a working RO treatment plant [12]. The plant operated using a cleaning method that exposed the biofilms to permeate from RO treatment, a biocide at basic pH, and a mixed acid detergent descaler, in that order. The pressure drop, or the pressure difference between feed and concentrate streams, was measured to indicate the performance of the membrane system, with a smaller pressure drop associated with higher system efficiency. Cleaning achieved reduction in the pressure drop and inactivation of bacteria. However, microscopy showed that EPS was not fully removed from the membrane surface and remained attached in a collapsed biofilm structure. This remaining EPS provided nutrients for any bacteria still surviving, leading to colony regrowth and reestablishment of a full biofilm within a week.

Baker and Dudley published a review of data collected from over a hundred RO membrane autopsies performed when membrane performance did not improve following cleaning [7]. These autopsies showed intractable biofouling layers with recalcitrant EPS. In addition, they showed that introducing chlorine into a system inactivates bacteria but can cause increased EPS production [7]. This increase in EPS production may be a defense mechanism enacted by bacteria that survive exposure to disinfectants. The failure of conventional cleaning methods to efficiently eliminate biofouling demonstrates the need for researchers to investigate other means of sustaining water production rates without increasing energy inputs.

5.4 Membrane Modification with Polydopamine

Surface modification is a strategy utilized by researchers to improve the resistance of polymeric membranes to bacterial attachment and biofilm formation. Dopamine is a chemical of interest in membrane modification due to the mild conditions under which it forms a hydrophilic and reactive coating. Dopamine contains amine and catechol groups, the same functional groups in the adhesive proteins excreted by mussels. These functional groups allow a coating to form on a wide array of materials, including metals, ceramics, and polymers [13]. While other surface modifications often require the application of pressure, heat, or light [14, 15], dopamine only requires a slightly basic solution and the presence of oxygen to polymerize and form a uniform polydopamine coating tens of nm thick [13]. Since Lee et al. first introduced polydopamine, several theories regarding its structure have been developed [13, 16-19]. Generally, polydopamine is believed to be a supramolecular aggregation of covalently linked dihydroxyindole oligomers of varying degrees of saturation as well as open-chain dopamine monomer units. Adhesion to nonpolar polymers, such as polysulfone, is thought to be the result of hydrophobic or Π - Π interactions [15]. Dopamine analogs, such as norepinephrine, have been developed, but the coating processes associated with these analogs are more complex and less controllable [15].

Hydrophilic surfaces like polydopamine are less prone to fouling than base polymeric membranes. This fouling resistance is attributed to the attraction between water molecules and the surface, creating an additional barrier to contaminant contact and subsequent attachment [14, 20]. The Freeman group at the University of Texas at Austin has looked extensively into applying the hydrophilic nature of polydopamine to organic

and biological membrane fouling control [21-24]. Araujo et al. conducted a 10-day biofouling study where researchers coated both the polysulfone membrane and the feed spacer with polydopamine [22]. This surface modification did not significantly decrease membrane biofouling, quantified as biomass accumulation on the membrane surface. The modification also failed to ameliorate the pressure increase that resulted from fouling. Miller et al. modified polysulfone ultrafiltration membranes with polydopamine and hydrophilic poly (ethylene glycol) and tested for both shorter-term and longer-term biofouling [23]. While modification was able to delay initial adhesion, the improvement in membrane performance was not sustained over the 10-day course of the experiment. McCloskey et al. modified reverse osmosis, nanofiltration, ultrafiltration, and microfiltration membranes with polydopamine to improve membrane performance during a 24-hour oil/water emulsion filtration [24]. They found that polydopamine modification increased permeate flux across all polymeric membrane types. Additional modification with poly (ethylene glycol) further increased flux, affecting microfiltration membranes most significantly. Kasemet et al. modified polyamide reverse osmosis membranes with polydopamine at different concentrations, deposition time, and initial pH [21]. All modifications resulted in increased permeate flux over 2 hours of oil/water emulsion filtration except for the modification conducted at acidic pH. Taken together, these results indicate that although hydrophilic polydopamine modifications may successfully delay organic fouling, this ability may not extend timescales enough to significantly improve treatment plant performance.

Finally, the reactivity of the polydopamine coating strengthens its appeal for use in membrane modification as it allows for the inclusion of additional anti-fouling

materials. The catechol groups contained in polydopamine react with thiol and amine groups, allowing for the addition of organic layers and functionalized polymers via Michael addition or Schiff base reactions [13]. For instance, antibacterial metallic nanoparticles like silver and copper can be incorporated into the polydopamine layer through reduction of their associated salts (i.e. silver nitrate and copper chloride) [13, 25]. Time-of-Flight Secondary Ion Mass Spectrometry (TOF-SIMS) and X-ray Photoelectron Spectroscopy (XPS) have been used to verify the presence of these metals on the polydopamine coating [13, 25-28]. Following silver nitrate exposure, Scanning Electron Microscopy (SEM) with Energy Dispersive X-ray (EDX) analysis revealed an even distribution of spherical silver nanoparticles, tens of nm in diameter, across the polydopamine surface [25, 27, 28]. Unlike other modifications that distribute additives throughout the membrane matrix, this process concentrates additives at the surface, where interaction with foulants takes place.

The ease with which antibacterial agents can be attached to a hydrophilic polydopamine coating makes this method attractive for creating anti-adhesive, antibacterial membrane surfaces. If bacteria are inactivated, they cannot proliferate and excrete the EPS that is primarily responsible for increasing membrane hydraulic resistance. Ye et al. utilized polydopamine to facilitate modification of RO thin film composite membranes with zwitterionic polymer brushes and quaternary ammonium salt brushes [29]. After three hours of exposure, the modification resulted in lower bacterial adhesion and increased bacterial inactivation, measured using a LIVE/DEAD fluorescent staining assay. Hegab et al. modified forward osmosis (FO) thin film composite membranes with polydopamine and graphene oxide and showed that under 24 hours of

constant pressure filtration, modification resulted in increased flux and decreased biofouling, quantified by the amount of adenosine triphosphate accumulated on the membrane surface [30]. The combination of anti-adhesive and anti-bacterial effects shows promise in reducing biofouling in membrane treatment applications.

The strong antibacterial properties of silver nanoparticles have made the combination polydopamine/silver modification particularly attractive [25-27, 31-35]. Discussed in more detail in the following chapter, previous work has demonstrated the ability of membranes modified with polydopamine and silver nanoparticles to resist foulant adhesion over the course of short-term (< 90 minute) filtration studies [27, 34]. Modification has also been demonstrated to be effective in decreasing the bacterial growth that develops on membrane surfaces following incubation with bacterial solutions [25-27, 32-34]. While several studies have investigated the anti-adhesive and antibacterial nature of membranes modified with polydopamine and silver nanoparticles, the methods used to demonstrate the ability of these modifications to delay biofouling are not uniform. In addition, they do not involve the applied pressure or extended periods of filtration that occur in membrane treatment plants and do not necessarily reflect long-term success in a treatment system [23].

5.4 Environmental Fate of Silver Nanoparticles

Silver nanoparticles used for membrane modification are predicted to slowly dissolve and move through wastewater treatment processes in the form of silver ions. However, given the possibility of a breakthrough event, the fate of silver nanoparticles in the treatment system is worth considering. Removal of silver nanoparticles by sedimentation has shown a wide range of efficacy. Li et al. looked at nine full-scale

wastewater treatment plants in Germany and found mechanical processes were responsible for removing 35% of influent silver nanoparticles [36]. A variety of lab-scale to full-scale studies have reported a wide range of removal efficiencies (10-95%) prior to biological treatment [37]. With regard to biological treatment, several studies investigating the silver nanoparticle content of microbial sludges found biosolids were able to contain more than 88% of influent nanoparticle concentrations [38]. However, the presence of silver nanoparticles can negatively impact biological treatment as concentrations as low as 0.05 mg/L have been shown to hinder the activity of nitrifying communities [39].

Silver nanoparticles have been detected in wastewater effluent and environmental waters at concentrations on the scale of ng/L [38]. In the environment, silver nanoparticles may dissolve, agglomerate into larger particles, or react to form new Ag products [40]. Silver can experience several reactions and is not expected to remain untransformed in surface waters. The sulfidation of silver will occur quickly, within the span of a few hours or days [41]. This transformation often occurs during wastewater treatment, as dissolved silver ions are exposed to reduced sulfur. In fact, the majority of silver nanoparticles will precipitate in the form of Ag_2S through the course of anaerobic wastewater treatment [42]. Ag_2S products are less soluble and toxic than silver nanoparticles [38]. Other common interactions include reactions with ozone to form aggregated Ag_2O_2 particles and with chloride to form AgCl particles [43]. Dissolution of silver nanoparticles under environmental conditions is slow, with the formation of surface layers like AgCl decreasing the dissolution rate even further [43, 44].

5.6 Silver Nanoparticle Toxicity

Exposure to silver nanoparticles can inactivate cells through oxidative stress, DNA damage, and apoptosis [45]. This toxicity is mainly associated with the large surface area of nanoparticles releasing high concentrations of toxic Ag^+ ions in close proximity to cells [46]. These ions will subsequently bind to ligands including thiol groups in structural and functional proteins, causing damage to the cell membrane and other cellular components [47, 48]. In addition, the release of silver ions has been associated with the generation of reactive oxygen species (ROS) and subsequent DNA damage. Silver nanotoxicity is size-dependent, with particles on the order of 10 nm producing the greatest levels of cellular inactivation [46]. Silver nanoparticles have been used in a variety of commercial products (e.g. food storage containers, clothing, and soaps) for their antibacterial functionality [49].

The *in vivo* toxicity of silver nanoparticles has been investigated in a few studies. Sung et al. found the no-observable-adverse-effects-level (NOAEL) in rats to be 100 $\mu\text{g}/\text{m}^3$ [50]. This study also determined that silver nanoparticles target the lungs and liver. However, Ag primarily passed through rat intestines in ion form. In another study involving rat exposures, Kim et al. found a NOAEL of 30 mg/kg following 90 days of ingestion, determining the liver as the target organ [51]. Munger et al. exposed humans to silver nanoparticles for a maximum of 14 days at an ingestion rate of 480 $\mu\text{g}/\text{day}$ [52], observing no significant effects in the lungs, heart, or abdominal organs. Therefore, they concluded that the human health risk posed by silver nanoparticle ingestion is low.

The EPA regulates the silver levels in drinking water through a secondary maximum contaminant level of 0.1 mg/L. Secondary standards are un-enforceable but

provide guidelines to avoid unwanted aesthetic effects. With regard to silver, this amounts to preventing argyria, a bluish-gray discoloration of the skin or eyes [46]. Argylial silver deposits can form as a result of the secondary particles produced following partial dissolution of Ag nanoparticles [47].

5.7 Summary

Membranes modified with polydopamine and silver nanoparticles may be less prone to fouling in water treatment systems due to their proven hydrophilic and anti-bacterial nature. However, literature previously published evaluating these membranes has focused on short-term modification effects, despite evidence that these effects cannot be extrapolated to improvements in longer term membrane performance. To determine the benefits of this membrane modification in real treatment systems, membranes modified with polydopamine and silver nanoparticles must be evaluated under longer time periods in which biofilms are allowed to form. This work will investigate initial bacterial adhesion to the membrane surface, longer term biofilm development, and silver leaching, to assess the effects of modifying low pressure polymeric membranes with polydopamine and silver nanoparticles.

5.8 References

1. Huang, H., K. Schwab, and J.G. Jacangelo, *Pretreatment for low pressure membranes in water treatment: a review*. Environ Sci Technol, 2009. **43**(9): p. 3011-9.
2. Geise, G.M., et al., *Water purification by membranes: The role of polymer science*. Journal of Polymer Science, Part B: Polymer Physics, 2010. **48**(15): p. 1685-1718.
3. Mallevalle, J., et al., *Water treatment membrane processes*. 1996, New York, NY: McGraw-Hill.
4. Furukawa, D.H., *NWRI Final Project Report: a Global Perspective of Low Pressure Membranes*. 2008.
5. Gijssbertsen-Abrahamse, A.J., E.R. Cornelissen, and J.A.M.H. Hofman, *Fiber failure frequency and causes of hollow fiber integrity loss*. Desalination, 2006. **194**(1-3): p. 251-258.
6. Lin, H., et al., *A critical review of extracellular polymeric substances (EPSs) in membrane bioreactors: Characteristics, roles in membrane fouling and control strategies*. Journal of Membrane Science, 2014. **460**: p. 110-125.
7. Baker, J.S. and L.Y. Dudley, *Biofouling in membrane systems — A review*. Desalination, 1998. **118**(1-3): p. 81-89.
8. Herzberg, M. and M. Elimelech, *Biofouling of reverse osmosis membranes: Role of biofilm-enhanced osmotic pressure*. Journal of Membrane Science, 2007. **295**(1-2): p. 11-20.
9. Huisman, I.H. and K. Williams, *Autopsy and failure analysis of ultrafiltration membranes from a waste-water treatment system*. Desalination, 2004. **165**(1-3): p. 161-164.
10. Porcelli, N. and S. Judd, *Chemical cleaning of potable water membranes: A review*. Separation and Purification Technology, 2010. **71**(2): p. 137-143.
11. Bridier, A., et al., *Resistance of bacterial biofilms to disinfectants: a review*. Biofouling, 2011. **27**(9): p. 1017-1032.
12. Bereschenko, L.A., et al., *Effect of conventional chemical treatment on the microbial population in a biofouling layer of reverse osmosis systems*. Water Research, 2011. **45**(2): p. 405-416.
13. Lee, H., et al., *Mussel-inspired surface chemistry for multifunctional coatings*. Science, 2007. **318**(5849): p. 426-430.
14. Kochkodan, V. and N. Hilal, *A comprehensive review on surface modified polymer membranes for biofouling mitigation*. Desalination, 2015. **356**: p. 187-207.
15. Yang, H.C., et al., *Surface engineering of polymer membranes via mussel-inspired chemistry*. Journal of Membrane Science, 2015. **483**: p. 42-59.
16. Chen, C.T., et al., *Polydopamine and eumelanin molecular structures investigated with ab initio calculations*. Chemical Science, 2017. **8**(2): p. 1631-1641.
17. Dreyer, D.R., et al., *Elucidating the structure of poly(dopamine)*. Langmuir, 2012. **28**(15): p. 6428-6435.

18. Hong, S., et al., *Non-Covalent Self-Assembly and Covalent Polymerization Co-Contribute to Polydopamine Formation*. *Advanced Functional Materials*, 2012. **22**(22): p. 4711-4717.
19. Liebscher, J., et al., *Structure of polydopamine: A never-ending story?* *Langmuir*, 2013. **29**(33): p. 10539-10548.
20. Kim, S.H., et al., *Design of TiO₂ nanoparticle self-assembled aromatic polyamide thin-film-composite (TFC) membrane as an approach to solve biofouling problem*. *Journal of Membrane Science*, 2003. **211**(1): p. 157-165.
21. Kasemset, S., et al., *Effect of polydopamine deposition conditions on fouling resistance, physical properties, and permeation properties of reverse osmosis membranes in oil/water separation*. *Journal of Membrane Science*, 2013. **425-426**: p. 208-216.
22. Araujo, P.A., et al., *Impact of feed spacer and membrane modification by hydrophilic, bactericidal and biocidal coating on biofouling control*. *Desalination*, 2012. **295**: p. 1-10.
23. Miller, D.J., et al., *Short-term adhesion and long-term biofouling testing of polydopamine and poly(ethylene glycol) surface modifications of membranes and feed spacers for biofouling control*. *Water Research*, 2012. **46**(12): p. 3737-3753.
24. McCloskey, B.D., et al., *A bioinspired fouling-resistant surface modification for water purification membranes*. *Journal of Membrane Science*, 2012. **413-414**: p. 82-90.
25. Sureshkumar, M., P.N. Lee, and C.K. Lee, *Stepwise assembly of multimetallic nanoparticles via self-polymerized polydopamine*. *Journal of Materials Chemistry*, 2011. **21**(33): p. 12316-12320.
26. Yang, H., et al., *Polydopamine-coated nanofibrous mats as a versatile platform for producing porous functional membranes*. *Journal of Materials Chemistry*, 2012. **22**(33): p. 16994-17001.
27. Tang, L., K.J.T. Livi, and K.L. Chen, *Polysulfone Membranes Modified with Bioinspired Polydopamine and Silver Nanoparticles Formed in Situ To Mitigate Biofouling*. *Environmental Science & Technology Letters*, 2015. **2**(3): p. 59-65.
28. Wang, W., et al., *Preparation and characterization of polystyrene/Ag core-shell microspheres - A bio-inspired poly(dopamine) approach*. *Journal of Colloid and Interface Science*, 2012. **368**(1): p. 241-249.
29. Ye, G., et al., *Controlled Architecture of Dual-Functional Block Copolymer Brushes on Thin-Film Composite Membranes for Integrated "Defending" and "Attacking" Strategies against Biofouling*. *Acs Applied Materials & Interfaces*, 2015. **7**(41): p. 23069-23079.
30. Hegab, H.M., et al., *Effective in-situ chemical surface modification of forward osmosis membranes with polydopamine-induced graphene oxide for biofouling mitigation*. *Desalination*, 2016. **385**: p. 126-137.
31. Liu, Z. and Y. Hu, *Sustainable Antibiofouling Properties of Thin Film Composite Forward Osmosis Membrane with Rechargeable Silver Nanoparticles Loading*. *ACS Appl Mater Interfaces*, 2016. **8**(33): p. 21666-73.
32. Yang, Z., et al., *In Situ Reduction of Silver by Polydopamine: A Novel Antimicrobial Modification of a Thin-Film Composite Polyamide Membrane*. *Environ Sci Technol*, 2016. **50**(17): p. 9543-50.

33. Zhang, R.N., et al., *Manipulating the multifunctionalities of polydopamine to prepare high-flux anti-biofouling composite nanofiltration membranes*. Rsc Advances, 2016. **6**(39): p. 32863-32873.
34. Huang, L.C., et al., *In situ immobilization of silver nanoparticles for improving permeability, antifouling and anti-bacterial properties of ultrafiltration membrane*. Journal of Membrane Science, 2016. **499**: p. 269-281.
35. Yang, E., et al., *Concurrent performance improvement and biofouling mitigation in osmotic microbial fuel cells using a silver nanoparticle-polydopamine coated forward osmosis membrane*. Journal of Membrane Science, 2016. **513**: p. 217-225.
36. Li, L., et al., *Quantification of nanoscale silver particles removal and release from municipal wastewater treatment plants in Germany*. Environmental Science and Technology, 2013. **47**(13): p. 7317-7323.
37. Zhang, C., et al., *Governing factors affecting the impacts of silver nanoparticles on wastewater treatment*. Science of the Total Environment, 2016. **572**: p. 852-873.
38. Siripattanakul-Ratpukdi, S. and M. Fürhacker, *Review: Issues of silver nanoparticles in engineered environmental treatment systems*. Water, Air, and Soil Pollution, 2014. **225**(4).
39. Choi, O. and Z. Hu, *Size dependent and reactive oxygen species related nanosilver toxicity to nitrifying bacteria*. Environmental Science and Technology, 2008. **42**(12): p. 4583-4588.
40. De Marchi, L., et al., *Engineered nanomaterials: From their properties and applications, to their toxicity towards marine bivalves in a changing environment*. Environmental Research, 2019. **178**.
41. Thalmann, B., et al., *Sulfidation kinetics of silver nanoparticles reacted with metal sulfides*. Environmental Science and Technology, 2014. **48**(9): p. 4885-4892.
42. Kaegi, R., et al., *Behavior of metallic silver nanoparticles in a pilot wastewater treatment plant*. Environmental Science and Technology, 2011. **45**(9): p. 3902-3908.
43. Troester, M., H.J. Brauch, and T. Hofmann, *Vulnerability of drinking water supplies to engineered nanoparticles*. Water Research, 2016. **96**: p. 255-279.
44. Dwivedi, A.D., et al., *Fate of engineered nanoparticles: Implications in the environment*. Coordination Chemistry Reviews, 2015. **287**: p. 64-78.
45. Kim, S. and D.Y. Ryu, *Silver nanoparticle-induced oxidative stress, genotoxicity and apoptosis in cultured cells and animal tissues*. Journal of Applied Toxicology, 2013. **33**(2): p. 78-89.
46. Karlsson, H.L., M.S. Toprak, and B. Fadeel, *Toxicity of Metal and Metal Oxide Nanoparticles*, in *Handbook on the Toxicology of Metals: Fourth Edition*. 2015. p. 75-112.
47. Liu, J., et al., *Chemical transformations of nanosilver in biological environments*. ACS Nano, 2012. **6**(11): p. 9887-9899.
48. Kędziora, A., et al., *Similarities and differences between silver ions and silver in nanoforms as antibacterial agents*. International Journal of Molecular Sciences, 2018. **19**(2).

49. McGillicuddy, E., et al., *Silver nanoparticles in the environment: Sources, detection and ecotoxicology*. Science of the Total Environment, 2017. **575**: p. 231-246.
50. Sung, J.H., et al., *Subchronic inhalation toxicity of silver nanoparticles*. Toxicological Sciences, 2009. **108**(2): p. 452-461.
51. Kim, Y.S., et al., *Subchronic oral toxicity of silver nanoparticles*. Particle and Fibre Toxicology, 2010. **7**.
52. Munger, M.A., et al., *In vivo human time-exposure study of orally dosed commercial silver nanoparticles*. Nanomedicine: Nanotechnology, Biology, and Medicine, 2014. **10**(1): p. 1-9.

Chapter 6. Modifying Water Purification Membranes with Bioinspired Polydopamine and Silver Nanoparticles for Biofilm Prevention³

6.1 Abstract

Low pressure membranes provide high-quality water through physical removal of bacteria, cysts, and particles. Bacteria attach to the membrane surface and form biofilms that reduce energy efficiency and increase the frequency of membrane replacement. Modifying membranes with polydopamine, a chemical mimic of the adhesive proteins that mussels release, has the potential to delay biofilm formation. Dopamine polymerizes under mild conditions, forming a coating that is of interest in membrane applications due to its hydrophilic and reactive nature. Compared to hydrophobic base membranes, hydrophilic surfaces are resistant to bacterial attachment. In addition, when polydopamine is exposed to silver nitrate, a reduction reaction takes place that embeds antimicrobial silver nanoparticles into the polydopamine layer. This study paired short-term deposition experiments with longer-term filtration experiments to determine the efficacy of this modification when challenged with *Pseudomonas aeruginosa*. Modification with polydopamine resulted in an average 48% reduction in the initial deposition rate of *P. aeruginosa*. However, the hydrophilicity of the polydopamine layer did not have a significant impact on membrane performance over 3 days of

³ This chapter has been published as Fleming, M.L., Bouwer, E., Chen, K.L. “Biofouling response of laboratory-scale polysulfone membranes modified with bioinspired polydopamine and silver nanoparticles” *Environmental Engineering Science*, 36, 335-343, 2019. Dr. Kai Loon Chen and Dr. Ed Bouwer provided guidance on experimental methodology and data interpretation as well as editorial suggestions.

bacterial filtration. Only the combination of both polydopamine and silver nanoparticles improved the rate of water production, with an average flux 1.7 times greater than that of the unmodified membrane. Confocal microscopy revealed heterogeneous bacterial growth on all membrane types with a lack of association between membrane performance and biofilm structure. Modifying membranes with polydopamine and silver nanoparticles has the potential to ameliorate the effects of biofouling, thereby increasing the efficiency of membrane water treatment.

6.2 Introduction

As current water infrastructure ages and regional water shortages become more severe, we need alternative treatment technologies to safeguard our water supply. Low pressure membrane systems hold promise, requiring less land area and producing higher quality water than traditional water treatment systems [1-4]. With high removal of turbidity, bacteria, and cysts, membrane systems produce water that meets increasingly stringent quality standards [5]. The largest challenge to the long-term use of low pressure membranes is biofouling [6]. Biofouling is the process in which bacteria adhere to the membrane surface, proliferate, and excrete extracellular polymeric substances, forming a biofilm [7]. Biofilms significantly decrease the energy efficiency of the treatment system and are resistant to traditional cleaning methods [8].

Membrane modification can delay biofouling by altering the interactions between the membrane surface and the bacteria in the feed solution [9]. Dopamine is a chemical used for membrane modification that mimics the behavior of the adhesive proteins released by mussels, a bivalve mollusk. Mussels are known for their ability to stick to a wide range of materials due to the presence of catechol and amine groups in their

adhesive proteins [10]. Dopamine is the simplest compound containing these same functional groups [11] and polymerizes under mild conditions, requiring only the presence of oxygen and a pH slightly above neutral [10]. When dopamine polymerizes, it forms a thin coating (tens of nm) on any exposed surface [10]. Several theories have been developed regarding the reactions involved in the polymerization process [10-14]. Once polymerized, this coating, like its biological inspiration, adheres to a wide array of materials, including metals, semiconductors, ceramics, and polymers [10]. Dopamine deposition is uniform and can be regulated using dopamine concentration, deposition time, pH, and oxygen availability [15, 16].

Polydopamine modification is of interest in membrane applications as base polymeric membranes are hydrophobic, while the thin polydopamine coating is hydrophilic [17-23]. Hydrophilic materials are less prone to organic and biological fouling as they form hydrogen bonds with water molecules, tightly binding a layer of water to the membrane surface and resulting in reduced foulant adsorption [9, 24]. In addition, the polydopamine coating is reactive and can be used as a glue to attach materials to the membrane surface. Upon exposure to polydopamine, metallic salts like silver nitrate and copper (II) chloride are reduced and their associated metallic nanoparticles are embedded in the polydopamine layer [10, 25]. The hydrophilic/antibacterial pairing of polydopamine and silver nanoparticles has been of specific interest due to the high antimicrobial activity of silver ions. A modified membrane that has a hydrophilic, antimicrobial nature has the potential to both delay initial deposition of bacteria and inactivate bacteria that deposit, thereby preventing biofilm development. Methods of evaluating the anti-adhesive and antibacterial effects of

these membranes vary widely across groups with most studies focusing on short-term impacts.

Although previous publications have addressed the effects of membrane modification with polydopamine and silver nanoparticles on bacterial attachment and survival upon exposure [18-23], to our knowledge, studies that bridge the gap to applied use in a constant pressure system have not been conducted. The purpose of this paper is to provide an understanding of how modifying low pressure membranes with polydopamine and silver nanoparticles affects membrane performance. Through direct observation experiments, we quantified the initial rate of bacterial deposition onto the membrane surface. Through biofilm formation experiments, we simulated the conditions of a working treatment system and determined how modification affected flux decline in a constant pressure system. Finally, we used confocal microscopy to characterize biofilms formed in the system to assess how modification affected biofilm development. By pairing short and longer-term experimental methods, we elucidated the effects of modifying polysulfone ultrafiltration membranes with polydopamine and silver nanoparticles on biofouling.

6.3 Materials and Methods

6.3.1 Membrane Fabrication and Modification

Polysulfone membranes were made using the wet phase inversion method [26]. Polysulfone beads (15 wt %, Udel P3500; Solvay Advanced Polymers) were dissolved with LiCl in 1-methyl-2-pyrrolidone (NMP) at 55° C. For the biofilm formation experiments, the percentage of LiCl was increased (3.5 wt %) to increase porosity and permeate flux. This increase in initial flux was sought to better demonstrate the flux

decline over time. Once the polysulfone and LiCl dissolved, the solution was allowed to degas for at least 72 hours. The solution was then spread over a glass plate with a casting knife (Elcometer 3530/5 Adjustable Baker Film Applicator, Elcometer Limited) at a gate height of 50 μm . The glass plate was submerged in deionized (DI) water, resulting in the formation of a membrane sheet ca. 50 μm thick.

For polydopamine (PD) modification, the membrane was secured in a polycarbonate flow cell (90 mm \times 38 mm \times 2 mm), active-side facing solution. A solution of 1 g/L dopamine hydrochloride (Sigma-Aldrich) dissolved in Trizma hydrochloride (Sigma-Aldrich) buffer (pH 8.5) was pumped through the flow cell and recirculated for 6 hours at a rate of 10 cm/s. Dopamine polymerized and formed a thin PD coating on the membrane surface. Following PD modification, the membrane was removed from the flow cell and rinsed with DI water. To incorporate silver nanoparticles into the PD coating (PD/Ag), the PD modified membrane was exposed to 50 mM AgNO_3 for two hours and then rinsed with DI water. Membranes prepared according to these methods have previously been characterized [18]. The PD/Ag coating was verified through elemental analysis with X-ray photoelectron spectroscopy and energy-dispersive X-ray spectroscopy. In addition, the distribution of silver nanoparticles on the membrane surface was shown using scanning electron microscopy.

6.3.2 Preparation of Bacterial Solution

The bacterial species *Pseudomonas aeruginosa PA01* was chosen for its ubiquity in the environment and its tendency to form biofilms. The species used in this study also has carbenicillin resistance which was used to prevent the growth of other organisms. The *P. aeruginosa* is labeled with green fluorescent protein. Bacterial solutions were prepared

by streaking *P. aeruginosa* onto an agar plate and leaving the plate overnight in an incubator at 30° C. A single colony was taken from the agar plate and transferred to LB Broth, Miller (Fisher Scientific) with 150 mg/L carbenicillin. The LB media was then left overnight in an incubator at 30° C. The next day, an aliquot of this overnight solution was pipetted into fresh LB media with 150 mg/L carbenicillin. When this bacterial solution reached the stationary growth phase (optical density = 0.8), it was removed from the incubator and washed [18]. The bacterial solution was centrifuged at 4,300 rpm for 10 minutes followed by resuspension in 154 mM NaCl. The solution was centrifuged and resuspended twice more. Finally, the solution was resuspended in 10 mM NaCl and adjusted to an optical density of 1.0 [27].

6.3.3 Direct Observation System

The short-term system (Figure 6.1) was used to characterize the attraction between bacteria in the feed solution and the membrane surface [18]. A 10 mM NaCl solution adjusted to pH 7 using NaHCO₃ was pumped from a pressurized feed tank through a flow cell holding the membrane. The system recirculates both the crossflow and permeate streams back to the feed tank. The flow cell was secured on the stage of an epifluorescence microscope (Nikon Eclipse E600W). The washed bacterial solution was injected into the feed tank, resulting in a system cell concentration of ca. 10⁵ cells/L. The crossflow rate, permeate flow rate, and pressure were maintained at 10 cm/s, 26 μm/s, and 20 psi, respectively. As the bacterial solution circulated through the system, cells deposited on the membrane surface. Pictures of the membrane surface were taken with IPLab software every 2 to 3 minutes for 20 minutes. The bacteria in each picture were counted using ImageJ software and the number of cells deposited were plotted as a

function of time. The slope of the resulting line was normalized by the initial cell concentration in the feed and the membrane surface area under the microscope ($870 \mu\text{m} \times 729 \mu\text{m}$) to calculate the initial deposition rate.

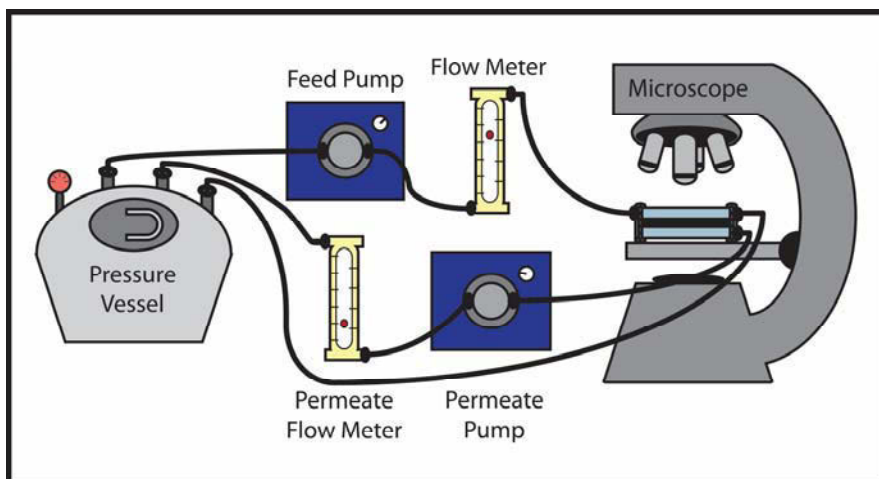


Figure 6.1. Direct observation system schematic. The system is pressurized to 20 psi. Bacterial feed solution in the pressure vessel is pumped through a flow meter and a polycarbonate flow cell set on the stage of a fluorescent microscope. The polycarbonate flow cell holds the membrane. The crossflow stream runs over the surface of the membrane, while the permeate stream passes through the membrane. Both the crossflow and permeate streams are recirculated to the pressure vessel.

6.3.4 Biofilm Formation System

The biofilm formation system (Figure 6.2) contains a feed tank, a pump, a flow cell containing the membrane, and crossflow and permeate lines recirculating solution back into the feed tank. The system was cleaned before and after each experiment using the method described by Kwan et al. [28]. 15% bleach was circulated for 30 minutes followed by two 10 minute rinses with DI water. Then, 5 mM EDTA adjusted to pH 11 was circulated for 30 minutes followed by two 10 minute rinses with DI water. Finally, 95% ethanol was circulated for 60 minutes followed by three 10 minute rinses with DI water. Following cleaning, the membrane was secured in the flow cell, and the pressure

and crossflow velocity were set at 25 psi and 8.5 cm/s, respectively. The membrane was subjected to compaction for at least 19 hours using 3 L of 200 mg/L NaN_3 . After compaction, the solution was replaced with 5 L of high nutrient synthetic wastewater to promote bacterial growth. The synthetic wastewater consisted of 0.6 mM $\text{Na}_3\text{C}_6\text{H}_5\text{O}_7$, 0.4 mM NH_4Cl , 0.2 mM KH_2PO_4 , 0.2 mM CaCl_2 , 0.5 mM NaHCO_3 , 8 mM NaCl , and 0.15 mM MgSO_4 [28]. The system was equilibrated for at least 5 hours before bacterial addition. The pressure was then decreased to 5 psi, resulting in an initial flux of $37 \text{ Lm}^{-2}\text{h}^{-1} \pm 9.7 \text{ Lm}^{-2}\text{h}^{-1}$ ($1.2 \text{ mL/min} \pm 0.3 \text{ mL/min}$). Initial flux was uncorrelated with membrane type and membrane performance. The washed bacteria were injected into the system resulting in a cell concentration of ca. 10^5 cells/mL. To determine permeate flux at a time point, the permeate stream was collected for three minutes and weighed. Then, the weight was converted into a volume and divided by the filtration area (membrane area) and the filtration time (3 minutes). The same experiment was run without the addition of bacteria to isolate the effects of biofouling on membrane flux.

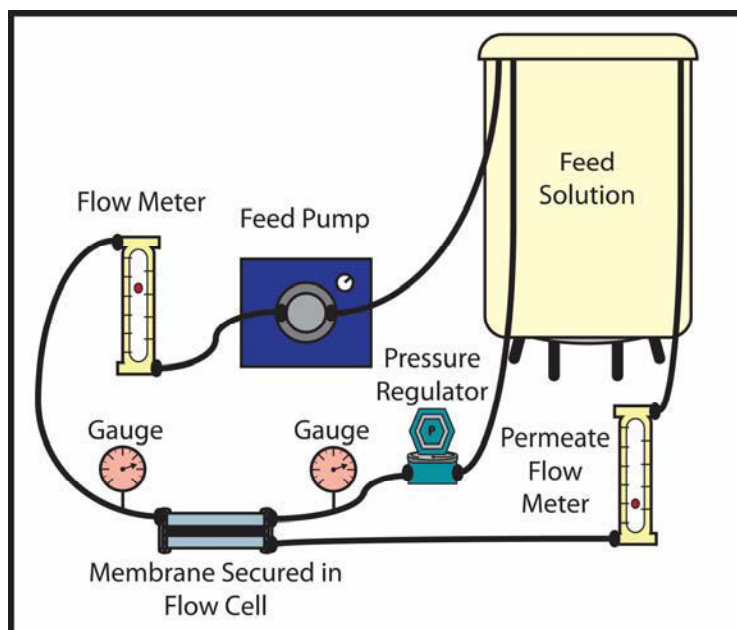


Figure 6.2. Biofilm formation system schematic. The system is pressurized to 5 psi, maintained using a pressure regulator and two pressure gauges. Bacterial feed solution is pumped through a flow meter and a polycarbonate flow cell which holds the membrane. The crossflow stream runs over the surface of the membrane, while the permeate stream passes through the membrane. Both the crossflow and permeate streams are recirculated to the feed solution container.

6.3.5 Silver Leaching

To determine the extent of silver leaching from the PD/Ag modified membranes over the period of compaction (ca. 19 hours of recirculating 3 L of 200 mg/L NaN_3) and the period of bacterial filtration (72 hours of recirculating 5 L of high nutrient synthetic wastewater), ca. 40 mL of the feed solution was collected and tested for dissolved silver using inductively coupled mass spectrometry (ICP-MS, PerkinElmer ELAN DRC II). The samples were filtered through a 0.2 μm polysulfone membrane (PALL Corporation) and acidified to a 2% HNO_3 concentration prior to ICP-MS analysis. Silver dissolution rate was calculated by dividing the mass of silver dissolved by the total membrane area and the time of exposure.

6.3.6 Biofilm Imaging

Following membrane performance evaluation in the biofilm formation system, membranes were removed from the flow cells. The membranes were stained with SYTO 9, propidium iodide (Live/Dead Biofilm Viability Kit, Invitrogen), and concanavalin A (Con A, Alexa Fluor 633, Invitrogen) to visualize live cells, dead cells, and extracellular polysaccharides, respectively. The biofilm was set in place using VectaShield Mounting Medium (Vector Laboratories). In addition, imaging spacers (Grace Bio-labs) were set between the glass slide and cover slip to protect the sample from compression. These samples were then imaged with a Zeiss LSM 510 Multiphoton Confocor 3 laser scanning microscope under a 40x objective. Image stacks (between 3 and 9 per membrane sample) were taken at an interval of 2 μm and analyzed using COMSTAT 2 to quantify biomass accumulation [29].

6.4 Results and Discussion

6.4.1 Direct Observation System

Figure 6.3a shows the number of bacteria depositing on base, PD modified, and PD/Ag modified membranes over a period of 20 minutes. PD modification decreased the initial rate of bacterial deposition by 48% while the PD/Ag modification decreased the rate by 38% (Figure 6.3b). The deposition rates associated with the two modifications were not significantly different at the 95% confidence level, but both modifications resulted in a substantial decline in initial bacterial adhesion compared to the unmodified membrane. The lack of distinction between the PD modification and the PD/Ag modification shows that the hydrophilic PD layer is likely responsible for delaying initial

bacterial attachment and is not significantly impacted by the additional incorporation of silver nanoparticles.

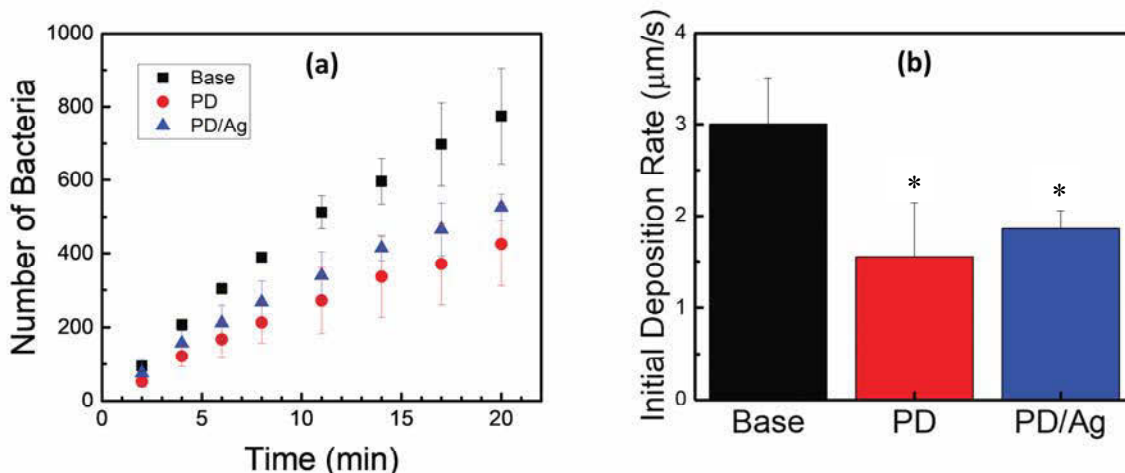


Figure 6.3. (a) Number of bacteria deposited on base polysulfone, PD modified, and PD/Ag modified membranes over 20 minutes of filtration through the direct observation system. Data represent average and standard deviation of triplicate experiments. (b) Initial deposition rate of *P. aeruginosa* onto base polysulfone, PD modified, and PD/Ag modified membranes. Rate calculated by normalizing the initial slopes presented in (a) by the membrane area ($870 \mu\text{m} \times 729 \mu\text{m}$) and the concentration of bacteria in the feed solution (ca. 10^5 cells/L). Asterisk (*) indicates $p < 0.025$.

This finding is consistent with the literature that has investigated the anti-adhesive nature of PD/Ag modified membranes by quantifying the attraction between the membrane surface and proteins or bacteria. Huang et al. modified polysulfone ultrafiltration membranes with PD/Ag and characterized their performance during a 70-minute lab scale filtration of bovine serum albumin (BSA) solution [22]. Modification increased water flux and demonstrated a small increase in BSA rejection. Our previous work also showed that PD/Ag modification decreased initial deposition of *Escherichia coli* over a period of twenty minutes [18]. Consequently, over short-term exposures,

membranes modified with PD/Ag have demonstrated increased resistance to foulant adhesion.

6.4.2 Biofilm Formation System

Figure 6.4 shows the decline in membrane permeate flux over three days of *P. aeruginosa* filtration. The rate of water filtering through the base, PD modified, and PD/Ag modified membranes decreased to 18%, 28%, and 33% of the initial values, respectively. These flux losses can be attributed to biofouling as the base membrane used in the control experiment retained 98% of the initial flux (data not shown). The flux of the base and PD/Ag modified membranes were consistently significantly different throughout filtration ($p < 0.1$). From hours 19-72 of filtration, the flux of the PD/Ag modified membrane remained between 1.77 and 1.98 times greater than that of the unmodified membrane. PD modification by itself, however, did not result in significantly improved membrane performance compared to base membranes. The anti-adhesive nature of PD, therefore, was not enough to significantly alter the effects of biofouling on the membrane surface. The additional modification with antimicrobial silver nanoparticles was required to see an improvement in membrane performance.

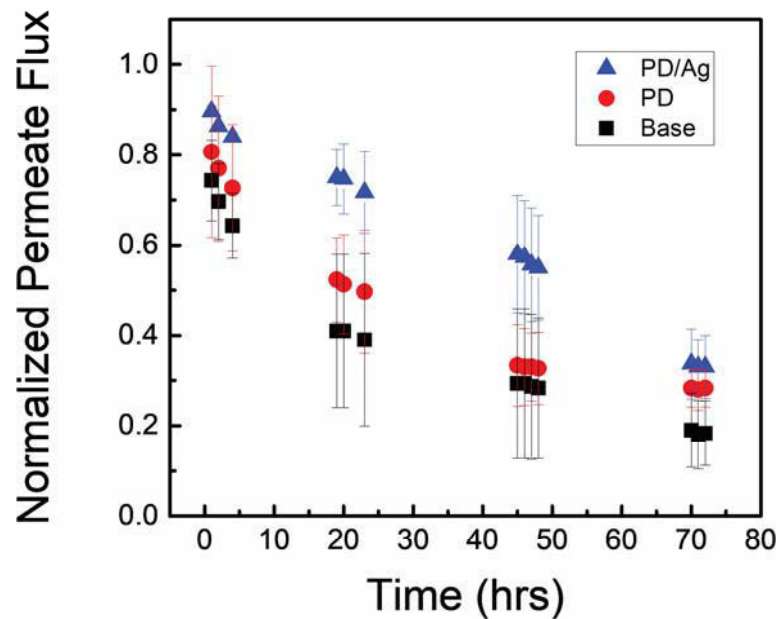


Figure 6.4. Flux decline over three days of *P. aeruginosa* filtration in the biofilm formation system through base, PD modified, and PD/Ag modified membranes. Flux measured by weighing the output of the permeate stream collected over a period of three minutes and converting to a flow rate. Data represent average and standard deviation of triplicate experiments.

This inconsistency in the results of the short and long-term tests supports previous assertions that while hydrophilic membrane modifications can delay initial fouling, they do not provide sufficient protection over longer filtration periods [30, 31]. Throughout the literature, hydrophilicity is shown to be one of the primary surface characteristics influencing bacterial adhesion [2, 32, 33]. However, Xu et al. showed that the improvement in temperature corrected specific flux provided by a hydrophilic, neutral surface was only exhibited during the initial stages of fouling (< 48 hours) [31]. After the initial stages, all membrane types were subject to flux decline due to bacterial attachment. Miller et al. also found a discrepancy in the impact of hydrophilic modifications on membrane efficiency over short-term and long-term periods of filtration [30]. While the PD and poly (ethylene glycol) modification delayed adhesion after 1 hour of exposure, it

did not lessen the pressure increase the system experienced during longer-term fouling runs that lasted up to 10 days. Our findings reinforce the conclusion that Miller et al. drew, that accurate assessments of anti-biofouling coatings require longer-term filtration studies [30].

The improvement in membrane performance seen in this study was due to the antibacterial character of PD/Ag modified membranes. The antibacterial effects of the membrane modification have generally been measured by tests that put bacteria in direct contact with the membrane following modification. The studies that included disk diffusion assays found that silver modification resulted in zones of inhibition surrounding the membrane surface [20-22, 25, 34]. Tang et al. demonstrated the antimicrobial character of the modification by quantifying the colony forming units (CFU) that grew on the membrane surface following filtration [18]. This antibacterial effect was also shown in various studies that used the spread plate method to determine the concentration of bacteria able to survive 2-24 hours of incubation with the modified membranes [19-22]. In addition, Huang et al. measured the water flux through the membrane before and after incubation with bacterial solution for 48 hours [22]. The modification resulted in a higher flux following incubation. All of these studies show that membrane modification results in inactivation of bacteria, but the impact of these findings was unclear as the studies were not conducted in realistic membrane filtration systems where bacteria is continually pushed to the membrane surface by applied pressure, building up layers over time. This study demonstrates the translation of the antibacterial character of PD/Ag modified membranes to an improvement in membrane performance in a constant pressure filtration system.

6.4.3 Silver Leaching

The total load of silver on membranes modified using this method is ca. 9.6 $\mu\text{g}/\text{cm}^2$ [18]. Triplicate compaction runs yielded silver dissolution rates of 0.22 $\mu\text{gcm}^{-2}\text{d}^{-1}$, 0.15 $\mu\text{gcm}^{-2}\text{d}^{-1}$, and 0.13 $\mu\text{gcm}^{-2}\text{d}^{-1}$, resulting in an average silver dissolution rate of 0.17 $\mu\text{gcm}^{-2}\text{d}^{-1}$ and a standard deviation of 0.05 $\mu\text{gcm}^{-2}\text{d}^{-1}$. Silver dissolution rates of 0.04 $\mu\text{gcm}^{-2}\text{d}^{-1}$, 0.02 $\mu\text{gcm}^{-2}\text{d}^{-1}$, and 0.05 $\mu\text{gcm}^{-2}\text{d}^{-1}$ were measured following triplicate bacterial filtration runs, resulting in an average silver dissolution rate of 0.04 $\mu\text{gcm}^{-2}\text{d}^{-1}$ with a standard deviation of 0.02 $\mu\text{gcm}^{-2}\text{d}^{-1}$. The concentrations of silver in the recirculated synthetic wastewater were 2 orders of magnitude below the silver drinking water standard of 100 $\mu\text{g}/\text{L}$ [35]. These dissolution rates, including the overall trend of the rate of dissolution decreasing after the initial silver release, are consistent with those reported in similar studies [19-21]. The membranes lost about 1.8% of their silver over one day of compaction and 1.3% over the following three days of bacterial filtration. Liu and Hu also demonstrated that reintroduction of silver nitrate results in a recharge of silver nanoparticles on the membrane surface [19]. Given the mild conditions required (ambient temperature and pressure), this modification technique has the potential to be reapplied *in situ*.

6.4.4 Biofilm Imaging

Representative images showing the wide range of bacterial growth that developed on each type of membrane surface are shown in Figure 6.5. No clear pattern emerged in these images.

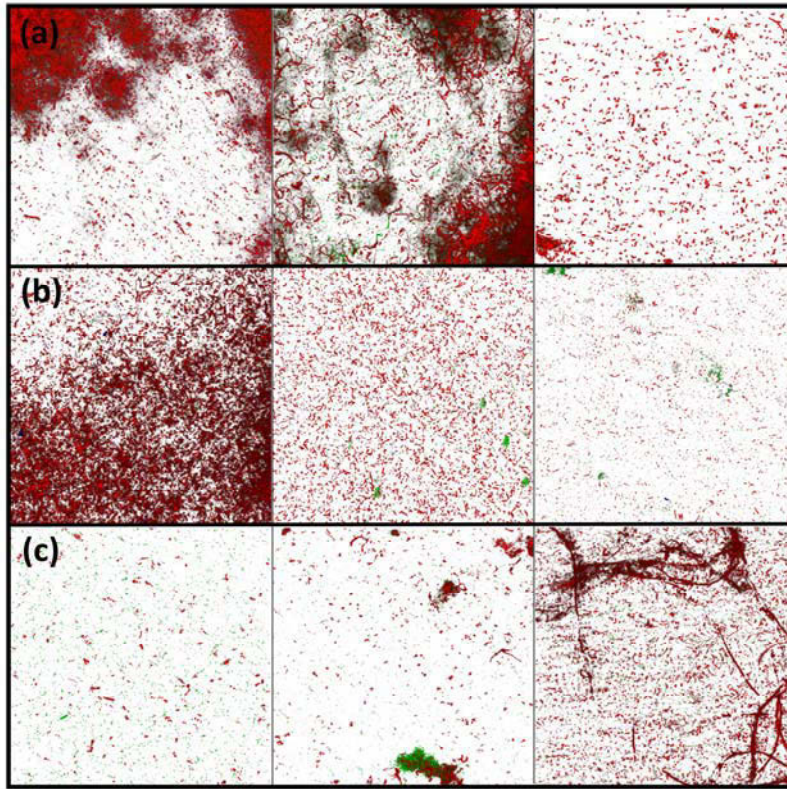


Figure 6.5. Representative top view confocal images of the live cells (green) and dead cells (red) attached to the surfaces of (a) base membranes, (b) PD modified membranes, and (c) PD/Ag modified membranes after three days of bacterial filtration. Each row contains three images to demonstrate the wide range of bacterial growth that developed on each type of membrane surface in the biofilm formation system. Each image is 225 μm x 225 μm .

The live cell, dead cell, and extracellular polysaccharide biovolumes quantified through analysis of these image stacks using COMSTAT 2 were too varied to be conclusive (Figure 6.6). Although extracellular polysaccharide biomass, an indicator of total EPS, is too wide ranging for differences to be statistically significant, the average accumulation on PD/Ag modified membranes is three orders of magnitude lower than that on base and PD modified membranes. This disparity suggests that EPS biomass accumulation is most indicative of membrane performance, supported by previous literature which asserts that it is the viscoelastic property of EPS, rather than the presence of deposited bacteria, which drastically increases the hydraulic resistance of the

membrane during biofouling [36, 37]. Overall, the biofilm imaging conducted here did not reveal a meaningful relationship between membrane performance and biomass accumulation. Literature studies using similar biofilm imaging techniques were examined in an attempt to identify factors contributing to the inconclusive observations reported.

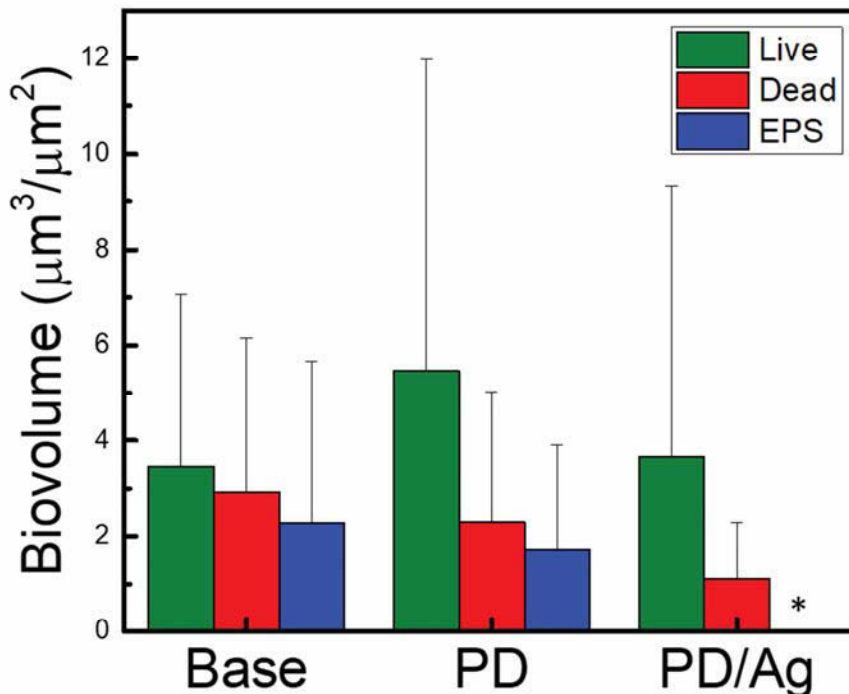


Figure 6.6. Live cell, dead cell, and extracellular polysaccharide (used as an indicator of EPS) COMSTAT biovolumes measured on base, PD modified, and PD/Ag modified membranes. The extracellular polysaccharide biovolume associated with PD/Ag modified membranes (*) cannot be seen as the average value is 0.0025 +/- 0.003 μm. Data represent average and standard deviation of triplicate experiments.

The biofilm heterogeneity observed in this experiment was not reported in some previous studies that used confocal microscopy to quantify bacterial accumulation on membrane surfaces [28, 37-41]. While these studies used *Pseudomonas sp.* in the feed, other pertinent factors including membrane type, nutrient conditions, cell concentration, and sample preparation, varied. The active layer of the membranes used in previous

studies were polyamide, while the membranes in this study are polysulfone. This material change is not likely to account for the differences in bacterial coverage as polyamide membranes are more hydrophilic than polysulfone membranes and thus should be less prone to fouling [27]. Furthermore, Flemming and Schaule demonstrated that 2-4 hours of contact with various bacterial suspensions (*Pseudomonas vesicularis*, *Acinetobacter calcoaceticus*, *Staphylococcus warneri*, and mixed culture) did not result in significantly different attachment to polyamide and polysulfone membranes [42]. In addition, modifying the membranes with positively charged, negatively charged, or zwitterionic hydrophilic polymers and/or silver nanoparticles [38, 39, 41] did not significantly affect the variance in previous studies. The heterogeneity in our study was also consistent between the hydrophobic base and hydrophilic modified membranes. Therefore, it seems unlikely that the membrane surfaces can account for the discrepancy in results.

Nutrient conditions are known to affect the development of the biofilm structure. Flemming and Schaule showed that starved cells tend to form islands of bacterial growth rather than a smooth homogeneous biofilm [42]. The nutrient composition of the synthetic wastewater used in this study was consistent with those used in Bar-Zeev et al. and Kwan et al. [28, 40]. Although the initial conditions were the same, the duration of filtration and initial cell concentrations, and therefore the nutrient availability, varied. The filtration in this study ran two days longer than the previous studies, while the initial cell concentration was 1-2 orders of magnitude smaller. Even with these considerations, given the high carbon content of the synthetic wastewater we consider it unlikely that the nutrient concentration would be so depleted as to significantly alter biofilm development.

Initial cell concentration may affect biofilm development independent of nutrient limitations. Previous studies [42, 43] have attempted to determine a range in which there is a linear relationship between the concentration of cells in suspension and the number of cells attached to the membrane surface. Ridgway et al. found this linear range to exist between 0 cells/mL and 10^6 cells/mL for *Mycobacterium sp.* in contact with a cellulose diacetate membrane for 3 hours [43]. Flemming and Schaule reported a higher range, between 10^6 cells/mL and 10^8 cells/mL, for *Pseudomonas sp.* exposed to a polyethersulfone membrane for 4 hours [42]. A sharp drop in bacterial adhesion below detection limits was associated with a suspended cell concentration less than 10^6 cells/mL. Given the comparable bacterial species and membrane type used in our study, the initial concentration of 10^5 cells/mL (1-4 orders of magnitude below similar studies that saw the formation of homogeneous biofilms [28, 37-41]) may fall below a concentration threshold, resulting in significantly different biofilm growth. However, in our constant pressure system, permeate drag will bring bacteria in contact with the membrane surface, limiting the impact of cell concentration as a factor in bacterial attachment.

Bar-Zeev et al. demonstrated that confinement of the biofilm results in a compacted biofilm structure [40]. In addition, they show that a more accurate evaluation of the biofilm can be achieved by utilizing a custom-made chamber to avoid this confinement [28, 40, 41]. In lieu of a custom-made chamber, we placed spacers between the glass slide and the cover slip to avoid compaction of the samples. Although some effects may still be present, we have not seen any evidence to suggest that confinement results in increased biofilm heterogeneity.

The magnification used in this study (40x) was higher than those used in the previous studies (20x) [28, 37-41]. However, Bernstein et al. included an evaluation of images taken at 40x magnification in the Supporting Information [38]. By comparing the analysis done on image stacks taken at 40x and 20x magnification, Bernstein et al. found that both image sets demonstrated the same overall trend in biomass attachment. In addition, increasing the magnification did not result in increased variance in the analysis of the image stacks.

We were unable to use confocal microscopy to distinguish between the mass of live cells, dead cells, and extracellular polysaccharides that accumulated on the different membrane surfaces. The heterogeneity of the biofilms that developed was so great that biovolume could not be related to membrane performance. However, as modifying the membrane with PD/Ag resulted in demonstrably higher flux over the course of *P. aeruginosa* filtration, we must assume that there are differences in bacterial attachment and growth that we were unsuccessful in capturing through confocal microscopy. Comparison with literature on biofilm imaging did not reveal factors contributing to the inconclusive results obtained in this study.

6.5 Conclusions

This study demonstrated the need for researchers investigating membrane modification to use long-term fouling systems (i.e., several days) instead of short-term tests (i.e., minutes to hours). During short-term adhesion experiments, the hydrophilic nature of the polydopamine coating was able to decrease the initial deposition rate of *P. aeruginosa* by almost 50%. However, this anti-adhesive effect did not translate to an improvement in membrane flux over three days of bacterial filtration. Instead, it was the

antibacterial character of the silver that significantly improved membrane performance in a more realistic system. Future studies should probe the effects of the PD/Ag modification on cleaning efficiency, as the anti-adhesive character of the PD coating is likely to improve flux recovery [22, 44]. Overall, PD/Ag membrane modification shows potential for application in membrane treatment systems. While surface modifications lose their efficacy over time, PD/Ag modification has potential for reapplication *in situ* due to mild modification conditions and proven recharge ability. The cost/benefit analysis will vary depending on the circumstances of the specific treatment site (scale, water quality, bacterial community) and should be considered in future studies. For water sources in which biofouling is a strong limiting factor in clean water production, such as feed waters with high nutrient conditions, decreased energy costs and frequency of membrane replacement will result in a significant reduction in the overall cost of membrane treatment, making high quality water more accessible.

6.6 References

1. Huang, H., K. Schwab, and J.G. Jacangelo, *Pretreatment for low pressure membranes in water treatment: a review*. Environ Sci Technol, 2009. **43**(9): p. 3011-9.
2. Geise, G.M., et al., *Water purification by membranes: The role of polymer science*. Journal of Polymer Science, Part B: Polymer Physics, 2010. **48**(15): p. 1685-1718.
3. Chang, H., et al., *Hydraulic backwashing for low-pressure membranes in drinking water treatment: A review*. Journal of Membrane Science, 2017. **540**: p. 362-380.
4. Gonzalez-Perez, A., K.M. Persson, and F. Lipnizki, *Functional channel membranes for drinking water production*. Water (Switzerland), 2018. **10**(7).
5. Freeman, S., et al., *Integrating low-pressure membranes into water treatment plants*. Journal American Water Works Association, 2006. **98**(12): p. 26-30.
6. Huisman, I.H. and K. Williams, *Autopsy and failure analysis of ultrafiltration membranes from a waste-water treatment system*. Desalination, 2004. **165**(1-3): p. 161-164.
7. Gijsbertsen-Abrahamse, A.J., E.R. Cornelissen, and J.A.M.H. Hofman, *Fiber failure frequency and causes of hollow fiber integrity loss*. Desalination, 2006. **194**(1-3): p. 251-258.
8. Kochkodan, V., D.J. Johnson, and N. Hilal, *Polymeric membranes: surface modification for minimizing (bio)colloidal fouling*. Adv Colloid Interface Sci, 2014. **206**: p. 116-40.
9. Kochkodan, V. and N. Hilal, *A comprehensive review on surface modified polymer membranes for biofouling mitigation*. Desalination, 2015. **356**: p. 187-207.
10. Lee, H., et al., *Mussel-inspired surface chemistry for multifunctional coatings*. Science, 2007. **318**(5849): p. 426-430.
11. Chen, C.T., et al., *Polydopamine and eumelanin molecular structures investigated with ab initio calculations*. Chemical Science, 2017. **8**(2): p. 1631-1641.
12. Dreyer, D.R., et al., *Elucidating the structure of poly(dopamine)*. Langmuir, 2012. **28**(15): p. 6428-6435.
13. Hong, S., et al., *Non-Covalent Self-Assembly and Covalent Polymerization Co-Contribute to Polydopamine Formation*. Advanced Functional Materials, 2012. **22**(22): p. 4711-4717.
14. Liebscher, J., et al., *Structure of polydopamine: A never-ending story?* Langmuir, 2013. **29**(33): p. 10539-10548.
15. Kasemset, S., et al., *Effect of polydopamine deposition conditions on fouling resistance, physical properties, and permeation properties of reverse osmosis membranes in oil/water separation*. Journal of Membrane Science, 2013. **425-426**: p. 208-216.
16. Yang, H.C., et al., *Surface engineering of polymer membranes via mussel-inspired chemistry*. Journal of Membrane Science, 2015. **483**: p. 42-59.
17. Arena, J.T., et al., *Solute and water transport in forward osmosis using polydopamine modified thin film composite membranes*. Desalination, 2014. **343**: p. 8-16.

18. Tang, L., K.J.T. Livi, and K.L. Chen, *Polysulfone Membranes Modified with Bioinspired Polydopamine and Silver Nanoparticles Formed in Situ To Mitigate Biofouling*. Environmental Science & Technology Letters, 2015. **2**(3): p. 59-65.
19. Liu, Z. and Y. Hu, *Sustainable Antibiofouling Properties of Thin Film Composite Forward Osmosis Membrane with Rechargeable Silver Nanoparticles Loading*. ACS Appl Mater Interfaces, 2016. **8**(33): p. 21666-73.
20. Yang, Z., et al., *In Situ Reduction of Silver by Polydopamine: A Novel Antimicrobial Modification of a Thin-Film Composite Polyamide Membrane*. Environ Sci Technol, 2016. **50**(17): p. 9543-50.
21. Zhang, R.N., et al., *Manipulating the multifunctionalities of polydopamine to prepare high-flux anti-biofouling composite nanofiltration membranes*. Rsc Advances, 2016. **6**(39): p. 32863-32873.
22. Huang, L.C., et al., *In situ immobilization of silver nanoparticles for improving permeability, antifouling and anti-bacterial properties of ultrafiltration membrane*. Journal of Membrane Science, 2016. **499**: p. 269-281.
23. Yang, E., et al., *Concurrent performance improvement and biofouling mitigation in osmotic microbial fuel cells using a silver nanoparticle-polydopamine coated forward osmosis membrane*. Journal of Membrane Science, 2016. **513**: p. 217-225.
24. Kim, S.H., et al., *Design of TiO₂ nanoparticle self-assembled aromatic polyamide thin-film-composite (TFC) membrane as an approach to solve biofouling problem*. Journal of Membrane Science, 2003. **211**(1): p. 157-165.
25. Sureshkumar, M., P.N. Lee, and C.K. Lee, *Stepwise assembly of multimetallic nanoparticles via self-polymerized polydopamine*. Journal of Materials Chemistry, 2011. **21**(33): p. 12316-12320.
26. Strathmann, H. and K. Kock, *Formation Mechanism of Phase Inversion Membranes*. Desalination, 1977. **21**(3): p. 241-255.
27. Benjamin, M.M. and D.F. Lawler, *Water quality engineering: Physical/chemical treatment processes*. 2013: John Wiley & Sons.
28. Kwan, S.E., E. Bar-Zeev, and M. Elimelech, *Biofouling in forward osmosis and reverse osmosis: Measurements and mechanisms*. Journal of Membrane Science, 2015. **493**: p. 703-708.
29. Heydorn, A., et al., *Quantification of biofilm structures by the novel computer program COMSTAT*. Microbiology, 2000. **146**(10): p. 2395-2407.
30. Miller, D.J., et al., *Short-term adhesion and long-term biofouling testing of polydopamine and poly(ethylene glycol) surface modifications of membranes and feed spacers for biofouling control*. Water Research, 2012. **46**(12): p. 3737-3753.
31. Xu, P., C. Bellona, and J.E. Drewes, *Fouling of nanofiltration and reverse osmosis membranes during municipal wastewater reclamation: Membrane autopsy results from pilot-scale investigations*. Journal of Membrane Science, 2010. **353**(1-2): p. 111-121.
32. Pasmore, M., et al., *Effects of ultrafiltration membrane surface properties on Pseudomonas aeruginosa biofilm initiation for the purpose of reducing biofouling*. Journal of Membrane Science, 2001. **194**(1): p. 15-32.
33. Habimana, O., A.J.C. Semião, and E. Casey, *The role of cell-surface interactions in bacterial initial adhesion and consequent biofilm formation on*

- nanofiltration/reverse osmosis membranes*. Journal of Membrane Science, 2014. **454**: p. 82-96.
34. Yang, H., et al., *Polydopamine-coated nanofibrous mats as a versatile platform for producing porous functional membranes*. Journal of Materials Chemistry, 2012. **22**(33): p. 16994-17001.
 35. Ratte, H.T., *Bioaccumulation and toxicity of silver compounds: A review*. Environmental Toxicology and Chemistry, 1999. **18**(1): p. 89-108.
 36. Baker, J.S. and L.Y. Dudley, *Biofouling in membrane systems — A review*. Desalination, 1998. **118**(1-3): p. 81-89.
 37. Herzberg, M. and M. Elimelech, *Biofouling of reverse osmosis membranes: Role of biofilm-enhanced osmotic pressure*. Journal of Membrane Science, 2007. **295**(1-2): p. 11-20.
 38. Bernstein, R., et al., *'Should I stay or should I go?' Bacterial attachment vs biofilm formation on surface-modified membranes*. Biofouling, 2014. **30**(3): p. 367-376.
 39. Ben-Sasson, M., et al., *In situ formation of silver nanoparticles on thin-film composite reverse osmosis membranes for biofouling mitigation*. Water Research, 2014. **62**: p. 260-270.
 40. Bar-Zeev, E., et al., *The importance of microscopic characterization of membrane biofilms in an unconfined environment*. Desalination, 2014. **348**: p. 8-15.
 41. Liu, C., et al., *Mitigation of Biofilm Development on Thin-Film Composite Membranes Functionalized with Zwitterionic Polymers and Silver Nanoparticles*. Environmental Science and Technology, 2017. **51**(1): p. 182-191.
 42. Flemming, H.C. and G. Schaule, *Biofouling on membranes - A microbiological approach*. Desalination, 1988. **70**(1-3): p. 95-119.
 43. Ridgway, H.F., M.G. Rigby, and D.G. Argo, *Adhesion of a Mycobacterium sp. to cellulose diacetate membranes used in reverse osmosis*. Applied and Environmental Microbiology, 1984. **47**(1): p. 61-67.
 44. Pasmore, M., et al., *Effect of polymer surface properties on the reversibility of attachment of Pseudomonas aeruginosa in the early stages of biofilm development*. Biofouling, 2002. **18**(1): p. 65-71.

Chapter 7. Conclusions, Significance, and Suggestions for Future Work

7.1 Impact of CMP on Nanoparticle Characteristics

No changes were observed in the physicochemical characterization of nanoparticles following CMP exposure. Diluted in aqueous solutions containing up to 1 M NaCl or 1 M NaNO₃, silica, ceria, and alumina nanoparticles retained sizes of ca. 170 nm, 140 nm, and 350 nm, respectively. Silica nanoparticles, unlike ceria and alumina nanoparticles, did show aggregation in the presence of CaCl₂ at concentrations ranging from 10-500 mM. This indicates the possibility of silica nanoparticle homo-aggregation in environmental waters. Silica, ceria, and alumina nanoparticles were negatively charged, negatively charged, and positively charged, respectively, in neutral pH NaCl solutions ranging from 1-100 mM. All charges approached neutral as the NaCl concentration increased due to charge screening. As the salt concentration increases and the charge is screened, silica and ceria nanoparticles are more likely to aggregate with negatively charged organic matter in saline surface waters. For positively charged alumina nanoparticles, electrostatic attraction to organic matter will be strongest at low salt concentrations, such as those present in lakes and rivers (ionic strength ca. 1-5 mM).

In addition, no changes to nanoparticle-model cell membrane interactions were observed that indicated exposure to the CMP process increased the environmental or human health risks posed by nanoparticle release. Silica nanoparticles at concentrations of 1 mg/L attached to SLBs in the presence of NaCl concentrations ranging from 10-150 mM NaCl. Under solution conditions that mimic physiological fluids (150 mM NaCl, pH

7.4), silica nanoparticles showed substantial attachment at concentrations ranging from 1-500 mg/L, with the initial rate of attachment increasing linearly with concentration. Ceria and alumina nanoparticles, both before and after CMP, showed only weak interactions with the SLB.

None of the CMP nanoparticles were associated with substantial vesicle disruption, with all 40-minute exposures resulting in the leakage of less than 1% of the fluorescent dye contained within the vesicles. Even though the dye leakage signal was either weak or undetectable for all CMP nanoparticles, the only statistically significant ($p < 0.05$) effect of CMP exposure was associated with ceria nanoparticle exposure to DOPC vesicles. While pre-CMP ceria nanoparticle runs resulted in slight dye leakage (<1% of total), post CMP-ceria nanoparticles did not result in any detectable dye leakage compared with the negative control. This change in ceria nanoparticle behavior is likely due to the erosion of sharper edges that may occur during CMP and only indicates less potential damage to cell membranes.

7.2 Stabilization Effects of Slurry Additives

Slurry dispersants governed the aggregation behaviors and model cell membrane interactions of alumina and ceria nanoparticles, even at high dilutions (>100,000x). While the resistance of the silica nanoparticles to aggregation was anticipated based on earlier studies [1-3], ceria and alumina nanoparticles have previously shown less stability with associated critical coagulation concentrations of 2 mM NaCl and 25 mM NaCl respectively [3]. In this work, even at high salt concentrations (1 M NaCl, 1 M NaNO₃, 0.5 M CaCl₂) no ceria or alumina nanoparticle aggregation was detected. Furthermore, only weak interactions with model cell membranes were observed, indicating steric

stabilization. The Material Safety Data Sheet (MSDS) of the ceria CMP slurry identifies polyacrylic acid as an additive with chemical properties such that it likely acts as a stabilizing agent in our systems. However, for the alumina nanoparticle slurries the dispersants that may be present remain unspecified. Given the information provided by the manufacturer and the alumina nanoparticles' retention of positive charge, lack of attachment to the negatively charged lipid bilayer, and slight removal of lipids from the bilayer at high concentrations, the stabilizer is likely a positively charged ammonium-based polymer.

7.3 Pairing Model Cell Membrane and Cytotoxicity Studies

Mechanistic studies investigating the interactions of CMP nanoparticles with model cell membranes were compared with cell viability and cell membrane damage studies conducted by our collaborators. The tendency of nanoparticles to attach to the DOPC SLB during QCM-D experiments appears to correlate with observed A549 lung epithelial cell membrane damage. Silica nanoparticles showed significant attachment to SLBs at concentrations ranging from 1-500 mg/L under conditions comparable to the cell media used in the cytotoxicity assays (150 mM NaCl, pH 7.4). At silica nanoparticle concentrations in this same range (50-500 mg/L), significant release (1.5-3x negative control) of the cytoplasmic enzyme lactate dehydrogenase (LDH) was also demonstrated. In contrast, ceria and alumina nanoparticles showed very weak interaction with SLBs. During the QCM-D experiments, the rates of mass change associated with exposure to alumina and ceria concentrations of 500 mg/L were on the same scale as those that occur in response to the introduction of 1 mg/L silica nanoparticles. In accordance with this

observed lack of SLB interaction, ceria and alumina exposures did not cause significant cell membrane damage assessed through the LDH assays.

The limited signals detected in the vesicle disruption and cell viability studies make effectively interpreting and comparing their results difficult. Cell viability was assessed using the IC₅₀ metric, or the concentration at which 50% of cells are unable to metabolize a resazurin dye. No IC₅₀ concentrations were determined for ceria nanoparticles, as 50% of cells, including A549 lung epithelial cells, HepG2 liver epithelial cells, and RAW 264.7 macrophages, were not inactivated following 48-hr exposures to concentrations up to 2 g/L. The lowest alumina nanoparticle IC₅₀ value, associated with HepG2 liver epithelial cells, was 3.5 g/L, 7 times the greatest concentration tested in the model cell membrane studies. Silica nanoparticles were associated with IC₅₀ values ranging from 220 mg/L-620 mg/L, overlapping with model cell membrane study concentrations. However, as no CMP nanoparticles showed substantial vesicle disruption, a correlation is not readily apparent.

7.4 Improving Polymeric Membrane Performance with Polydopamine and Silver Nanoparticle Modification

Low pressure polysulfone membranes were modified with hydrophilic polydopamine and antibacterial silver nanoparticles to prevent bacterial attachment and biofilm formation. This modification was assessed using both short-term (20 minutes) bacterial deposition and longer-term (3 days) membrane filtration experiments. Both the polydopamine modification and polydopamine/silver nanoparticle modification significantly decreased the initial rate of *Pseudomonas aeruginosa* attachment, with declines of 48% and 38% respectively. Therefore, this short-term reduction in bacterial

attachment can be attributed to the anti-adhesive polydopamine layer, irrespective of further modification with silver nanoparticles.

However, in a longer-term, constant-pressure filtration system, only the modification that included antibacterial silver nanoparticles was able to improve the rate of clean water production. The anti-adhesive property of polydopamine was not effective in significantly improving permeate flux as the applied pressure pushed bacteria up against the membrane surface over longer time periods. Instead, the ability of silver nanoparticles to inactivate the bacteria that attached to the membrane surface was necessary in delaying the effects of bacterial growth. For membranes modified with polydopamine and silver nanoparticles, the permeate flux remained over 1.7 times that of the unmodified membranes.

After 3 days of filtration, the biofilms that formed on the membrane surfaces were imaged to determine how modification affected biofilm structure. While the distributions of live cells, dead cells, and extracellular polymeric substances (EPS) were too varied to make definitive conclusions, the polydopamine and silver nanoparticle modification was associated with the smallest average EPS biovolume. This decrease in EPS levels provides further evidence that the inactivation of bacteria by silver nanoparticles allows for delayed biofilm formation and improved membrane performance.

7.5 Engineering and Research Significance

7.5.1 Metal Oxide Nanoparticles Applied in Chemical Mechanical Planarization

The abrasive metal oxide nanoparticles used in CMP are currently unregulated; however, given the societal unease around nanoparticle use and the continuously evolving regulatory landscape, it benefits the semiconductor industry to evaluate the

environmental fate and toxicity of CMP nanoparticles. While engineered nanomaterials released to surface waters are generally predicted to aggregate with natural organic matter and settle out of the water column [4], this work demonstrates the ability of slurry dispersants to stabilize nanoparticles even at high dilutions. As persistence in the water column is believed to increase bioavailability [5], these stabilizing effects are important to consider during the CMP slurry design process.

No changes in physicochemical characteristics or model cell membrane interactions were observed during our studies that indicate that exposure to CMP processing increases the hazard posed by silica, ceria, or alumina nanoparticle release [6]. However, the goal of this work was not to provide an assessment of CMP nanoparticle cytotoxicity and no specific conclusions regarding their associated risks can be made without further study. Regarding the use of QCM-D model membrane studies as a tool to provide insights into the mechanisms of cytotoxicity, measured SLB attachment showed potential as useful indicators of membrane damage. The results of vesicle disruption studies were not correlated with membrane damage or cellular inhibition however, and so these particular studies were not useful in elucidating the results of the cytotoxicity assays.

7.5.2 Silver Nanoparticles Applied in Membrane Water Treatment

Low land requirement allows membranes to be used in decentralized systems while high quality water delivery allows them to aid access to previously unusable water sources including seawater and wastewater. The largest barrier to membrane use is the associated energy requirements, greater than those of traditional water treatment systems. The energy efficiency of membrane filtration has increased substantially over the last

decades due to advances in membrane materials [7]. Since membrane permeability has been thoroughly developed for commercial application, controlling membrane fouling is the next critical step to improving the energy efficiency of membrane treatment [7]. Polydopamine and silver nanoparticle membrane modification can be administered to produce a uniform, controlled coating under mild conditions [8]. This hydrophilic/antibacterial combination showed the ability to sustain increased water flux over 3 days of constant-pressure bacterial filtration. Given the common cleaning protocol involving tens of backwashes per day [9], increased permeate flux is likely to be sustained over even longer time periods. The low dissolution rate of the silver nanoparticles is beneficial for maintaining the antibacterial quality of the modified membranes as well as complying with secondary drinking water standards. Finally, the potential for membranes to be re-modified *in situ* makes polydopamine/silver nanoparticle modification an exciting prospective solution for membrane treatment systems that are compromised by the effects of biofouling.

The research evaluating membrane modifications covers a wide range of experimental methods that are difficult to compare, and many consider only short-term effects. The polydopamine modification itself has received a great deal of attention as an anti-fouling coating. Our observations reinforce the conclusions reached by the Freeman group through studies that challenged polydopamine modified membranes with bacterial filtration over 10 days. As in our study, polydopamine modification decreased initial bacterial adhesion but did not significantly improve membrane performance over longer-term filtration [10, 11]. These results call into question the ability of hydrophilic coatings to decrease the effects of biofouling under realistic conditions. The work presented here,

which demonstrates the lack of applicability of short-term anti-adhesive improvements to longer-term performance, should aid in redirecting research efforts towards methods that more accurately assess the efficacy of membrane modification. Such assessment will ensure this technology is properly developed to help meet the increasing need for alternative water treatment systems.

7.6 Future Research Directions

7.6.1 CMP Nanoparticle Characterization

The next step for the CMP nanoparticle characterization work is to identify the stabilizing agent that governs the behavior of the alumina nanoparticles. While we can deduce the dispersant is a positively charged polymer based on our observations of steric stabilization, determining the specific material is of immediate importance. Polymeric materials in general can be identified through several techniques, including High Performance Liquid Chromatography (HPLC), Nuclear Magnetic Resonance Spectroscopy (NMR), Gel Permeation Chromatography (GPC), and Fourier Transform Infrared Spectroscopy (FTIR). FTIR is currently being pursued by our collaborators at North Carolina A&T State University as part of our joint CMP slurry characterization research study.

CMP nanoparticle physicochemical and model cell membrane interaction characterization could be expanded to other slurry types. Although this work considered three of the most common nanoparticle/wafer combinations, numerous slurries are available through several different manufacturers. Based on our findings, future studies should be designed with an emphasis on distinct nanoparticle/dispersant combinations. Future studies should also include positive controls to better elucidate the ways in which

SLB attachment and vesicle disruption are related to cytotoxicity. This work would have benefited through comparison with a nanomaterial known to physically damage lipid bilayers upon attachment, such as graphene oxide nanosheets [12]. This control would have been useful in interpreting the results of the vesicle disruption studies and their application to cytotoxicity assays.

CMP nanoparticle characterization would also benefit from observation of behaviors in environmental systems, including surface waters. This experimentation would generate more accurate predictions of interactions and sinks, including the likelihood of homo- and hetero-aggregation, under the dilution and salt conditions present in the environment. It would also allow for the detection of organic matter coatings that are likely to form on nanoparticle surfaces, altering their surface properties. For instance, while organic matter has been shown to increase the resistance of nanoparticles to aggregation, they have also been associated with decreased toxicity [13]. An area of particular interest in further waste CMP nanoparticle ecotoxicity testing is the impact of nanoparticle exposure on benthic organisms, as predicted sedimentation is likely to put these organisms at higher risk [14].

Just as a layer of organic matter is expected to coat engineered nanomaterials in surface waters, a protein corona is expected to form in physiological fluids. “Protein corona” is the term for the layer of proteins and other biomolecules that will adhere to nanoparticle surfaces upon their introduction to blood plasma, pulmonary fluid, and digestive fluid. Over 80 proteins have been identified in nanoparticle protein coronas, including albumin, immunoglobulins, apolipoproteins, and fibrinogen [15]. The investigation of the direct interactions of engineered nanomaterials with cells is a

conservative method of assessing cytotoxicity because the formation of the corona reduces nanoparticle adhesion and uptake [16, 17]. However, the inevitability of corona formation makes its consideration crucial to the future development of toxicity profiles

7.6.2 Developing Membranes Modified with Polydopamine and Silver Nanoparticles

Further characterization of membranes modified with polydopamine and silver nanoparticles is required before large-scale implementation. Common cleaning procedures, including periodic backwashing, should be applied in realistic systems to quantify additional performance gains. Chemical cleaning procedures should be tested and optimized, as soaking with certain solutions may be damaging to the modified surface. In addition, over time as membrane performance fails, re-modification should be tested *in situ* to determine applicability to large-scale systems.

Taken together, these steps will provide a basis for the financial analysis of the incorporation of polydopamine and silver nanoparticle modification into membrane treatment systems. The usefulness of this modification will be site specific and depend on the quality of the source water, influence of other pre-treatment methods, and current levels of biofouling. Furthermore, research to assess the effects of membrane modification should be expanded to include high pressure membranes, since biofouling is a major problem in reverse osmosis systems. When polydopamine and silver nanoparticle membrane modification has been fully developed, it has the potential to increase the energy efficiency of membrane treatment systems, thereby increasing public access to clean water.

7.7 References

1. Vigil, G., et al., *Interactions of silica surfaces*. Journal of Colloid And Interface Science, 1994. **165**(2): p. 367-385.
2. Otero-González, L., et al., *Stability of alumina, ceria, and silica nanoparticles in municipal wastewater*. Water Science and Technology, 2014. **70**(9): p. 1533-1539.
3. Liu, X. and K.L. Chen, *Aggregation and interactions of chemical mechanical planarization nanoparticles with model biological membranes: Role of phosphate adsorption*. Environmental Science: Nano, 2016. **3**(1): p. 146-156.
4. Quik, J.T.K., et al., *Heteroaggregation and sedimentation rates for nanomaterials in natural waters*. Water Research, 2014. **48**(1): p. 269-279.
5. Goswami, L., et al., *Engineered nano particles: Nature, behavior, and effect on the environment*. Journal of Environmental Management, 2017. **196**: p. 297-315.
6. Speed, D., et al., *Physical, chemical, and in vitro toxicological characterization of nanoparticles in chemical mechanical planarization suspensions used in the semiconductor industry: Towards environmental health and safety assessments*. Environmental Science: Nano, 2015. **2**(3): p. 227-244.
7. Elimelech, M. and W.A. Phillip, *The future of seawater desalination: energy, technology, and the environment*. science, 2011. **333**(6043): p. 712-717.
8. Lee, H., et al., *Mussel-inspired surface chemistry for multifunctional coatings*. Science, 2007. **318**(5849): p. 426-430.
9. Porcelli, N. and S. Judd, *Chemical cleaning of potable water membranes: A review*. Separation and Purification Technology, 2010. **71**(2): p. 137-143.
10. Araujo, P.A., et al., *Impact of feed spacer and membrane modification by hydrophilic, bactericidal and biocidal coating on biofouling control*. Desalination, 2012. **295**: p. 1-10.
11. Miller, D.J., et al., *Short-term adhesion and long-term biofouling testing of polydopamine and poly(ethylene glycol) surface modifications of membranes and feed spacers for biofouling control*. Water Research, 2012. **46**(12): p. 3737-3753.
12. Hu, W., et al., *Protein corona-mediated mitigation of cytotoxicity of graphene oxide*. ACS Nano, 2011. **5**(5): p. 3693-3700.
13. Glisovic, S., et al., *Emerging technologies and safety concerns: a condensed review of environmental life cycle risks in the nano-world*. International Journal of Environmental Science and Technology, 2017. **14**(10): p. 2301-2320.
14. De Marchi, L., et al., *Engineered nanomaterials: From their properties and applications, to their toxicity towards marine bivalves in a changing environment*. Environmental Research, 2019. **178**.
15. Boyes, W.K., et al., *A comprehensive framework for evaluating the environmental health and safety implications of engineered nanomaterials*. Critical Reviews in Toxicology, 2017. **47**(9): p. 767-810.
16. Leroueil, P.R., et al., *Wide varieties of cationic nanoparticles induce defects in supported lipid bilayers*. Nano Letters, 2008. **8**(2): p. 420-424.
17. Yuan, H., et al., *Variable nanoparticle-cell adhesion strength regulates cellular uptake*. Physical Review Letters, 2010. **105**(13).

Curriculum Vitae

Margaret L. Fleming

EDUCATION

Johns Hopkins University, Whiting School of Engineering, *Baltimore, MD*

- Doctor of Philosophy in Environmental Engineering February 2020
- Master of Science in Environmental Process Engineering May 2018

Cornell University, College of Agriculture and Life Sciences, *Ithaca, NY*

- Bachelor of Science in Environmental Engineering May 2014

RESEARCH

Graduate Researcher

Dr. Edward Bouwer, Johns Hopkins University, *Baltimore, MD* Spring 2017 - Fall 2019

- Conducted physicochemical characterization of ceria, silica, and alumina nanoparticles to help determine their behavior and fate in aquatic environments
- Studied attachment of nanoparticles to model cell membranes
- Collaborated with researchers conducting cytotoxicity studies at N.C. A&T State University to assess environmental risk

Dr. Kai Loon Chen, Johns Hopkins University, *Baltimore, MD* Fall 2014 - Spring 2017

- Altered low-pressure filtration membranes with anti-bacterial silver nanoparticles to increase water treatment energy efficiency
- Investigated initial bacterial adhesion and subsequent biofilm formation

Undergraduate Researcher

Dr. Sheila Saia, Cornell University, *Ithaca, NY* Fall 2013 - Spring 2014

- Characterized stream water quality parameters including pH, dissolved oxygen, total organic carbon, soluble reactive phosphorus, and total suspended solids

Dr. Brian Buchanan, Cornell University, *Ithaca, NY* Fall 2012 - Spring 2013

- Collected field data including GPS coordinates and soil saturation measurements for use in a model associating soil thresholds with storm runoff and nonpoint source pollution

TEACHING

City Springs Science Outreach Program

Fall 2014 - Spring 2019

- Assisted in monthly activities for a class of 20-30 5th grade students
- Introduced concepts related to the water cycle, energy, and environmental engineering

Teaching Assistant

Dr. Ed Bouwer, Johns Hopkins University, *Baltimore, MD* Fall 2015 – Spring 2019

- Classes: Environmental Engineering Fundamentals, Engineering Microbiology, Biological Processes
- Acted as a guest lecturer
- Graded homework and lab write-ups

EMPLOYMENT

Technical Associate

Fall 2011 - Fall 2019

EcoSafety Sciences, *Marlborough, MA*

- Collected data on drug compounds found in pharmaceuticals and personal care products using relevant literature, databases, and EPI Suite
- Wrote study summaries to inform risk assessments and evaluate environmentally friendly replacement materials

SCIENCE POLICY AND COMMUNICATION

Johns Hopkins Homewood Science Policy Group

Fall 2018 - Fall 2019

- Organized and moderated panel of AAAS Fellows for doctoral students interested in policy careers
- Co-wrote a policy memo on the Baltimore Clean Air Act
- Attended Capitol Hill Day to advocate for science funding
- Participated in workshops on oral and written science communication

IGERT Water, Health and Climate Fellow

Fall 2014 - Spring 2018

- Tested bacterial contamination of drinking water in Iquitos, Peru over two weeks
- Summarized results and recommendations in a report for the local government
- Presented research to an industry advisory committee

AWARDS AND FELLOWSHIPS

- The National Science Policy Network and Journal of Science Policy and Governance International Memo Competition Honorable Mention - 2019
- Judges' Choice Award Department Poster Session – 2017, 2018, 2019
- American Chemical Society Graduate Student Award - 2016
- Cornell University College of Agriculture and Life Sciences Academic Excellence Award - 2014
- Integrative Graduate Education and Research Traineeship (IGERT) Water, Climate, and Health Fellow - 2014
- Duke University Center for the Environmental Implications of Nanotechnology (CEINT) Research Experience for Undergraduates (REU) Fellow - 2013

PUBLICATIONS

Peterson, E., Fleming, M.L., Saund, S., Stephens, B. "Baltimore Clean Air Act; the need for a new waste management system in Baltimore" *Journal of Science Policy and Governance*, 14, 2, 2019.

Fleming, M.L., Bouwer, E., Chen, K.L. "Biofouling response of laboratory-scale polysulfone membranes modified with bioinspired polydopamine and silver nanoparticles" *Environmental Engineering Science*, 36, 335-343, 2019.

Tang, L., Huynh, K.A., Fleming, M.L., Larronde-Larretche, M., Chen, K.L. "Imparting antimicrobial and antiadhesive properties to polysulfone membranes through modification with silver nanoparticles and polyelectrolyte multilayers" *Journal of Colloid and Interface Science*, 451, 125–133, 2015.

Buchanan, B.P., Fleming, M.L., Schneider, R. L., Richards, B.K., Archibald, J., Qiu, Z., Walter, M.T. "Evaluating topographic wetness indices across central New York agricultural landscapes" *Hydrology and Earth System Sciences*, 18, 3279-3299, 2014.